Altered regulation of adipogenesis with respect to disease processes

Stephanie Jane Davies
BSc

Submitted in fulfilment of the requirements for the degree of Doctor of Philosophy in Molecular Cell Biology

National University of Ireland, Cork
School of Biochemistry and Cell Biology

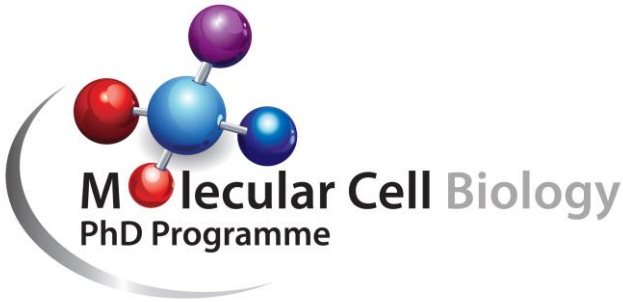

January 2017

Head of School: Professor Rosemary O'Connor

Supervisor: Professor Tommie V. McCarthy

This thesis is dedicated to my wonderful grandparents

Michael & Pauline Hughes

Dr Hilton & Heather Davies

Table of Contents

Declaration

The thesis submitted is my own work, except where explicit reference is made to the contribution of others, and has not been submitted for another degree, either at University College Cork or Elsewhere.

Signed: (Stephanie Jane Davies)

Date: _____

Acknowledgements

I would like to extend my sincerest gratitude to my supervisor Professor Tommie McCarthy. I am privileged to say that throughout this process he never lost enthusiasm.

I would like to thank my family for their unwavering support.

And finally, I would like to thank my fellow colleagues in the school of biochemistry, at University College Cork. They have made this experience unforgettable.

ABSTRACT

Dysregulation of adipose tissue metabolism is associated with multiple metabolic disorders. One such disease, known as Dunnigan-type familial partial lipodystrophy (FPLD2) is characterised by defective fat metabolism and storage. FPLD2 is caused by a specific subset of mutations in the LMNA gene. The mechanisms by which LMNA mutations lead to the adipose specific FPLD2 phenotype have yet to be determined in detail. Previous work employed RNA-Seq analysis to assess the effects of wild-type (WT) and mutant (R482W) LMNA on the expression profile of differentiating 3T3-L1 mouse preadipocytes and identified over 200 transcripts whose expression was altered. Four of these genes namely ITM2A, IGFBP5, PTPRQ and WNT6 were selected for detailed investigation using the 3T3-L1 model for adipogenesis. Extensive methodological work was carried out aimed at developing a system that facilitated robust analysis of transfected gene activity in the adipocyte differentiation 3T3-L1 cell model.

Preliminary investigations were carried out on IGFBP5, PTPRQ and WNT6 and while some progress was made in exploring these genes in adipogenesis, significant obstacles were encountered. A complex endogenous IGFBP5 expression profile is shown in 3T3-L1 differentiation, with IGFBP5 over-expression and shRNA mediated knockdown leading to inhibited and enhanced differentiation, respectively. Investigation into the effects of LMNA over-expression on IGFBP5 yielded conflicting results and further analysis is required to elucidate the mechanisms regulating IGFBP5 expression in adipogenesis. PTPRQ and WNT6 are lowly expressed in pre-adipocytes and further down-regulated during 3T3-L1 differentiation. PTPRQ over-expression is reported to inhibit the adipogenic programme, and in this thesis shRNA mediated knockdown of PTPRQ is shown to inhibit differentiation as well. WNT6 knockdown is reported to enhance adipogenesis, however technical difficulties in the accurate detection of WNT6 mRNA render this gene challenging to study in the context of adipogenesis.

Detailed investigations were carried out on ITM2A. In this thesis ITM2A is identified as a novel modulator of adipogenesis and results show that endogenous ITM2A expression is transiently down-regulated during induction of 3T3-L1 differentiation.

ITM2A over-expression was seen to moderately inhibit differentiation of 3T3-L1 preadipocytes while shRNA mediated knockdown of ITM2A significantly enhanced 3T3-L1 differentiation. Investigation of PPARγ levels indicate that this enhanced adipogenesis is mediated through the stabilization of the PPARγ protein at specific time points during differentiation. The results demonstrate that ITM2A knockdown is sufficient to rescue the inhibitory effects of LMNA WT and R482W mutant over-expression on 3T3-L1 differentiation and indicate a novel therapeutic approach for FPLD2.

ABBREVIATIONS

3-Isobutyl-1-methylxanthine ..... IBMX
5α-Androstan-17β-ol-3-one .....DHT
A Disintegrin and metalloproteinase domain-containing protein 10 .....ADAM10
Acyl-CoA synthetase ..... ACS
Acyl-CoA-binding protein ..... ACBP
Adipocyte stem cells ..... ASC
Atherosclerotic cardiovascular disease .....ACVD
Autophagy protein 5/7.....ATG5/7
Autosomal Emery-Dreifuss muscular dystrophy .....A-EDMD
Bafilomycin A1 ..... BafA1
Basic-helix-loop-helix-leucine zipper..... bHLH-LZ
Bone morphogenetic protein ..... BMP
Bovine serum albumin ..... BSA
Brown adipose tissue .....BAT
C/EBP homologous protein CHOP10
cAMP response element-binding protein ..... CREB
CCAAT/enhancer binding protein .....C/EBP
CCAAT/enhancer binding protein .....C/EBP
Cell death-inducing Dffa-like effector C .....CIDEC
Charcot-Marie-Tooth disorder type 2B.....CMT2B
Chicken ovalbumin upstream promoter transcription factor II.....COUP-TFII
Cluster of differentiation 36 ..... CD36
Congenital generalised lipodystrophy.....CGL
Cyclic adenosine monophosphate ..... cAMP
Cytomegalovirus .....CMV
Deoxyribonucleic acid ..... DNA
Dilated cardiomyopathy.....DCM
Dimethylsulfoxide ..... DMSO
Dublecco's modified eagle medium ..... DMEM
Dunnigan-type familial partial lipodystrophy..... FPLD2
Empty vector.....EV
Ethylenediaminetetraacetic acid..... EDTA
Extracellular matrix..... ECM
Farnesyltransferase..... FTase
Fatty acid binding protein 2 .....aP2
Fetal Bovine serum .....FBS
Forkhead box O1 ..... FOXO1
Fragile X-related protein 1 .....FXR1P
Glucose transporter 4 .....Glut4
Glycerol kinase..... GyK
Glycogen synthase kinase 3 β GSK-3β

Low density lipoprotein receptor-related protein 5/6 ..... LRP5/6
Human adipocyte stem cell ..... hASC
Ribonucleic acid ..... RNA
Untranslated region ..... UTR
Complementary DNA ..... cDNA
Short hairpin RNA ..... shRNA
Protein tyrosine kinase ..... PTK
Protein tyrosine phosphatase ..... PTP
Autosomal recessive non-syndromic hearing impairment ..... arNSHI
Transmembrane domain ..... TM
Juxtamembrane ..... JM
Phosphatidylinositol phosphatase ..... PIP
Phosphatase and tensin homologue ..... PTEN
Phosphoglycerate kinase ..... PGK
T-cell factor/lymphoid enhancer factor ..... TCF/LEF
Custom primers ..... CP
Postnatal fibroblasts ..... MAFs
Androgen receptor ..... AR
Androgen deprivation therapy ..... ADT
HAART-associated lipodystrophy syndrome ..... HALS
Herpes simplex virus – thymidine kinase ..... HSV-TK
High fat diet ..... HFD
Highly active antiretroviral therapy ..... HAART
Histone deacetylase-1 ..... HDAC1
Hutchinson-Gilford progeria syndrome ..... HGPS
Hydrochloric acid ..... HCL
Insulin growth factor binding protein IGFBP5
Insulin growth factor ..... IGF
Insulin receptor substrate ..... IRS
Integral membrane protein 2A ITM2A
Integrated DNA technologies ..... IDT
Internal ribosome entry site ..... IRES
Isoprenylcysteine carboxyl methyltransferase ..... ICMT
Knockdown ..... KD
Knockout ..... KO
Kobberling-type lipodystrophy FPLD1
Limb-girdle muscular dystrophy 1B LGMD1B
Lipoprotein-lipase ..... LPL
Lithium chloride LiCl
Liver X receptor ..... LXR
LMNA-related congenital muscular dystrophy ..... L-CMD
Luria-Bertani ..... LB
Mechanistic target of rapamycin complex 1 ..... mTORC1
Meningioma 1 ..... MN1

Mesenchymal stem cell ..... MSC
Mitogen-activated protein kinase ..... MAPK
Mitotic clonal expansion ..... MCE
Mouse embryonic fibroblasts ..... MEFs
Murine stem cell virus ..... MSCV
New England biolabs ..... NEB
Nuclear factor 1 ..... NF1
Parathyroid hormone ..... PTH
Passive lysis buffer ..... PLB
Peroxisome proliferator-activated receptor γ ..... PPARγ
Phosphate buffer saline ..... PBS
Phosphoenolpyruvate carboxykinase ..... PEPCK
Phosphoinositide 3 kinase PI3K
piggyBac ..... PB
Polymerase chain reaction ..... PCR
Protein Kinase B ..... AKT/PKB
Protein tyrosine phosphatase receptor type Q ..... PTPRQ
Quantitative real-time PCR ..... qPCR
RAR-related orphan receptor a ..... RORa
Restrictive dermopathy ..... RD
Retinoic acid ..... RA
Retinoic acid receptor ..... RAR
Retinoid X receptor ..... RXR
r-metHuLeptin-replacement therapy ..... metreleptin
Signal peptide peptidase-like 2 ..... SPPL2
Signal transducer and activator of transcription ..... STAT
Simian virus 40 ..... SV40
Sodium dodecyl sulphate ..... SDS
Sterol regulatory element ..... SRE
Sterol response element binding protein 1 ..... SREBP1
Stromal vascular cells ..... SVC
Terminal repeats ..... TR
Tetramethylethylenediamine ..... TEMED
Thiazolidinedione ..... TZD
Thyroid hormone receptor ..... TR
Transcriptional start site ..... TSS
Triacylglycerol ..... TAG
Trichloroacetic acid ..... TCA
Tris-acetate-EDTA ..... TAE
Tumor necrosis factor - α ..... TNFα
Type II diabetes mellitus T2DM
Vacuolar-type H^+ ATPase ..... v-ATPase
White adipose tissue ..... WAT
Wild type ..... WT

Wingless-type MMTV integration site .....WNT
B-Nicotinamide adenine dinucleotide.....NAD^+

LIST OF FIGURES

LIST OF TABLES

CHAPTER 1: INTRODUCTION

Nuclear Lamins

Nuclear lamins are type V intermediate filament proteins that polymerise to form components of the nuclear lamina; a fibrous meshwork associated with the inner nuclear membrane [1].The localisation of lamin filaments within the nuclear lamina in relation to the nuclear envelope is illustrated in figure 1.1 along with the main components of the nuclear envelope environment. The inner and outer nuclear membranes depicted below contain nuclear pore complexes, which function to regulate active transport of molecules between the nuclear and cytoplasmic compartments [2]. Several of the many known integral inner membrane proteins, such as emerin and lamin-associated polypeptide 1/2β, are shown to interact with lamins and mediate the tight association between the nuclear lamina and inner membrane of the nuclear envelope [3,4].

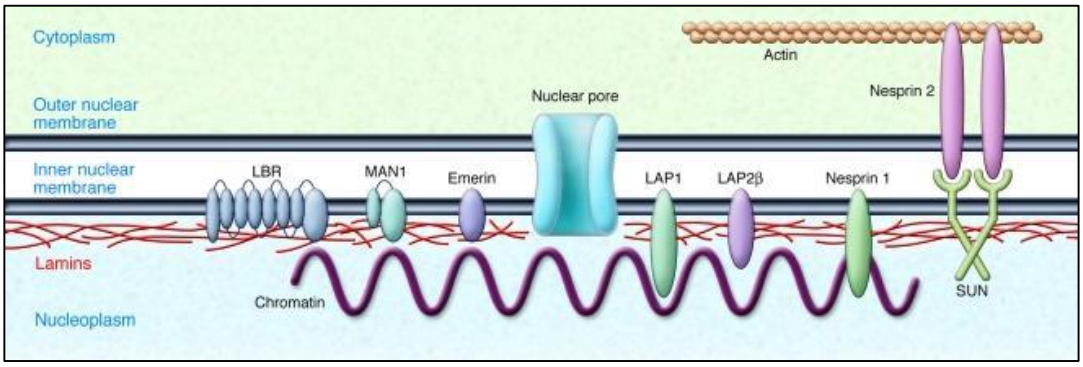

Figure 1.1: The nuclear lamina is shown in red at the nucleoplasmic side of the inner nuclear membrane. Taken from Worman et al., (2009) (4).

The mammalian genome contains three lamin genes; LMNA, LMNB1 and LMNB2 that encode lamin A/C, lamin B1 and lamin B2 respectively. The LMNA gene is alternatively spliced to produce two main isoforms, lamin A and lamin C, the expression of which is developmentally regulated [6]. Unlike B type lamins, which are ubiquitously expressed during development, A type lamins are not detected in undifferentiated cells but are expressed in most differentiated somatic cells [7]. A type lamins are found both at the nuclear periphery and within the nucleoplasm [8].

Lamins have a tripartite structure, characteristic of intermediate filament proteins, consisting of a conserved central α-helical coiled-coil rod domain flanked by variable tail and head domains [4,9]. The carboxy (C)-terminal tail domain of Lamin A is globular in nature, it contains a conserved immunoglobulin-like fold, a nuclear localization signal and a C-terminal CaaX (cysteine - aliphatic amino acid - aliphatic amino acid - any amino acid) motif [3,9]. The CaaX motif directs a series of sequential enzymatic reactions, which function to process the lamin A precursor (prelamin A) into mature Lamin A. This post-translational modification involves the farnesylation of the CaaX motif, followed by C terminal cleavage by the protease ZMPSTE24. This in turn is followed by the methylation of the now exposed farnesylcysteine. Finally, Prelamin A is cleaved again by ZMPSTE24, and the removal of the terminal 15 amino acids results in the generation of mature lamin A [4]. This process is thought to be essential for the future assembly and integration of lamin A filaments into the nuclear lamina and is illustrated in figure 1.2 [10].

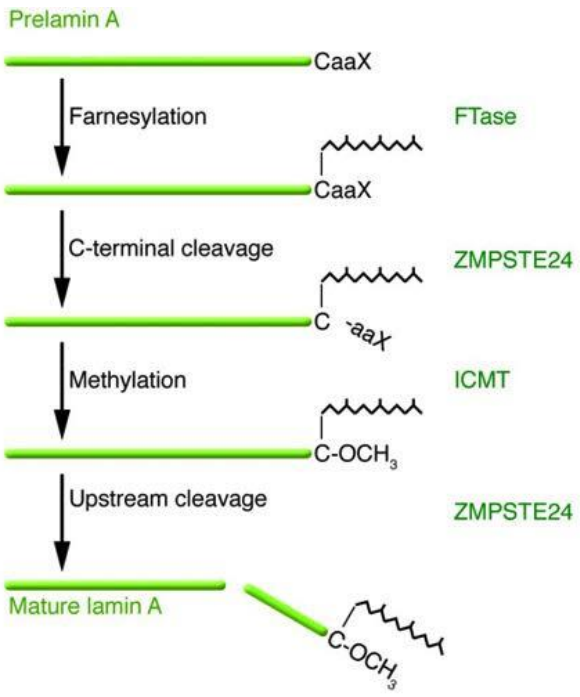

Figure 1.2: Post-translational processing of prelamin A. Enzymes responsible for farnesylation (FTase), C-terminal cleavage (ZMPSTE24), methylation (ICMT) and upstream cleavage (ZMPSTE24) are shown on the right of the schematic in green. Adapted from Worman et al., 2009 [5]. Abbreviation; FTase – farnesyltransferase, ICMT – isoprenylcysteine carboxyl methyltransferase.

Lamins are important structural components of the nucleus and are essential for nuclear integrity (1). The lamina contributes to the mechanical stability of the nucleus and plays a role in complex interactions between the nuclear envelope and various cytoskeletal components [4,12]. In addition to providing structural support lamins play a role in regulating many nuclear processes. These include DNA replication and repair where alterations in lamin organization can block DNA repair and generate genomic instability [13,14]. Disruption of nuclear lamins can influence gene transcription by inhibition RNA-Polymerase II activity [15] and modulate cell proliferation by regulating retinoblastoma protein function [16,17]. In addition, lamins have been shown to play a role in the differentiation of various tissue types, through their ability to cause diverse disease phenotypes such as Emery-Dreifuss muscular dystrophy [18], Hutchinson-Gilford progeria syndrome [19] and Familial Partial Lipodystrophy [20].Lamins interact directly with chromatin as well as indirectly, through lamin binding proteins [21–25]. They have been shown to modulate chromatin organization in a number of different contexts and determine chromosome positioning within the nucleus in conjunction with their associated internal membrane proteins [8,26]. Transcriptionally silent heterochromatin is 'anchored' at the nuclear periphery through interactions with the lamina although lamin-chromatin interactions are not exclusively associated with a transcriptionally repressive state [8,27,28]. The diverse nature of lamin A function is evident upon examination of the LMNA null mouse phenotype. Distinct changes appear in nuclear morphology where LMNA deficient cells display irregular and elongated nuclei, loss of heterochromatin association at the nuclear periphery and dramatic alterations in emerin localization in a tissue specific manner [29,30]. Homozygous LMNA null mice display severe skeletal and cardiac muscular dystrophy along with complete loss of white adipose tissue [29,30].

Laminopathies

Mutations in the LMNA gene are responsible for a wide spectrum of inherited disorders. Collectively known as primary 'laminopathies', these disorders can affect various tissues in either a systemic or specific manner [31]. Affected tissues include striated muscle (Emery-Dreifuss muscular dystrophy, dilated cardiomyopathy and limb-girdle muscular dystrophy 1B), adipose tissue (Dunnigan-type familial partial lipodystrophy), skeletal tissue (mandibular dysplasia) and peripheral nerve tissues (Charcot-Marie-Tooth disorder type 2B), while premature ageing syndromes (Hutchinson-Gilford progeria syndrome and atypical Werner's syndrome) are multi-systemic [31,32]. Secondary laminopathies derive from mutations in the ZMPSTE24 gene that encodes the enzyme responsible for post-translational processing of prelamin A [33], and have been reported to affect skeletal, muscle and adipose tissues [34–36], and cause restrictive dermopathy (RD) [37,38].

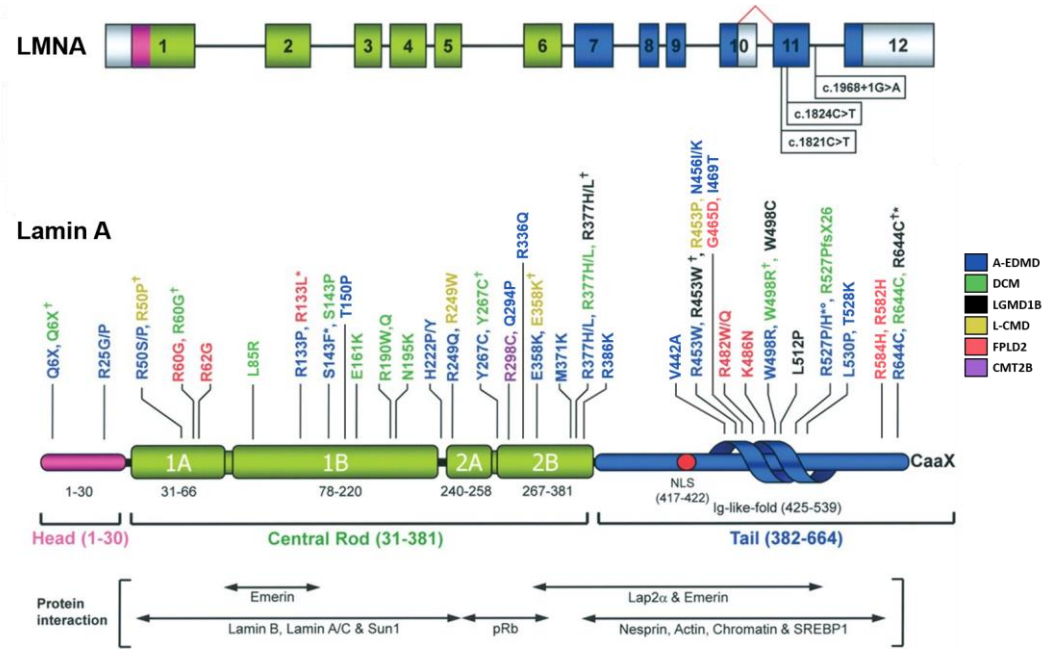

Figure 1.3: LMNA mutations and associated laminopathies. LMNA gene exons and their corresponding lamin A protein domains are shown in the same colour. The LMNA splice site is shown in red on the LMNA gene schematic and HGPS mutations that lead to the generation of alternative splice sites are shown in black (c.1824C>T, c.1968+1G>A and c.1821G>A). Mutations causing various laminopathies and their locations are shown along the lamin A protein. The colour legend on the right indicates which mutations lead to which diseases. Lamin A protein regions and their associated

interacting proteins are shown in black. Abbreviations; A-EDMD – Autosomal Emery-Dreifuss muscular dystrophy, DCM - dilated cardiomyopathy, LGMD1B - limb-girdle muscular dystrophy 1B, L-CMD - *LMNA*-related congenital muscular dystrophy, FPLD2 – Dunnigan-type familial partial lipodystrophy 2, CMT2B - Charcot-Marie-Tooth disorder type 2B. †; same amino acid substitution generates different laminopathies. Adapted from Scharner et al., 2010 and Burk and Stewart 2002 [33,39].

Figure 1.3 illustrates a subset (<20%) of the many mutations that lead to the development of various laminopathies. The locations of these mutations within the different lamin A protein domains are shown, along with the known lamin A interacting proteins [40]. Laminopathies are most commonly produced by missense or frame shift mutations in the LMNA gene [39]. One of the better-studied laminopathies, HGPS, is caused by mutations in exon 11 that generate alternative splice sites resulting in a truncated lamin A protein. This protein product is known as 'progerin' and bears a 50 amino acids internal deletion within the carboxy (C)-terminal tail domain [9,37,41]. In addition, the most common HGPS mutation (G608G) leads to loss of the second ZMPSTE24 cleavage site resulting in a permanently farnesylated form of the progerin protein [42]. Accumulation of progerin in the cell is thought to drive the HGPS multi-systemic premature ageing phenotype through distortion of normal nuclear morphology and function [43].

Dunnigan-type familial partial lipodystrophy

Dunnigan-type familial partial lipodystrophy (FPLD2) is caused almost exclusively by heterozygous missense mutations in the 8th and 11th exons of the LMNA gene [4]. Mutations that result in lipodystrophies are mainly found in the immunoglobulin-like fold of the lamin A protein. They do not alter the three-dimensional structure of the protein, however the majority of these mutations generate amino acid substitutions that lead to a decrease in the surface positive charge of the immunoglobulin-like domain, which may affect protein-protein interactions [9,31]. Common mutations leading to FPLD2 occur at amino acid 482, in which the positively charged arginine if often substituted with a neutral amino acid such as tryptophan (R482W) or glutamine (R482Q) [44,45].

FPLD2 is an autosomal dominant laminopathy characterized by defective fat metabolism and storage [46]. Symptoms of this disorder manifest at puberty and include the loss of peripheral, subcutaneous adipose tissue from the extremities (limbs, truncal and gluteal regions) with a build-up of visceral and nuchal adipose tissue. This is accompanied by a myriad of metabolic symptoms such as hepatic steatosis, atherosclerosis and insulin resistance, which leads to type II diabetes mellitus [44]. Defective energy storage is thought to be the primary pathogenic factor in such lipodystrophies, leading to the development of the characteristic metabolic disease state [47]. The biochemical and clinical study of FPLD2 patients has identified a sex dependent aspect of the disease phenotype, where symptoms appear significantly more severe in female patients [48,49]. In addition, the first case of homozygous LMNA R482Q mutations has recently been reported, and these individuals appear to have a combination of EDMD and generalized lipodystrophy [49].

FPLD2 mouse models

A number of mouse knock-in models exist for different laminopathies, including AD-EDMD (L530P, H222P), DCM (N195K) and progeria (LMNA $^{HG/+}$, LMNA $^{HG/HG}$), however currently there is no data published on an FPLD2 mutation knock-in mouse model [50–54]. Interestingly a few of these laminopathy models do exhibit a complete or partial loss of adipose tissue (AD-EDMD L530P Knock-in, LMNA $^{HG/+}$, LMNA $^{HG/HG}$, Zmpste24$^{-/-}$), along with the distinct symptoms associated with each respective laminopathy mutation. A transgenic mouse model of FPLD2 has previously been generated where human LMNA R482Q mutant was expressed from the aP2 adipose tissue specific promoter [55]. These mice expressed endogenous levels of wild type LMNA as well as additional aP2 driven R482Q mutant LMNA in their adipose tissue, as transgene expression was not detected in most other tissues. FPLD2 transgenic mice accumulated significantly less white and brown adipose tissue than wild type littermates and acquired FPLD2 metabolic symptoms including decreased insulin sensitivity and hepatic steatosis. Wojtanik et al., (2009) determined that their FPLD2 transgenic mice exhibited reduced adipocyte differentiation by comparing the in vitro differentiation potential of epididymal fat-pad stromovascular fractions from FPLD2 versus wild-type mice. They propose that defective adipocyte differentiation rather than impaired lipid droplet accumulation or fat loss leads to the lipodystrophic phenotype in FPLD2.

Adipose tissue

Adipose tissue is a complex organ that plays an important role in the regulation of whole body metabolism. As well as providing energy storage, it functions to modulate energy homeostasis and has key endocrine/paracrine functions [56].

There are two types of adipose tissue in mammals, white adipose tissue (WAT) and brown adipose tissue (BAT), which differ in cell composition, morphology and function. White adipocytes contain a single large lipid droplet and relatively few small elongated mitochondrial around the periphery of the cell whereas brown adipocytes contain many smaller lipid droplets and are rich in large mitochondria The adipose organ comprises a number of distinct anatomical depots including WAT subcutaneous (femoral, truncal and gluteal) and intra-abdominal (visceral and omental) fat depots which differ in biological function as well associated disease risk [57,58]. These depots are composed of mature white adipocytes and stromal vascular cells (SVC) which include fibroblasts, adipocyte progenitors (ASC), preadipocytes, endothelial cells, pericytes and immune cells [57,59]. BAT depots are most commonly observed in new-borns and are found mainly around the neck and upper chest regions [58]. They are highly vascularized, containing brown adipocytes, adipocyte progenitors and a dense network of capillaries [60,61]. BAT functions primarily to generate heat in a process called non-shivering thermogenesis, and plays an important role in maintaining body temperatures in a cold environment [61]. Recently, numerous studies have reported BAT function in adults [62,63], and a role for BAT has been described in protection against obesity [58]. The microenvironment of fat depots is influenced by various factors including cellular composition, extracellular matrix (ECM) composition, metabolic characteristics and secretory products. These differences in microenvironment are responsible for the distinct endocrine and metabolic functions of the different adipose depots within the body [57]. The notion of adipose tissue functioning as a secretory endocrine organ was first suggested after the discovery of circulating factor leptin [64] and adipose tissue derived tumour necrosis factor- α (TNFα)[65]. Since then, numerous adipocyte derived secreted proteins or adipokines have been identified, such as resistin and adiponectin, establishing adipose tissue as a dynamic endocrine organ, that plays an integral role in the regulation of metabolism [66].

The differences in adipose tissue depot development and control are of interest as fat distribution plays an important role in metabolic disease pathogenesis, with the accumulation of fat in visceral or intra-abdominal depots being strongly associated with obesity related metabolic syndrome [67]. Numerous factors are known to affect adipose tissue distribution, including age, sex, energy balance, endocrine signalling and genetic factors [68]. Metabolic syndrome is characterised as group of related physiological and metabolic factors that lead to increased risk of type II diabetes mellitus (T2DM) and atherosclerotic cardiovascular disease (ACVD). These factors include hypertension, insulin resistance, glucose intolerance and dyslipidaemia, which are usually associated with an excess in body weight [69].

Lipodystrophies

Lipodystrophy refers to a disease state in which adipose tissue is deficient or defective. Impaired adipose tissue function leads to the development of metabolic syndrome symptoms, surprisingly similar to those observed in obesity [70]. These include insulin resistance, type 2 diabetes mellitus, hepatic steatosis and the ectopic accumulation of lipids in non-adipose tissues such as the liver and muscle [71]. Genetic lipodystrophies include familial partial lipodystrophy and congenital generalized lipodystrophy (CGL), the latter of which is caused by mutations in AGPAT2, BSC12 or CAV1 [71,72]. Acquired lipodystrophies are not associated with any genetic mutations but rather are thought to develop as a result of immune-mediated fat loss [71]. Currently the most common acquired form of the disease is HIV-associated lipodystrophy, driven by HIV treatment with highly active antiretroviral therapy (HAART). The mechanism by which fat redistribution occurs in these patients is currently unknown [73,74].

Partial lipodystrophies are more common than general lipodystrophies and exhibit a milder phenotype, characterised specifically by the re-distribution of adipose tissue as well as total fat loss. FPLD1, also known as Köbberling-type lipodystrophy, is considered to be familial although a specific genetic mutation has yet to be linked to this disease [75]. FPLD2 arises from mutations in the LMNA gene (as previously described) and FPLD3 is caused by loss-of-function mutations in peroxisome proliferator-activated receptor-γ (PPARγ), a key adipogenic factor, essential for the development of mature adipocytes [76]. Although FPLD2 and FPLD3 are genetically distinct they exhibit similar clinical features, most notably the specific pattern of fat loss from the gluteal and limb regions, insulin resistance, hepatic steatosis and type II

diabetes mellitus [77,78]. Considering these similarities, it could be suggested that FPLD2 LMNA mutations might lead to reduced or impaired PPARγ function during adipogenesis. Several additional genes have been implicated in the development of partial lipodystrophies. Mutations in ZMPSTE24, AKT2 and CIDEC have been reported to cause the lipodystrophic phenotype (34,36,80,81). ZMPSTE24 plays a key role in LMNA processing as previously described and its mutation most likely leads to a lipodystrophy through similar mechanisms as LMNA mutation [78]. AKT is involved in downstream insulin signalling and its mutation has been reported to result in the autosomal dominant inheritance of a lipodystrophic state with severe insulin resistance and type 2 diabetes [80]. Finally, mutation of the cell death-inducing Dffa-like effector C (CIDEC) gene that is involved in the formation of lipid droplets in adipose tissue, has recently been reported to produce a new subtype of familial partial lipodystrophy identified by the characteristic loss of subcutaneous fat from the limbs and insulin-resistance driven diabetes [81].

The mechanisms by which these distinct mutations lead to either partial or generalised lipodystrophy are not all clear, but can be divided into various functional categories. AGPAT2 and BSCL2 are involved in triacylglycerol (TAG) synthesis, CAV1 effects fatty acid uptake by adipocytes and CIDEC is involved in the process of lipid droplet formation. In contrast, LMNA, PPARG, ZMPSTE24 and AKT2 mutations are considered to drive the lipodystrophic phenotype by affecting the expression of genes involved in adipogenic differentiation [78].

Lipodystrophy mouse models

A number of knock-out mouse models have been produced in order to study adipose tissue development and related diseases. AGPAT2 and CAV1 null mice appear to mimic the CGL disease state in humans with varying degrees of metabolic syndrome [82,83] while PPARγ and CEBPα knockout (KO) mice fail to develop WAT [71,84,85]. An unexpected lipodystrophy mouse model was generated when over-expression of a dominant-positive form of sterol regulatory element-binding protein 1 (nSREBP1c) was directed from the adipose specific aP2 promoter in transgenic mice. SREBP1 is a key transcription factor in the regulation of lipogenesis and nSREBP1c is the active form of this transcription factor [86]. Shimomura et al., (1998) reported reduced and

defective WAT development with the expansion of a large intrascapular fat pad consisting of pale adipose tissue where BAT is normally found. These mice exhibited severe hepatic steatosis, insulin resistance and diabetes mellitus [87]. The over-expression of nSREBP1c in these mice was seen to perturb development of both white and brown adipose tissue. An incomplete block in WAT differentiation was observed as transgenic mouse fat pads contained immature white adipocytes with interspersed islands of normal mature adipocytes. Brown adipocyte depots were dramatically enlarged and cells within these depots contained more fat in comparison to those of wild type littermates [87]. SREBP1 regulates many lipogenic genes and is up-regulated during the early stages of adipogenic differentiation [88]. It has been shown to promote adipogenesis in an in vitro differentiation context [89]. It is therefore surprising that increased SREBP1c in mouse adipose tissue leads to lipodystrophy. Interestingly, transgenic mice overexpressing nSREBP1a (a more potent transcriptional activator isoform of SREBP1c) in their adipose tissue exhibit a completely different phenotype, exhibiting normal plasma insulin and glucose levels, white and brown adipocyte hypertrophy and hepatic steatosis [90]. These contrasting phenotypes suggest distinct roles for SREBP1a and SREBP1c in mouse adipocyte metabolism.

Adipogenesis

The development of adipose tissue and the regulation of fat metabolism are not fully understood. Mesenchymal stem cells (MCS) have the potential to differentiate into numerous cell types including chondrocytes, osteocytes, myocytes and adipocytes. In an in-vivo setting these cells respond to various signals to undergo determination towards one of the above cell lineages [91]. The process of adipogenesis involves commitment of pluripotent MSC to the adipocyte lineage, followed by terminal differentiation of pre-adipocytes into mature adipocytes [88]. In an undifferentiated state, MSCs express low levels of respective lineage specific factors which repress each other and function to maintain the pluripotent state [92]. Although the exact mechanism of adipogenic commitment is unclear, various factors are known to be involved. In vivo, prolonged excessive intake of energy leads to a metabolic state that produces various signals that stimulate MSC commitment to the adipogenic cell lineage [88]. In vitro studies have identified bone morphogenetic protein (BMP) 4 [93], BMP2 [94] and Wnt [95,96] as activators of adipogenic commitment while Hedgehog is reported to inhibit this process [97]. Finally, mechanical cues have been shown to affect MSC

lineage commitment, where cell shape, density and cytoskeleton tension influence cell fate [98].

Primary pre-adipocytes, harvested from the vascular stroma of in-vivo adipose tissue, have a limited capacity to proliferate and a finite potential to differentiate in vitro [99]. As a result, the signalling transduction pathways and molecular mechanisms that regulate adipogenesis have largely been studied in pluripotent (C3H10T1/2) or preadipocyte cell lines (3T3-L1).

Terminal Differentiation

Adipocyte terminal differentiation involves a transcriptional cascade in which the expression of pro-adipogenic factors is temporally induced alongside the down-regulation of various anti-adipogenic factors [92].Preadipocyte cell lines have been used to characterise key events of the adipogenic differentiation programme, and terminal differentiation of mouse pre-adipocytes has been studied extensively using the 3T3-L1 cell model. In this well-established system, the pre-adipocytes are grown to confluency and undergo growth arrest, after which point an adipogenic cocktail is applied to activate insulin growth factor (Insulin/IGF-1), cAMP (IBMX/Forskolin) and glucocorticoid (dexamethasone) signalling pathways. Figure 1.4 illustrates the temporal cascade of differentiation events that occur post-induction.

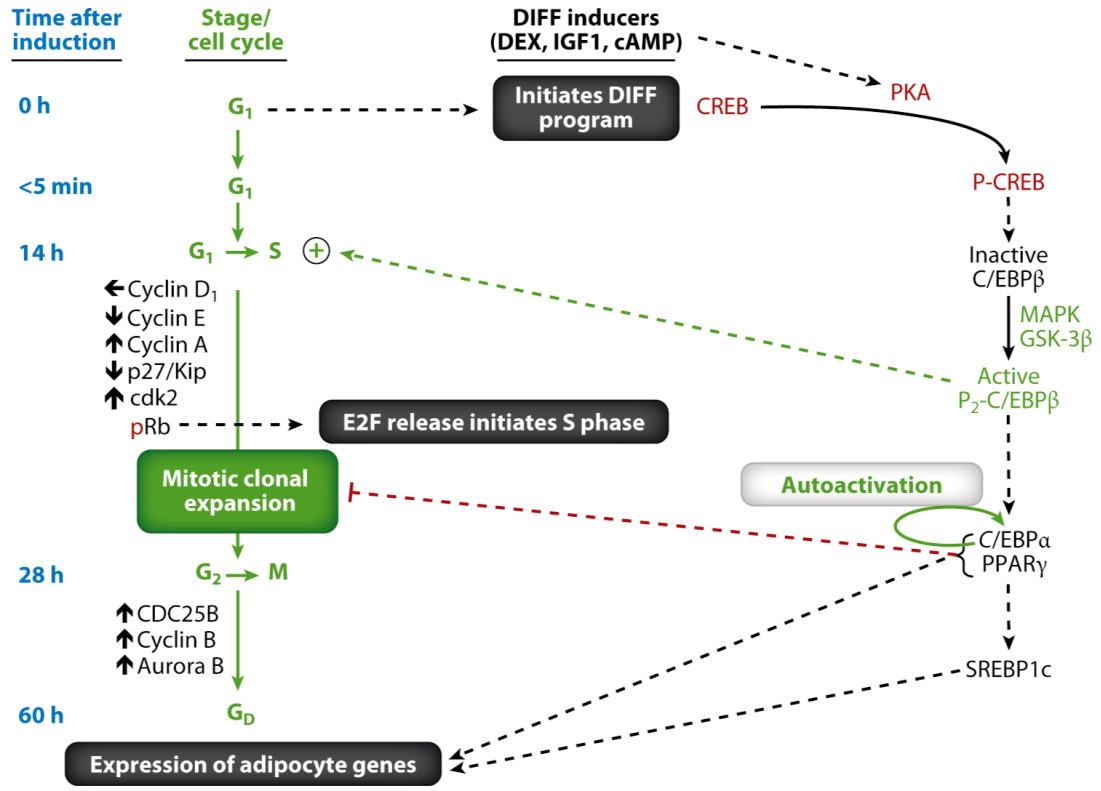

Figure 1.4 : The in-vitro adipogenic differentiation programme, taken from Tang and Lane (2012) [88].

Directly after addition of the induction cocktail, cyclic AMP response element-binding protein (CREB) phosphorylation induced expression of the CCAAT- enhancer-binding protein β (C/EBPβ) transcription factor [100]. However, at this stage C/EBPβ is unable to bind DNA [101]. At approximately 16 to 20 h post induction, 3T3-L1 cells re-enter the cell cycle to undergo a few rounds of mitotic clonal expansion (MCE), at which point C/EBPβ acquires the ability to bind DNA, and initiates the adipogenic transcriptional cascade [102]. Sequential phosphorylation of C/EBPβ by MAP kinase and GSK-3β are important post-translation modifications that confer DNA-binding activity [103]. Once able to bind DNA, C/EBPβ activates C/EBPα and PPARγ expression through C/EBP elements in their respective promoters [103].Subsequently, C/EBPα and PPARγ cross-regulate each other, in a positive-feedback loop that plays an important role in maintaining the differentiated state [104,105]. C/EBPα stimulates both PPARγ expression [103,106] and its own expression through auto-regulation [107]. PPARγ and C/EBPα are considered the master regulators of adipogenesis and are transcriptionally activated approximately 18-24hrs post induction [88]. These transcription factors then

function to activate the expression of various adipogenic genes through regulatory elements in their promoters [108,109].

CCAAT- enhancer-binding proteins

The importance of these factors in adipogenesis has been highlighted in various in-vitro and in-vivo studies. Constitutively active CREB has been shown to promote 3T3-L1 differentiation through C/EBPβ activation (100). Both C/EBPβ KO MEFs and 3T3-L1 cells over-expressing a dominant negative C/EBPβ with no DNA-binding capacity, are unable to undergo MCE, which is essential for MEF and 3T3-L1 adipogenic differentiation (102,103,100). A certain amount of redundancy has been demonstrated between the CCAAT- enhancer-binding proteins in adipogenesis. C/EBPβ KO and C/EBPδ KO mice show relatively normal WAT accumulation while C/EBPβ and C/EBPδ double KO mice show significantly reduced WAT volume, due to a reduced number of adipocytes [111]. C/EBPα over-expression is sufficient to stimulate 3T3-L1 differentiation [112], while C/EBPα silencing has been shown to suppress adipogenesis in these cells [113]. C/EBPα KO mice die shortly after birth due to hypoglycaemia and their adipocytes are unable to accumulate lipid droplets [114]. Although clearly important in the process of adipogenesis, ectopic expression of C/EBPα is unable to rescue adipogenesis in PPARγ KO fibroblasts (105). In addition, Zuo et al., (2006) demonstrated that C/EBPβ is unable to induce C/EBPα in the absence of PPARγ during 3T3-L1 cell differentiation. In this context PPARγ is required to dislodge the repressive histone deacetylase-1 (HDAC1) from the C/EBPα proximal promoter [116]. C/EBPα is however essential for efficient insulin-sensitive glucose transport, as demonstrated by PPARγ over-expression in C/EBPα KO fibroblasts that are able to differentiate but lack insulin-sensitivity [117].

Peroxisome proliferator-activated receptor γ (PPARγ)

PPARγ is a member of the nuclear hormone receptor superfamily that controls the expression of adipogenic and lipogenic genes through binding to PPAR-response regulatory elements as heterodimers with the retinoid X receptor (RXR) [118–120]. PPARγ action is essential in adipogenesis as the numerous signalling pathways and pro/anti-adipogenic factors that influence this process converge on the regulation of

PPARγ activity and expression [92]. Figure 1.5 illustrates the transcriptional regulation of adipocyte differentiation and depicts the role of pro- and anti- adipogenic factors in modulating PPARγ expression and activity during this process [121].

Through the use of distinct promoters and alternative splicing, the PPARγ gene encodes a number of splice variants and two principle protein isoforms, PPARγ2 and PPARγ1 [122]. These proteins have differential abilities to promote adipogenesis. PPARγ2 has an additional 28 N terminal amino acids and is exclusively expressed in adipose tissue, where it functions as a master regulator of adipogenesis (118,124,125). PPARγ1 is expressed in various tissues and cell types, including fat, liver, muscle and macrophages [126–128].

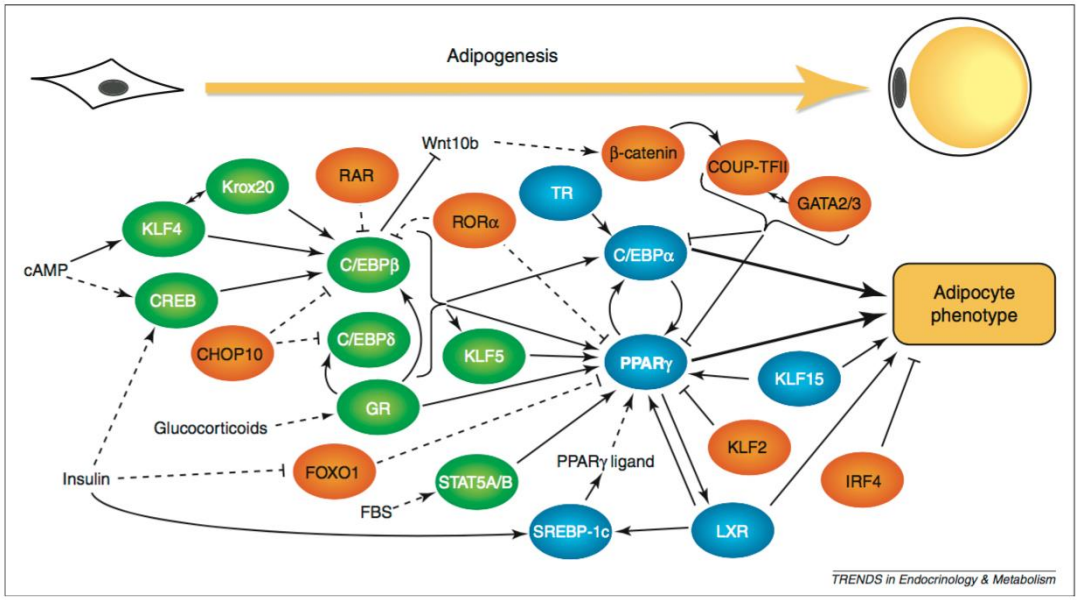

Figure 1.5: Transcriptional regulation of adipogenesis. Early (green), late (blue) and anti- (orange) adipogenic factors are shown. Solid lines represent modulation of gene expression and dashed lines represent modulation of activity. Abbreviations: COUP-TFII - chicken ovalbumin upstream promoter transcription factor II, FOXO1- forkhead box O1, LXR- liver X receptor, TR- thyroid hormone receptor, CHOP10- C/EBP homologous protein, RAR - retinoic acid receptor, RORa - RAR-related orphan receptor a. Taken from Siersback et al., (2011) (121).

PPARγ is a ligand-inducible transcription factor, where ligand binding results in a conformational change that leads to interactions with various co-activating proteins to

modify PPARγ activity [130]. To date, no endogenous high-affinity PPARγ ligands have been identified, however potent synthetic PPARγ agonists known as Thiazolidinediones (TZDs) have been used as insulin-sensitizers in the treatment of type II diabetes for some time [131].

Various studies have shown that PPARγ2 is both necessary and sufficient to induce adipogenesis, and is also required for the maintenance of a differentiated adipogenic state [92]. Ectopic expression of PPARγ2 in non-adipogenic fibroblasts was shown to stimulate the adipogenic differentiation of these cells [132], and since then numerous in-vitro and in-vivo studies have characterised the role of PPARγ2 in adipogenesis and lipid metabolism. PPARγ KO in mice leads to embryonic lethality due to impaired placental development, however a chimeric WT/KO model produced a lipodystrophic phenotype in which any adipose tissue present was derived from PPARγ WT cells (117). Several PPARγ mouse models have been generated in which adipocyte specific PPARγ KO or PPARγ2 isoform specific KO in adipose tissue lead to insulin resistance and varying degrees of lipodystrophy (127,135–137). Dominant negative PPARγ knock-in models exhibit abnormal fat distribution [138] and features of metabolic syndrome [139]. These models have played an important part in dissecting the complex physiological functions of PPARγ in vivo, and highlight its role in regulation of energy metabolism and metabolic disease development [130,140]. Figure 1.6 summarises PPARγ regulation of adipogenic and lipogenic pathways, as well as its modulation of glucose homeostasis and adipose secreted factors, all of which combine to influence insulin sensitivity [118].

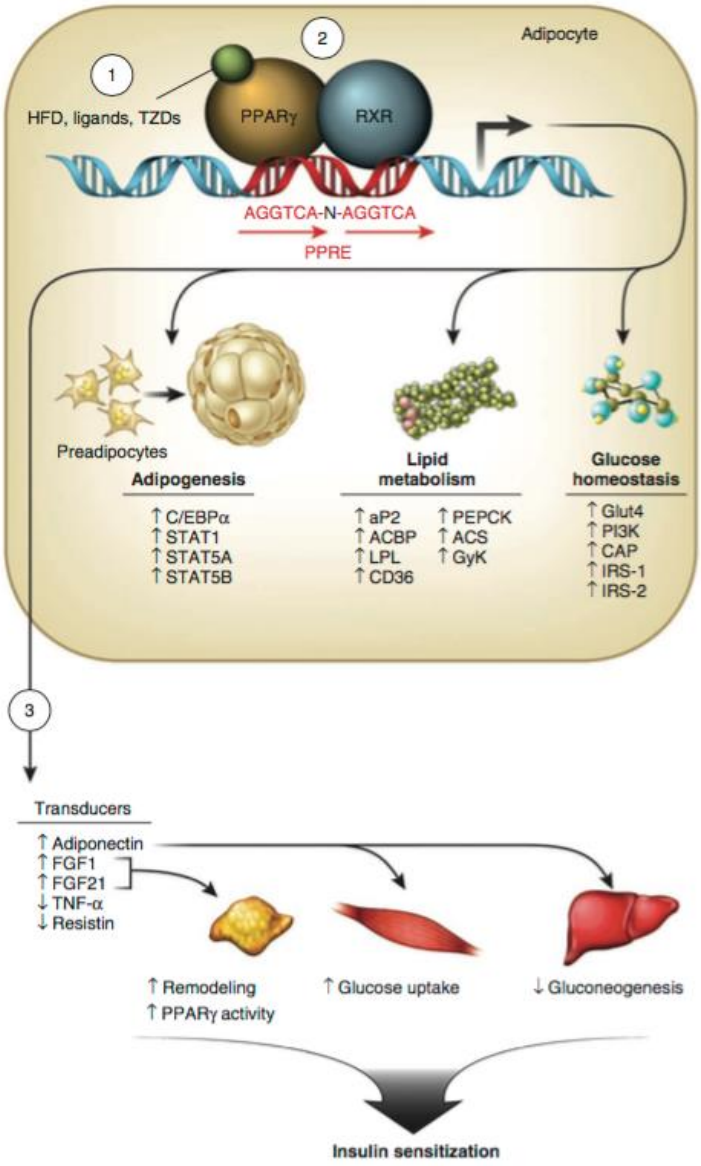

Figure 1.6: PPARγ mediated control of adipose tissue development and metabolism. (1) High fat diet (HFD), ligand and TZD activation of PPARγ-RXR heterodimerization and (2) binding to PPAR-response regulatory elements of genes involved in adipocyte differentiation and maintenance of metabolic homeostasis, (3) as well as genes responsible for adipose secreted proteins. Abbreviations: STAT1/STAT5A/STAT5B - signal transducer and activator of transcription 1, 5A and 5B, ACBP - acyl-CoA–binding protein, LPL- lipoprotein lipase, aP2 - fatty acid binding protein 2, CD36 - cluster of differentiation 36, ACS - acyl-CoA synthetase, PEPCK - phosphoenolpyruvate carboxykinase, PI3K - phosphoinositide 3 kinase, IRS-1/IRS-2 - insulin receptor substrate 1 and 2, GyK- glycerol kinase and Glut4 - glucose transporter 4. Taken from Ahmadian et al., (2013).

FPLD2 biology

The physiological characteristics of FPLD2 support the hypothesis that LMNA mutation leads to altered or impaired lamin A function, which in turn influences the dynamic process of adipogenesis. Although the exact molecular mechanisms leading to the disease phenotype remain unclear, a number of factors have been implicated.

Nuclear organization and transcription

Recently the relationship between A type lamins and chromatin state has been described in human adipocyte stem cells (ASC) both pre, and post terminal differentiation. In this context A type lamins are reported to interact with thousands of promoters within the genome, and to modulate chromatin modifications at these sites. In addition, lamin A-promoter interactions are shown to be remodelled during the adipogenic programme, with variable impact on the transcriptional outcome of the genes involved (28). Characterisation of the immunoglobulin like fold in the lamin A carboxyl-terminal tail has identified reduced DNA binding affinity of this peptide in response to FPLD2 R482W and R482Q mutation [142]. It is therefore possible that reduced or altered lamin-DNA interaction influences the remodelling of lamin A-promoter interactions during adipogenesis, and play a role in FPLD2 disease pathophysiology.

Prelamin A

Abnormal accumulation of progerin or farnesylated prelamin A is reported to contribute to nuclear distortion in HGPS [43,143]. Previously, a number of studies have described mutant prelamin A accumulation in FPLD2 patient fibroblasts [144,145]. The accumulation of this unprocessed form of the lamin A protein was suggested to generate the lipodystrophic disease phenotype by sequestering the SREBP1 transcription factor at the nuclear membrane and preventing its action in adipocyte differentiation [145]. In contrast, a recent study has reported no prelamin A accumulation in fibroblasts carrying a number of FPLD2 LMNA mutations [146]. As the mutations that cause FPLD2 are distant from the sequences required for LMNA farnesylation and cleavage, it is unlikely that prelamin A processing plays a role in the mechanism of FPLD2 pathophysiology.

Altered SREBP1 activity

The SREBP transcription factors play important roles in lipid metabolism, and SREBP1 is known to promote adipocyte differentiation through activation of PPARγ [89,147]. The SREBP1 gene produces SREBP1a and SREBP1c through the use of distinct promoters and alternative splicing [148,149]. SREBP1 is a basic-helix-loop-helix-leucine zipper (bHLH-LZ) transcription factor, and is synthesized as an endoplasmic reticulum membrane bound precursor protein that undergoes a two-step proteolytic cleavage to release an active nuclear SREBP1. Once translocated into the nucleus SREBP1 binds to sterol regulatory elements (SRE) and activates the transcription of target genes involved in lipid biosynthesis [150].

Numerous studies have suggested FPLD2 mutant mediated dysregulation of SREBP1 transcription factors as the primary mechanism driving the lipodystrophic phenotype. Lloyd et al (2002) first identified SREBP1 and 2 as binding partners of lamin A, and reported that FPLD2 mutation (R482W) resulted in reduced lamin A binding to SREBP1 [151]. They proposed that lamin A might play a role in the import of the SREBP transcription factors into the nucleus and that lamin A mutations could lead to lipodystrophy through the dysregulation of the SREBP activity. Since then several studies have reported lamin A-SREBP interactions [144,152,153], the most recent of which reported that the LMNA Ig fold is important in LMNA-SREBP interactions and that LMNA R482W mutation reduced LMNA-SREBP interaction leading to the up-regulation of SREBP1 target genes in FPLD2 patient fibroblasts [154].

Finally, a recent publication reported reduced binding of FPLD2 mutant LMNA to the fragile X-related protein 1 (FXR1P), leading to elevated FXR1P expression in FPLD2 patient fibroblasts. Ectopic expression of FXR1P was shown to stimulate a myogenic differentiation programme in human adipocyte progenitors and a model was proposed in which FPLD2 LMNA mutation leads to a remodelling of the adipogenic programme towards a myogenic lineage, through FXR1P up-regulation [155].

Treatment

Currently, limited therapy options are available to FPLD2 patients. Lipodystrophy treatments vary depending on the type of lipodystrophy and the severity of symptoms observed in individual patients. Current treatments include lifestyle modifications (Nutrition and exercise) as well as a number of therapeutic drugs or hormones such as TZDs, lipid-lowering drugs, metformin and metreleptin or insulin administration [156,157]. Numerous reports have described improvements in glucose metabolism, reduced serum triglyceride concentrations and improvements in insulin sensitivity through treatment with the PPARγ agonist rosiglitazone (TZD) [158–160]. TZD treatment leads to increased body fat which is credited with the improved metabolic control, however there are adverse side effects associated with this therapy, including a risk of hepatoxicity [161]. In addition TZD treatment is seen to produce inconsistent results across different studies and patients [156]. In recent years, the development of recombinant methionyl human leptin replacement therapy (r-metHuLeptin-replacement therapy / metreleptin), has led to trials in patients with varying lipodystrophic syndromes. Severe lipodystrophy in characterised by a complete loss of adipose tissue. It follows that individuals suffering from severe forms of lipodystrophic syndrome would be deficient in adipose secreted compounds [162]. However only moderate effects have been observed with this treatment in FPLD2 [163]. In recent years, there has been increased interest in the development of partial lipodystrophy therapies as numerous patients with HIV/AIDS that are receiving highly active antiretroviral therapy (HAART) develop HAART-associated lipodystrophy syndrome (HALS). HALS is associated with a redistribution of adipose tissue similar to that observed in FPLD2, as well as numerous metabolic symptoms, and while the antiretroviral treatment is implicated in the pathophysiology of the disease, the mechanisms involved are not understood [156].

THESIS AIMS

The aim of this research is to investigate the effects of LMNA overexpression on the transcriptional profile of 3T3-L1 cell differentiation. The terminal differentiation of mouse preadipocytes has been studied extensively using the 3T3-L1 cell model, and the over-expression of both wild-type and R482W mutant LMNA are reported to have a similar inhibitory effects on 3T3-L1 differentiation. During the adipogenic programme, PPARγ expression is up-regulated approximately 24 to 48hrs post induction [88]. Boguslavsky et al., (2006) [20] observed a decrease in PPARγ expression and a significant reduction in lipid droplet accumulation in LMNA transfected cells when compared to an empty vector control. In addition, numerous PPARγ loss of function mutations are seen to generate a disease phenotype similar to that of FPLD2, referred to as FPLD3 (78,77) . Due to these similarities observed in FPLD phenotype and the previously described LMNA effect on PPARγ expression [20], it follows that FPLD2 LMNA mutations may lead to reduced or impaired PPARγ function during adipogenesis. Previously in the McCarthy lab, RNA-Seq analysis was performed at 36hrs post induction of 3T3-L1 pre-adipocytes in order to investigate the effects of wild-type and R482W mutant LMNA on gene expression profiles at this initial phase of terminal differentiation, around the time of PPARγ induction. 3T3-L1 preadipocytes were stably transfected with human LMNA overexpression constructs (pCDNA3-LMNA-WT and pCDNA3-LMNA-R482W) or empty vector control (pCDNA3) and induced to differentiate. Total RNA was isolated 36 h post application of the induction cocktail and RNA-Seq analysis was performed.

Significant changes in the expression of 212 and 232 transcripts were identified when comparing the empty vector control transfected cells to cells over-expressing LMNA WT and LMNA R482W, respectively. Analysis of these data sets identified 76 common transcripts, affected by both LMNA WT and R482W mutant in comparison to the control. Table 1 and 2 list the transcripts up-regulated and down-regulated by LMNA overexpression.

The ultimate aim of this research is to identify novel therapeutic approaches for reversal of the FPLD2 phenotype through exploring genes altered by LMNA overexpression in adipogenesis. Based on the literature and transcripts identified in

the previously described RNA-Seq analysis, a number of genes were investigated in this context. Genes highlighted in red in tables 1 and 2 are considered in this thesis.

Table 1.1: Transcripts up-regulated in response to LMNA WT and R482W mutant overexpression. Fold down-regulation in comparison to empty vector control.

	Fold Increase	
Gene ID	LMNA WT	LMNA R482W
Alcam	1.53	1.34
Apod	3.92	2.52
Atp6v0c-ps2	2.98	3.56
Cacna1c	1.38	1.46
Ces2g	3.14	2.40
Cpm	2.02	2.55
Fgf10	1.37	1.46
Gas2l3	1.31	1.43
Gm14440	19.30	7.89
Gm5886	2.38	2.13
H2-M1	2.89	3.15
Heph	1.67	1.81
Hr	1.81	1.73
Igfbp3	1.53	2.21
Il1rn	6.23	2.24
Itga11	2.43	2.13
Itm2a	16.27	8.28
Kcnj15	1.61	1.72
Kif21a	1.23	1.24
Lgals3	1.26	1.29
Lmo7	1.47	1.49
Malat1	1.72	1.66
Nfat5	1.26	1.27
Nptxr	7.92	4.37
Nqo1	1.42	1.44
Nrp2	1.15	2.77
Pcdh19	1.25	1.26
Pi15	2.60	1.48
Ptprq	4.15	10.65
Rap1gap2	1.64	1.53
Rassf5	1.61	1.57
S100a8	2.08	2.37
Saa3	1.79	1.84
Sertad4	1.45	1.38
Slc29a1	1.31	1.24
Slc38a1	1.89	1.47
Srgap3	1.36	1.47
Syne1	1.63	2.27
Sytl2	1.42	1.42
Tgfbi	1.36	1.38
Timeless	1.27	1.27
Wnt6	5.98	7.49

Table 1.2: Transcripts down-regulated in response to LMNA WT and R482W mutant overexpression. Fold down-regulation in comparison to empty vector control.

	Fold Decrease	
Gene ID	**LMNA WT**	**LMNA R482W**
Adamts15	4.57	3.61
Angptl7	5.28	5.04
Cacna2d1	1.19	1.19
Cd36	1.95	2.06
Clec14a	1.36	2.59
Col23a1	2.77	5.63
Ddx51	1.48	1.45
Dkk3	1.90	1.67
Dlk1	1.14	1.25
Dpt	1.87	2.70
Elfn1	1.78	1.83
Epha4	1.62	1.86
Hs6st2	1.25	1.33
Igfbp5	50.15	5.21
Il1r2	2.59	3.80
Il1rl1	1.57	1.59
Lars2	3.34	3.62
Ndrg1	1.94	1.56
Nlrp4e	3.36	5.05
Nod1	1.27	1.36
Pcdh17	2.49	0.40
Pvrl2	1.30	1.47
Retnla	3.86	4.07
Rmrp	3.16	42.58
Sema3a	1.30	1.62
Stc1	1.43	1.66
3110007F17Rik	1.57	1.96
5730469M10Rik	1.56	1.75
9630013A20Rik	2.60	3.13

CHAPTER 2: MATERIALS AND METHODS

MATERIALS

Cell Lines

3T3-L1 cell lines were purchased from ZenBio (SP-L1-F), 3T3-L1 cells originally from ATCC (ATCC CL-173) were a kind gift from Professor Rosemary O'Connor (UCC, Cork, Ireland), and a third 3T3-L1 cell line indicated as 3T3-L1 M.S. was a kind gift from Professor Michael Schupp (Charite, CCR, Berlin, Germany). 3T3-NIH cells were a kind gift from Professor Tom Moore (UCC, Cork, Ireland). LMNA WT and KO MEF cells were kindly provided by Professor Colin Stewart (Institute of Medical Biology, Singapore).

Bacterial strains

The E. coli DH5α strain from McCarthy lab was used for all cloning transformations and plasmid preparations. The bacterial cells were grown in Luria-Bertani (LB) broth and agar.

Chemicals, consumables and reagents

Table 2.1: Chemicals, consumables and reagents used in the experiments outlined in this thesis.

Product	Brand/Company
Tissue Culture	
Dublecco's Modified Eagle Medium (DMEM)	Sigma-Aldrich D6429
L-Glutamine solution	Sigma-Aldrich G7513
Penicillin-Streptomycin	Sigma-Aldrich P4333
Trypsin-EDTA	Sigma-Aldrich T4049
G418 disulfate salt	Sigma-Aldrich A1720
Puromycin dihydrochloride	Sigma-Aldrich P8833
Dublecco's Phosphate buffered Saline (PBS)	Sigma-Aldrich D8537
Gibco Fetal Bovine Serum, South American	Bio Sciences 10270-106
Fetal Bovine Serum	Sigma-Aldrich F7524
3-Isobutyl-1-methylxanthine	Sigma-Aldrich I7018
Insulin solution human	Sigma-Aldrich I9278
Dexamethasone	Sigma-Aldrich D4902
Formaldehyde solution 36.5-38% in H2O	Sigma-Aldrich F8775
Oil Red O solution	Sigma-Aldrich O1391
Lipofectamine 2000 reagent	Invitrogen, Bio-Sciences 11668-027
TurboFect in vitro Transfection reagent	Fermentas, Fisher Scientific R0531
Testosterone	Applichem A0671,0010

5α-Androstan-17β-ol-3-one (DHT)	Sigma-Aldrich A8380
Cell culture dishes/flasks	Sarstedt
Cell scrapers	Sarstedt 83.183
Dimethylsulfoxide (DMSO) - MTT	Sigma-Aldrich D8418
Dimethylsulfoxide (DMSO) sterile	Sigma-Aldrich D2438
100% Ethanol	Central stock
MycoAlert™ mycoplasma detection kit	Lonza
Trypan Blue	Sigma-Aldrich
Quantitative RT-PCR	
Fluka, BioUltra, Phenol, 99.5%	Sigma-Aldrich 77608
Guanidine thiocyanate	Promega V2791
Ammonium thiocyanate	Sigma-Aldrich A7149
Sodium acetate	Sigma-Aldrich S7545
Glycerol	Sigma-Aldrich G5516
Tetro cDNA Synthesis Kit	Bioline BIO-65043
PrimeTime qPCR Assays	Integrated DNA Technologies (IDT)
5X HOT FIREPol Probe pPCR mix plus (ROX)	Solis BioDyne 08-14-00001
96 well Multiply PCR plate	Sarstedt 72.1980.232
Lighcycler 480 sealing foil	Roche 4729757001
Rnase Zap	Bio-Sciences AM9780
Isopropanol	Sigma-Aldrich 19516
Molecular biology	
dNTP	New England Biolabs N0446S
Q5 –High-Fidelity DNA Polymerase	New England Biolabs M0491S
Phusion High-Fidelity DNA Polymerase	New England Biolabs M0530S
Taq DNA Ligase	New England Biolabs M0208S
T5 Exonuclease	New England Biolabs M0363S
β-Nicotinamide adenine dinucleotide (NAD^+)	New England Biolabs B9007S
Instant Sticky-end Ligase Master Mix	New England Biolabs M0370S
T4 DNA Ligase	New England Biolabs M0202S
100-bp DNA ladder	New England Biolabs N3231S
1kb DNA Ladder	New England Biolabs N3232S
Agarose Molecular Biology Reagent	Sigma-Aldrich A9539
SafeView Nucleic acid stain	NBS Biologicals NBS-SV5
QIAquick PCR purification Kit	Qiagen 28104
QIAprep Spin Miniprep Kit	Qiagen 27106
LB Broth	Sigma-Aldrich L3022
Agar	MERCK Millipore 111925
Ampicillin sodium salt	Sigma-Aldrich A9518
Kanamycin sulfate	Sigma-Aldrich K4000
Chloramphenicol	Boehringer Mannheim 634 433
Restriction Endonucleases	New England Biolabs
PureYield Plasmid Midiprep system	Promega A2492
Primers	Sigma-Aldrich and IDT
Taq DNA polymerase	New England Biolabs M0267S
Polyethylene glycol 8000	Sigma-Aldrich P2139
Lithium hydroxide monohydrate	Sigma-Aldrich L4533
Boric Acid	Sigma-Aldrich
Luciferase assay	
Solid assay microplate 96 well solid white	Fisher Scientific 10167481
Coelenterazine native	Nanolight technologies 303-01
LAR II buffer	Recoding Lab
Passive Lysis Buffer (PLB)	Promega
Western Blotting	
Trizma HCL	Sigma-Aldrich T5941

Trizma Base	Sigma-Aldrich
Glycine	Sigma-Aldrich
Sodium Chloride (NaCL)	Sigma-Aldrich
Potassium Chloride (KCL)	Sigma-Aldrich
Monopotassium phosphate (KH_2PO_4)	Sigma-Aldrich
Disodium phosphate (Na_2HPO_4)	Sigma-Aldrich
Sodium dodecyl sulphate (SDS)	Sigma-Aldrich L4390
Bromophenol Blue	BDH Chemicals ltd.
Dithiothreitol (DTT)	Sigma-Aldrich D9779
30% Acrylamide	Sigma-Aldrich A3574
Ammonium persulfate	Sigma-Aldrich A3678
Tetramethylethylenediamine (TEMED)	Sigma-Aldrich T9281
Protein Ladder EZ-run	Fisher Scientific, Fermentas, BPE3603
Whatman Protran nitrocellulose membranes	Sigma-Aldrich Z613657
Chromatography paper	GE healthcare and life sciences 3030672
Methanol	Sigma-Aldrich 34860-2
Ponceaux S	Sigma-Aldrich P3504
Marvel dried skimmed milk	Centra Ireland
Tween 20	Sigma-Aldrich P2287
Bovine serum albumin (BSA)	Sigma-Aldrich A7906
CL-XPosure™ Films	Fisher Scientific 34090
Parafilm	
Restore™ stripping buffer	Thermo Scientific 21059
SuperSignal™ West Pico and Femto substrates	Thermo Scientific, 34087 and 34094
Trichloroacetic acid	Sigma-Aldrich
Acetone	Sigma-Aldrich 270725

Antibodies

Table 2.2: Antibodies used in the Western blotting experiments described in this thesis.

Antibody	**Clone**	**Company**
THE™ DYKDDDDK Tag antibody		GenScript
Anti-Flag	M2	Sigma-Aldrich
Anti-B-actin	AC-15	Sigma-Aldrich
Anti-α-tubulin	B-5-1-2	Sigma-Aldrich
Anti-MYC	9E10	Santa Cruz Biotechnology
Anti-PPARγ	81B8	Cell Signalling Technology
Anti-Lamin A/C (2032)		Cell Signalling Technology
Anti-ITM2A (14407)		Proteintech

PrimeTime® qPCR Assays

Table 2.3: All PrimeTime qPCR probe-based assays utilised in quantitative RT-PCR experiments. All assays were purchased from IDT.

Gene	Assay ID	Primer 1	Primer 2
NoNo	**Mm.PT.58.16299938**	5'CATCATCAGCATCACCACCA3'	5'TCTTCAGGTCAATAGTCAAGCC3'
LMNA	**Hs.PT.58.39267032**	5'GGTCACCCTCCTTCTTGGTAT3'	5'AGACCCTTGACTCAGTAGCC3'
ITM2A	**Mm.PT.58.11424567**	5'CTGTCCGAGCTCAAATCCTG3'	5'ACAATCAGTCCTGCC AAGATG3'
ITM2A	**Mm.PT.58.6163978.gs**	5'TCACTCCTGACAGATCTTGGT3'	5'AAATCCTTCCGCCTTAGACG3'
C/EBPα	**Mm.PT.58.30061639.g**	5'TCATTGTCACTGGTCAACTCC3'	5'ACAAGAACAGCAACGAGTACC3'
PPARγ	**Mm.PT.56a.31161924**	5'CTGCTCCACACTATGAAGACAT3'	5'TGCAGGTTCTACTTT GATCGC3'
IGFBP5	**Mm.PT.56a.11593699**	5'GTACCTGCCCAACTGTGAC 3'	5'GCTTCATTCCGTACTTGTCCA3'
PTPRQ	**Mm.PT.58.30283019**	5'GTGAAGTTACACTGCCTGACA3'	5'AACAAGCCAGTGACAGTCTT3'
WNT6	**Mm.PT.58.5344953**	5'AGTCAAGACTCTTTATGGATGCG3'	5'CATGGCACTTACACTCGG T3'
WNT6 CP*		5'GCTCTCCAGATGCTAGCG 3'	5'CACCGAGTGTAAGTGCCAT3'

*CP denotes Custom Primer. These primers were designed and ordered as a probe-based assay from IDT. All other assays were pre-designed by IDT.

Plasmids

Table 2.4: Plasmids used in the experiments outlined in this thesis.

Plasmid	Source
pCDNA3-FLAG-LMNA WT	Worman lab
pCDNA3-FLAG-LMNA R482W	Worman lab
pCMV6.ITM2A	Origene MR203468
pCMV6.IGFBP5	Origene MR203605
pIRES-EGFP	Clontech - O'Connor Lab
pCMV(PB)	PB terminal repeats from pCyL50 amplified and cloned into pIRES-EGFP
pCMV(PB)- FLAG-LMNA WT	LMNA amplified from pCDNA3-FLAG-LMNA WT
pCMV(PB)-FLAG-LMNA R482W	LMNA amplified from pCDNA3-FLAG-LMNA R482W
pCMV(PB)ITM2A	ITM2A amplified from pCMV6.ITM2A
pMSCVpuro	Clontech - Schupp lab
pMSCV(PB)	PB terminal repeats from pCyL50 amplified and cloned into pMSCVpuro
pMSCV(PB)- FLAG-LMNA WT	LMNA amplified from pCDNA3-FLAG-LMNA WT
pMSCV(PB)-FLAG-LMNA R482W	LMNA amplified from pCDNA3-FLAG-LMNA R482W
pMSCV(PB)ITM2A	ITM2A amplified from pCMV6.ITM2A
pMSCV(PB)IGFBP5	IGFBP5 amplified from pCMV6.IGFBP5
pRFP-C-RS	Origene
pRFP-C-RS.shITM2A.1	Origene - TF501127C / FI540152
pRFP-C-RS.shITM2A.2	Origene - TF501127A / FI348274
pRFP-C-RS.shITM2A.3	Origene - TF501127D / FI540153
pRFP-C-RS.shITM2A.4	Origene - TF501127B / FI540151
pRFP-C-RS.shControl	Origene - TR30015
pRFP(PB)	PB terminal repeats from pCyL50 amplified and cloned into pRFP-C-RS
pRFP(PB).shITM2A.1	PB terminal repeats from pCyL50 amplified and cloned into pRFP-C-RS.shITM2A.1
pRFP(PB).shITM2A.2	PB terminal repeats from pCyL50 amplified and cloned into pRFP-C- RS.shITM2A.2
pRFP(PB).shControl	PB terminal repeats from pCyL50 amplified and cloned into pRFP-C-RS.shControl

pRFP(PB).shIGFBP5	IGFBP5 shRNA amplified and cloned into pRFP(PB)
pRFP(PB).shPTPRQ.1	PTPRQ shRNA.1 amplified and cloned into pRFP(PB)
pRFP(PB).shPTPRQ.2	PTPRQ shRNA.2 amplified and cloned into pRFP(PB)
pRFP(PB).shPTPRQ.3	PTPRQ shRNA.3 amplified and cloned into pRFP(PB)
pRFP(PB).WNT6	WNT6 shRNA amplified and cloned into pRFP(PB)
pCMV(PB)-Flag-LMNA-WT.shITM2A	shITM2A amplified and cloned into pMSCV(PB)- FLAG-LMNA WT
pCMV(PB)-Flag-LMNA-WT.shControl	shControl amplified and cloned into pMSCV(PB)- FLAG-LMNA WT
pCMV(PB)-Flag-LMNA-R482W.shITM2A	shITM2A amplified and cloned into pMSCV(PB)- FLAG-LMNA-R482W
pCMV(PB)-Flag-LMNA-R482W.shControl	shControl amplified and cloned into pMSCV(PB)- FLAG-LMNA-R482W
pCMV(PB).shITM2A	shITM2A amplified and cloned into pMSCV(PB)
pCMV(PB).shControl	shControl amplified and cloned into pMSCV(PB)
pGlucBasic	New England Biolabs
pGluc(PB)Basic	PB terminal repeats from pCyL50 amplified and cloned into pGlucBasic
pGluc(PB)ITM2A/2kb	ITM2A promoter amplified from genomic DNA and cloned into pGluc(PB)Basic
pGluc(PB)ITM2A/1.5kb	ITM2A promoter amplified from genomic DNA and cloned into pGluc(PB)Basic
pGluc(PB)ITM2A/1kb	ITM2A promoter amplified from genomic DNA and cloned into pGluc(PB)Basic
pGluc(PB)ITM2A/0.5kb	ITM2A promoter amplified from genomic DNA and cloned into pGluc(PB)Basic
pGluc(PB)ITM2A/0.35kb	gBlock purchased from IDT and cloned into pGluc(PB)Basic
pGluc(PB)ITM2A/GATA.mt	gBlock purchased from IDT and cloned into pGluc(PB)Basic
pGluc(PB)IGFBP5/1.2kb	IGFBP5 promoter amplified from genomic DNA and cloned into pGluc(PB)Basic
pGluc(PB)IGFBP5/2.4kb	IGFBP5 promoter amplified from genomic DNA and cloned into pGluc(PB)Basic
pCyL50	Wellcome Trust Sanger Institute, Ref (165)
mPB	Wellcome Trust Sanger Institute, Ref. [165]

METHODS

Tissue culture

3T3-L1 and mouse embryonic fibroblasts (MEFs) were maintained in standard growth medium; Dulbecco's modified Eagle's medium with 10% fetal bovine serum (Gibco – South American origin), 2 mM L-glutamine and 100U/ml penicillin, 100µg/ml streptomycin, at 37°C in a 5% CO2 incubator. 3T3-NIH cells were maintained in standard growth medium with alternatively sourced 10% fetal bovine serum (Sigma-Aldrich). 3T3-L1 and MEF cell lines were sub-cultured in fresh medium every 2 days at a 1:4 ratio. 3T3-NIH cells were sub-cultured in fresh medium every 2-3 days at a 1:10 ratio. To sub-culture, cells were washed once in PBS and Trypsin-EDTA was used to detach the cells from the growth surface. To cryopreserve, cells were washed

with PBS, tripsinised and spun at 1500 rpm for 5 minutes, at room temperature. Cell pellets were re-suspended in a mixture of 70% standard growth medium, 20% FBS and 10% sterile DMSO. Cell suspensions were initially stored at -80˚C and then in liquid nitrogen for long term storage. Cryopreserved cells were thawed at 37˚C and transferred to culture flask containing pre-warmed standard growth medium and cultured at 37˚C overnight. Fresh medium was applied the next day.

3T3-L1 differentiation

For differentiation, 3T3-L1 cells were grown to confluence in standard growth medium (day -2). Two days post confluence (day 0) cells were induced in fresh medium containing 0.5mM 3-Isobutyl-1-methylxanthine (IBMX), 1μM dexamethasone (D) and 10 μg/ml insulin (I). This induction cocktail is referred to as MDI. For submaximal induction fresh medium was applied containing 10 μg/ml insulin and 1μM dexamethasone (DI) or just 1μM dexamethasone (D) alone. Two days later (day 2) fresh medium containing 10 μg/ml insulin was applied. Fresh standard medium was applied every two days after that until day 8 when cells were fixed and stained with Oil Red O.

Oil Red O staining

3T3-L1 cells were washed with phosphate buffer saline (PBS) and fixed with 10% formaldehyde solution (Sigma-Aldrich) in PBS for 15-30 minutes at 37°C. Fixed cells were washed with water (x 2) and a working Oil Red O solution (0.5% in isopropanol – diluted 3:2 with ddH20) applied overnight with gentle rocking. Oil Red O quantification was performed using ImageJ as previously described [166] and expressed as Oil Red O absorbance units (ORO a.u.).

3T3-L1 stable transfection

For all stable transfections, 3T3-L1 cells were co-transfected with piggyBac transposable vectors and the mPB transposase using Lipofectamine 2000 transfection reagent (Invitrogen). Cells were seeded the day before in 60mm dishes, so that cells were at 50-70% confluency. Plasmid DNA and Lipofectamine were diluted in serum free DMEM separately and allowed to incubate at room temperature for 5 minutes. Diluted DNA was added to diluted Lipofectamine and incubated at room temperature

for 20 minutes. To transfect cells at 50-60% confluency in a 60mm dish, a total of 8µg DNA and 20µl of Lipofectamine were diluted in 0.5mls of serum free media respectively. For co-transfections, equal amounts of DNA were used i.e. 4µg of transposase and 4µg of overexpression/knockdown (KD)/luciferase construct. Prior to transfection fresh standard medium was applied to the cells and the DNA/Lipofectamine mix was added drop-wise. Cells were incubated with the transfection mix for 4-6hrs at 37°C in a 5% CO2 incubator, after which fresh standard medium was applied. Between 24 and 48hrs post transfection, depending on cell morphology and observed cell death, selection antibiotics were applied (800µg/ml G418 or 0.75-1.5ug/ml puromycin) and cells were selected for 1-2 weeks, depending on rate of cell growth.

3T3-NIH transient transfection

Transient transfection of 3T3-NIH cells was performed with TurboFect *in vitro* transfection reagent (Thermo Scientific). Cells were seeded the day before in 6-well plates, so that cells were at 70-80% confluency. Plasmid DNA and TurboFect reagent were diluted in 0.5mls of serum free media and incubated at room temperature for 20 minutes. A total of 4µg DNA and 6µl of TurboFect were used per well to transfect cells seeded in a 6-well plate. For shRNA mediated KD of over-expressed ITM2A a 3:1 ratio was used, where 3µg of shRNA were co-transfected with 1µg of the over-expression construct. Prior to transfection fresh standard medium was applied to the cells and the DNA/TurboFect mix was added drop-wise. Cells were incubated with the transfection mix for 6hrs at 37°C in a 5% CO2 incubator, after which fresh standard medium was applied. 48hrs post transfection the cells were lysed and ITM2A protein analysed by immunoblot.

Plasmid Construction

PiggyBac Transposable constructs

PiggyBac transposable constructs were generated as follows; piggyBac (PB) terminal repeats (TR) were amplified from pCyL50 and cloned into the overexpression vectors pIRES2-EGFP, and pMSCVpuro, the knockdown vector pRFP-C-RS, and the luciferase reporter pGlucBasic, such that they flanked the promoter/MSC, *Gaussia* luciferase gene (pGlucBasic) and mammalian antibiotic resistance markers. The 5'PBTR and 3'PBTR were amplified using primers listed below in table 5.

Table 2.5: PCR primers used to amplify piggyBac terminal repeats (PBTR).

Amplicon	Froward primer (5'>3')	Reverse primer (5'>3')
5'PBTR	GGTACCTCGCGCGACTTGGTTTGC	GCTAGCCAACAAGCTCGTCATCGC3
3'PBTR	TTAATTAACGAGAGCATAATATTGATAT	GAGCTCGGTATTCACGACAGCAGG

Gibson assembly was used to insert the TR into each construct, and the primers shown above in table 5 contained additional 'overlap' sequence of approximately 15bp at the 5' end, to complement each vector respectively and facilitate the assembly cloning. These primers are listed below in table 6. Lower case sequence represents the vector 'overlap' portion of the primer and uppercase sequence is complementary to the insert being amplified.

Table 2.6: Gibson assembly primers used to amplify piggyBac terminal repeats (PBTR) in the previously described vectors.

Primer name	Gibson primer sequence (5'>3')
5'PBTR.pIRES2-EGFP5'	cgccatgcattagttatGGTACCTCGCGCGACTTG
5'PBTR.pIRES2-EGFP3'	cccgtaattgattactatGCTAGCCAACAAGCTCGTC
3'PBTR.pIRES2-EGFP5'	cgccatgcattagttatTTAATTAACGAGAGCATAATATTGATAT
3'PBTR.pIRES2-EGFP3'	cccgtaattgattactatGAGCTCGGTATTCACGAC
5'PBTR.pMSCVpuro5'	tactgagagtgcaccaGGTACCTCGCGCGACTTG
5'PBTR.pMSCVpuro3'	ggtatttcacaccgcaGCTAGCCAACAAGCTCGTC
3'PBTR.pMSCVpuro5'	gataacgcaggaaagaaTTAATTAACGAGAGCATAATATTGATATC
3'PBTR.pMSCVpuro3'	gctggccttttgctcaGAGCTCGGTATTCACGAC
5'PBTR.pRFPCRS5'	ccggccggatcggtgGGTACCTCGCGCGACTTG
5'PBTR.pRFPCRS3'	gtctttccactggggGCTAGCCAACAAGCTCGTC
3'PBTR.pRFPCRS5'	cactggccaattggttTTAATTAACGAGAGCATAATATTGATAT
3'PBTR.pRFPCRS3'	cgcggctacaattgttGAGCTCGGTATTCACGAC

5'PBTR.pGlucbasic5'	agtgccacctgacgtGGTACCTCGCGCGACTTG
5'PBTR.pGlucbasic3'	ccgatccgtcgacgtGCTAGCCAACAAGCTCGTC
3'PBTR.pGlucbasic5'	gtatcttatcatgtctgtaTTAATTAACGAGAGCATAATATTGATAT
3'PBTR.pGlucbasic3'	ctagaggtcgacggtaGAGCTCGGTATTCACGAC

The 5'PBTR was inserted into the AseI site of pIRES2-EGFP, the NdeI sites of pMSCVpuro, the EcoR1 site of pRFP-C-RS and the Aat II site of pGlucBasic, while the 3'PBTR was inserted into the BsaI site of pIRES2-EGFP, the PciI sites of pMSCVpuro, the PciI site of pRFP-C-RS and BstZ17I site of pGlucBasic, to generate pCMV(PB), pMSCV(PB), pRFP(PB) and pGluc(PB)basic. The transposable pIRES2-EGFP plasmid with piggyBac terminal repeats will be referred to as pCMV(PB) to simplify nomenclature.

LMNA, ITM2A and IGFBP5 overexpression constructs

A human LMNA (WT and R482W mutant) cDNA plasmid was kindly provided by Howard J Worman (Department of Pathology and Cell Biology, Columbia University). LMNA was amplified from this plasmid and inserted into the XhoI and EcoRI sites of pCMV(PB) to produce pCMV(PB)-Flag-LMNA-WT and pCMV(PB)-Flag- LMNA-R482W. LMNA was also amplified and inserted into the XhoI and EcoRI sites of pMSCV(PB) to generate pMSCV(PB)-Flag-LMNA-WT and pMSCV(PB)-Flag- LMNA-R482W.

ITM2A mouse cDNA was purchased from Origene, amplified and inserted into the XhoI and EcoRI sites of pMSCV(PB), to generate a fusion protein with a 107aa C-terminal addition that included a Myc-DDK tag and generated pMSCV(PB)ITM2A. The ITM2A cDNA was also amplified and cloned into the EcoR1 and BamHI sites of pCMV(PB) with a separate 69aa C-terminal addition also including a Myc-DDK tag to generate pCMV(PB)ITM2A.

IGFBP5 mouse cDNA was purchased from Origene, amplified and inserted into the XhoI and EcoRI sites of pMSCV(PB), to generate a fusion protein with a 59aa C-terminal addition that included a Myc-DDK tag and generated pMSCV(PB)IGFBP5. Gibson assembly was used to insert LMNA, ITM2A and IGFBP5 into each vector backbone and the primers used to generate the above constructs are listed below (Table 7).

Table 2.7: Gibson assembly primers used to amplify LMNA, ITM2A and IGFBP5 into the previously described vectors.

Primer name	Gibson primer sequence (5'>3')
pIRES2-EGFP.LMNA.F	ctaccggactcagatcATCGAATTAATACGACTCATTATAG
pIRES2-EGFP.LMNA.R	taccgtcgactgcagCATGATGCTGCAGTTCTG
pMSCVpuro.LMNA.F	gccggaattagatctcATCGAATTAATACGACTCATTATAG
pMSCVpuro.LMNA.R	tcccctacccggtagTTACATGATGCTGCAGTTC
pIRES2-EGFP.ITM2A.F	cgagctcaagcttcgAATTCGTCGACTGGATCC
pIRES2-EGFP.ITM2A.R	ggagggagaggggcgTAAACCTTATCGTCGTCATC
pMSCVpuro.ITM2A.F	gccggaattagatctcAATTCGTCGACTGGATCC
pMSCVpuro.ITM2A.R	tcccctacccggtagTAAACCTTATCGTCGTCATC
pMSCVpuro.IGFBP5.F	gccggaattagatctcAATTCGTCGACTGGATCC
pMSCVpuro.IGFBP5.R	tcccctacccggtagTAAACCTTATCGTCGTCATC

ITM2A, IGFBP5, WNT6 and PTPRQ shRNA constructs

ITM2A shRNA constructs were purchased from Origene in pRFP-C-RS (Origene HuSH-29 shRNA, TF501127). Table 8 shows the 29mer sequence of the ITM2A shRNA constructs. PiggyBac transposable arms were then cloned into each construct individually, as previously described.

IGFBP5, WNT6 and PTPRQ shRNA sequences were ordered from IDT as ultramer oligonucleotides, amplified and inserted downstream of the U6 promoter in the BamHI and HindIII sites of pRFP(PB) plasmid, in the final format specified by Origene for their HUSH-29 shRNA. The shRNA cassette contains a 29mer target specific shRNA sequence, a 7 nucleotide hairpin loop and the reverse 29mer complimentary sequence, followed by a 6 nucleotide termination sequence (Origene HuSH-29 application guide). Ultramer sequences and Gibson assembly primers used to amplify each ultramer are listed below in table 9. Gibson assembly was originally used to insert the shRNA sequences into the pRFP(PB) vector, however due to high frequency of recombination, as assessed by sequencing, classical cloning was employed instead. Ultramer sequences were amplified with Gibson assembly primers, digested with HindIII and Sau3A1 and inserted into the pRFP(PB) construct using standard ligation reactions.

Table 2.8: ITM2A shRNA sequences.

shRNA name	shRNA sequence
TF501127C / FI540152 (shITM2A.1)	CGTGCCATTGACAAATGCTGGAAGATTAG
TF501127A / FI348274 (shITM2A.2)	TGTTGGTGGAGCCTGCATTTACAAGTACT
TF501127D / FI540153 (shITM2A.3)	GGCGGCAATTATTCACGACTTTGAGAAGG
TF501127B / FI540151 (shITM2A.4)	GATGTAGAGGCGCTCGTCAGTCGCACTGT

Origene tube ID reference numbers are listed in shRNA name column. ITM2A shRNAs are numbered 1-4 throughout the thesis, and shRNA number i.e. shITM2A.1 is included in brackets beside the tube ID.

Table 2.9: Ultramer sequences and Gibson assembly primers for IGFBP5, WNT6 and PTPRQ shRNA constructs.

Oligonucleotide name	shRNA/Gibson primer sequence (5'>3')
shIGFBP5.1	GATCGCCAAGCACACTCGCATTTCCGAGCTGAAGTCAAGAGCT TCAGCTCGGAAATGCGAGTGTGCTTGGTTTTTTGAAGCT
pRFP.shIGFBP5.1.F	gtggaaaggacgcggGATCGCCAAGCACACTCG
pRFP.shIGFBP5.1.R	tccacagggtcgacaAGCTTCAAAAAACCAAGCACAC
sh.WNT6.1	GATCGGGAGGCTGCGGAGACGATGTGGACTTCGGTCAAGAGCC GAAGTCCACATCGTCTCCGCAGCCTCCTTTTTTGAAGCT
pRFP.shWNT6.1.F	gtggaaaggacgcggGATCGGGAGGCTGCGGAG
pRFP. shWNT6.1.R	tccacagggtcgacaAGCTTCAAAAAAGGAGGCTGCG
shPTPRQ.1	GATCGTGGAGACATACTGATTACAAAGCTTATGGTCAAGAGCC ATAAGCTTTGTAATCAGTATGTCTCCATTTTTTGAAGCT
pRFP.shPTPRQ.1.F	gtggaaaggacgcggGATCGTGGAGACATACTG
pRFP.shPTPRQ.1.R	tccacagggtcgacaAGCTTCAAAAAATGGAGAC
shPTPRQ.2	GATCGCAGAGTGAAGCTGATAGCTGATGTAAGCATCAAGAGTG CTTACATCAGCTATCAGCTTCACTCTGTTTTTTGAAGCT
pRFP.shPTPRQ.2.F	gtggaaaggacgcggGATCGCAGAGTGAAGCTG
pRFP.shPTPRQ.2.R	tccacagggtcgacaAGCTTCAAAAAACAGAGTGAAG
shPTPRQ.3	GATCGGGCACAGTATATCTTCTTACACCAGTGCATCAAGAGTG CACTGGTGTAAGAAGATATACTGTGCCTTTTTTGAAGCT
pRFP.shPTPRQ.3.F	gtggaaaggacgcggGATCGGGCACAGTATATC
pRFP.shPTPRQ.3.R	tccacagggtcgacaAGCTTCAAAAAAGGCACAG

Red sequence in the ultramer sequences represents the modified BamHI site (GATCG) hairpin loop (TCAAGAG), and termination sequence (TTTTTT).

Luciferase reporter constructs

ITM2A and IGFBP5 promoter regions were amplified from mouse genomic DNA and inserted into the EcoRI and HindIII (ITM2A) or BglII and HindIII sites (IGFBP5) of pGlucBasic or pGluc(PB)basic, directly upstream of the *Gaussia* secreted luciferase. Gibson assembly was used to insert the ITM2A promoter fragments into pGluc(PB)basic, and standard primers with BglII (F) and HindIII (R) restriction sites included were used to insert the IGFBP5 promoter fragments into pGlucBasic and pGluc(PB)basic. All primers used to generate the constructs are listed below, in table 10.

Four ITM2A promoter fragments were amplified of approximately 2kb, 1.5kb, 1kb and 0.5kb upstream of the translational start site. Exact positioning is shown in the schematic in Figure 3.3, chapter 3. Two IGFBP5 promoter fragments were amplified of approximately 2.4kb and 1.2kb upstream of the translational start site. Exact positioning is shown in the schematic in Figure 5, chapter 4.

Two further ITM2A promoter constructs were generated with a 0.35kb promoter fragment and a 0.5kb promoter fragment including a mutated GATA site as shown in the schematic in figure 3.4, chapter 3. The 0.35kb and GATA mutant 0.5kb fragments were purchased as gBlock gene fragments from IDT, amplified and inserted into the EcoRI and HindIII sites of pGluc(PB)basic using Gibson assembly.

Table 2.10: Gibson assembly and standard primers used to amplify ITM2A and IGFBP5 promoter fragments for insertion into pGlucBasic/pGluc(PB)basic.

Primer name	Gibson primer sequence (5'>3')
pGlucITM2A.2kb.F	gatcgggagatcttggTACTTTTCTGAATAATACAATGTGGACTT
pGlucITM2A.1.5kb.F	gatcgggagatcttggACATCCTGCTTCTAAGGTCC
pGlucITM2A.1kb.F	gatcgggagatcttggACACCAGCATCTGGTTATATTG
pGlucITM2A.0.5kb.F	gatcgggagatcttggGTTGCAGAACTCAGAAACC
pGlucITM2A.0.35kb.F	gatcgggagatcttggGTAGGAGCATGCCTGGGG
pGlucITM2A.0.5kb.GATA.mt	gatcgggagatcttggGCCAGGCCCAAGTTTGGG
pGlucITM2A.R	ccgagctcggtaccaGGTGAATCTTCGGGCTGC
pGlucIGFBP5.2.4kb.F	CTATAGATCT**gcacacagctcttcttccctct**
pGlucIGFBP5.1.2kb.F	CTATAGATCT**gaaaggacttcttgggcagggta**
pGlucIGFBP5.R	GCATTAAGCTT**tttctcggagtctggctttacct**

Gibson vector overlap sequences are shown in lower case in ITM2A primers. Additional bases and restriction sites (underlined) are shown in capitals in IGFBP5 primers, with promoter complementary sequence in bold lowercase.

Dual constructs

Dual piggyBac transposable LMNA over-expression and ITM2A/WNT6 shRNA constructs were generated by amplifying the shRNA cassette for either shITM2A.1 or shWNT6.1 (including U6 promoter) and inserting it into the AflII site of pCMV(PB)-FLAG-LMNA WT, pCMV(PB)- FLAG-LMNA R482W and pCMV(PB) empty vector. Gibson assembly primers used to amplify the shRNA cassettes are listed below (Table 11).

Table 2.11: Gibson assembly primers used to amplify shRNA cassettes.

Primer name	Gibson primer sequence (5'>3')
pCMV(PB).shRNA.F	caaactcatcaatgtatcAATTCCCCAGTGGAAAGAC
pCMV(PB).shRNA.R	cgcttacaatttacgccCTGACACACATTCCACAG

Agarose gel electrophoresis

Agarose powder was dissolved in Tris-acetate-EDTA (TAE) containing 40mM Tris-acetate and 1mM EDTA, by microwave heating. SafeView Nucleic Acid Stain was added (1µl/10ml agarose gel solution) and mixed well before gel was cast. Samples were mixed with 6X loading dye, loaded on the agarose gel and ran in 1X TAE buffer at 100 volts at room temperature. Running duration was modified depending on the size on the DNA product being visualised.

Lithium Borate agarose gel electrophoresis

A lithium borate system was used for high resolution agarose electrophoresis of the small amplified shRNA DNA molecules. Agarose powder was dissolved in 1X lithium borate (LB) buffer and SafeView Nucleic Acid Stain was added (1µl/10ml agarose gel solution) and mixed well before gel was cast. Samples were mixed at a 1:1 ratio with a LB loading dye, loaded on the agarose gel and ran in 0.1X LB buffer at 120 Volts at room temperature. LB buffer composition is listed below in Table 12.

Table 2.12: Lithium borate buffer and loading dye composition.

Component	Final Concentration
1X Lithium borate Buffer (pH 8.2-8.5)	
Lithium hydroxide monohydrate	10mM
Boric acid	0.6M
Loading Dye	
LB buffer	0.5X
Glycerol	50%
Bromophenol blue	0.2%

Polymerase chain reaction (PCR) amplification

LMNA, ITM2A, IGFBP5 cDNA, piggyBac terminal repeats, ITM2A and IGFBP5 promoter fragments, and ITM2A, IGFBP5, PTPRQ and WNT6 shRNA sequences were amplified using Q5 or Phusion high fidelity polymerases. PCR reactions were set up as recommended by the manufacturer for each polymerase. Briefly, all DNA and reagents were thawed and kept on ice while 50µl reactions were set up as described in Table 13.

Table 2.13: PCR reaction setup.

Component	50µl reaction	Final
5X reaction buffer	10µl	1X
10 mM dNTPs	1µl	200 µM
10 µM Forward Primer	2.5µl	0.5 µM
10 µM Reverse Primer	2.5µl	0.5 µM
Template DNA	Variable	<200ng
GC enhancer/DMSO	10µl/2.5µl	1X/5%
Polymerase	0.5µl	1 Unit
ddH2O	To 50µl	

GC enhancer (Q5), GC 5X reaction buffer (Phusion) or DMSO (Phusion) were used when appropriate. Template DNA concentrations varied depending on product being amplified, promoter fragments were amplified from approximately 100ng of mouse genomic DNA while piggyBac terminal repeats, gene cDNA and shRNA sequences were amplified from approximately 1-2ng of plasmid/ultramer template. All primers

are listed in the plasmid construction section above, and all annealing temperature used were as recommended by the NEBuilder assembly tool (www.neb.com) when generating Gibson assembly primers. Standard thermocycling conditions were used as shown below (Table 14). A hot start was used for all reactions; samples were heated to 95°C for 1 minute prior to the addition of polymerase. Duration of elongation was varied depending on the length of the product with approximately 30 seconds per kb.

Table 2.14: Thermocycling conditions for PCR reactions.

Step	Cycles	Temperature	Duration
Hot start	1	95°C	1 minute
Initial denaturation	1	98°C	30 seconds
Denaturation	35	98°C	10 seconds
Annealing		Variable	30 seconds
Elongation		72°C	variable
Final Extension	1	72°C	2 minutes
Cooling/Hold		4°C	unlimited

Promoter fragments, gene cDNA and piggyBac terminal repeat PCR products were separated on 1% agarose gels with a 1kb ladder. All shRNA PCR products were separated on 2% lithium borate gels with a 100bp ladder. Visualisation of all products was carried out using SafeView Nucleic Acid Stain, and the Bio-Rad Gel Doc™ EZ Gel documentation system. PCR products were purified using the QIAquick PCR purification kit for downstream applications.

Restriction endonuclease digestion

All restriction endonuclease enzymes were purchased from NEB and digestion reactions were carried out as recommended for each individual enzyme. Typically, 1μg of DNA (vector/insert) was digested with 10 units (1μl) of restriction enzyme, in a 50μl reaction containing 1X buffer, for 1 h at 37°C. The NEB double digest finder was used to select appropriate buffer for double-digests, and these reactions were incubated for 2 h at 37°C. In all cases, enzymes were added last and samples were mixed gently by pipetting. Digested products were separated on 1% agarose gels with a 1kb ladder and visualised using SafeView Nucleic Acid Stain, and the Bio-Rad Gel Doc™ EZ Gel documentation system. Digested products were purified using the QIAquick PCR purification kit for downstream applications.

Gibson assembly

All Gibson assembly primers were designed using the NEBuilder assembly tool, with 15 nucleotide overlaps. The Gibson assembly reaction is summarised in figure 2.1, where the key steps of the reaction are illustrated.

Gibson assembly reactions were carried out as described by Gibson et al., 2009. A stock of 5X isothermal reaction (ISO) buffer was prepared and stored at -20°C (500 mM Tris-HCl pH 7.5, 50 mM MgCl2, 1 mM of each dNTP, 50 mM DTT**,** 25% PEG-8000, 5 mM NAD). The assembly master mixture was prepared as outlined below (Table 15), and 15µl aliquots were stored at -20°C. For each Gibson assembly reaction, an assembly master mix aliquot was thawed on ice, to which 5µl of DNA was added, mixed well by pipetting and incubated at 50°C for 1 h. A total volume of 5µl of DNA was added to each reaction, with varying concentrations of insert and backbone. A 5:1 ratio of insert to vector backbone was used in all reactions, with total amounts varying depending on the concentrations of purified inserts and digested backbones. In all cases, empty vector control reactions were carried out; reactions were set up with ddH2O instead of the insert and transformed alongside each reaction. 5µl of each reaction was transformed into 50µl of DH5α E. coli bacterial cells.

Table 2.15: Gibson assembly master mixture.

Component	Volume
ISO Buffer	100µl
T5 exonuclease	0.2µl
Phusion polymerase	6.25µl
Taq DNA ligase	50µl
ddH2O	Up to 375µl

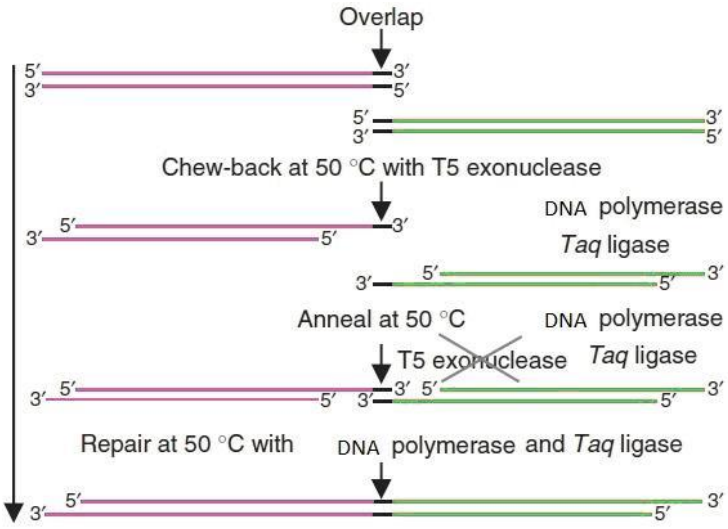

Figure 2.1: Schematic representation of Gibson assembly reaction. Taken from Gibson et al., 2009.

Standard ligation

Standard ligations were used instead of Gibson assembly for shRNA cloning. Amplified shRNA sequences were purified and ligated individually with digested pRFP(PB) using Sticky-end Ligase Master Mix or T4 DNA ligase with a 5:1 molar ratio of insert to vector. Standard protocols for both the Sticky-end Ligase Master Mix and T4 DNA ligase are described by the manufacturer (www.neb.com). Empty vector control ligations were set up with ddH2O instead of insert and transformed alongside each reaction. 5µl of each ligation reaction were transformed into 50µl of DH5α E. coli bacterial cells. IGFBP5 promoter fragments were inserted into pGluc basic and pGluc(PB) basic using standard ligations. Amplified promoter sequences were digested and purified, and ligated individually with digested and purified pGluc Basic and pGluc(PB)basic using T4 DNA ligase with a 5:1 ratio of insert to vector.

Bacterial transformation

Competent DH5α E. coli bacterial cells were thawed on ice, 5µl (20-100ng DNA) of Gibson assembly reactions or standard ligations was added to 50µl of competent cells, mixed gently by flicking and incubated on ice for 20 minutes. Cells were heat shocked at 42°C for 90 seconds using a water bath, and placed back on ice. 500µl of LB broth was added and cells were incubated at 37°C for 40-60 minutes. 100µl of cells were plated on LB agar plates containing a selection antibiotic, and incubated overnight at

37°C. pCMV(PB) vector reactions were plated with 50μg/ml Kanamycin, pMSCV(PB) and pGluc(PB) vector reactions were plated with 50μg/ml Ampicillin, and pRFP(PB) vector reactions were plated with 20μg/ml Chloramphenicol.

Identification of positive clones and plasmid purification

Positive clones were identified either by restriction digest or colony PCR. Bacterial colonies were used to inoculate 5 ml of LB broth containing an appropriate selection antibiotic (depending on vector backbone), and incubated overnight in a 37°C shaking incubator. Plasmids were extracted from the bacterial cultures using the QIAprep Spin Miniprep Kit and digested with the appropriate restriction enzymes to confirm the presence of the insert. Alternatively, colony PCR was performed prior to plasmid purification, to identify positive clones. PCR reactions were carried out using Taq polymerase as recommended by the manufacturer, individual bacterial colonies were added directly to each 25μl reaction and lysed during the initial denaturing step. PCR products were separated on 1% agarose gels with a 1kb ladder and visualised using SafeView Nucleic Acid Stain, and the Bio-Rad Gel Doc™ EZ Gel documentation system. Positive colonies were used to inoculate 5mls of LB broth containing selection antibiotic, incubated overnight in a 37°C shaking incubator, and plasmids extracted as previously described. Prior to plasmid extraction 25% glycerol stocks of positive colonies were made and stored at -20°C. Once the insert sequence was confirmed by sequencing, plasmids were purified on a larger scale for mammalian cell transfections, using the PureYield™ Plasmid Midiprep System. Briefly, 200-300 ml of LB broth with selection antibiotic was inoculated with a glycerol stock (50-100μl) and incubated overnight in a 37°C shaking incubator. The bacterial cells were then pelleted by centrifugation, re-suspended and lysed at room temperature. Lysates were neutralized and centrifuged again. The cleared lysate was then applied to a PureYield™ clearing and binding column, each column was washed with an endotoxin and column wash and the plasmid DNA eluted in 400μl of ddH2O.

Sequencing

All promoter fragment, gene cDNA and piggyBac terminal repeat sequences were verified by standard sanger sequencing by a service provider (www.gatc-biotech.com) and shRNA sequences were verified with an adapted sanger sequencing protocol (GATC Supreme run).

Ribonucleic acid (RNA) extraction and complementary (cDNA) synthesis

Total RNA was extracted from 3T3-L1/3T3-NIH/MEF cell biological triplicates using homemade Trizol. Cells were trypsinised and pelleted by centrifugation at 1500 rpm for 5 minutes, supernatant was removed gently and cell pellets were stored at -80°C until RNA extraction. Solid crystalline phenol was melted in a 50°C water bath and water saturated by adding ddH2O in excess and mixing well. The solution was allowed to settle overnight so that excess water separated and settled on top of the saturated phenol solution. The lower phenol phase was then used to make homemade Trizol with the reagents listed below in Table 16, and stored at 4°C.

Table 2.16: Homemade Trizol reagent (50 ml).

Reagent	Volume	Final
ddH2O saturated phenol	19 ml	38%
Guanidine thiocyanate	4.73g	0.8M
Ammonium thiocyanate	3.8g	0.4M
Sodium acetate, pH 5.0 (3M)	1.67 ml	0.1M
Glycerol	2.5 ml	5%
ddH2O	Up to 50 ml	

Trizol was added to the frozen cell pellets (approximately 500µl per 10cm^2 growth area) and complete cell lysis was aided by pipetting. Samples were centrifuged at 12,000 x g, for 10 minutes, at 4°C, to remove debris. Supernatant was transferred to a new sterile 1.5 ml Eppendorf tube. Chloroform was added to each tube (1/5th of Trizol volume) and samples were mixed well by vigorous shaking for 15 seconds. Samples were centrifuged at 12,000 x g, for 15 minutes, at 4°C. The upper aqueous phase was carefully transferred to a new sterile 1.5 ml Eppendorf tube and isopropanol was added (1/2 of Trizol volume). Samples were mixed well by vortexing and centrifuged at 12,000 x g, for 10 minutes, at 4°C, to pellet RNA. The RNA pellet was washed once

with 80% ethanol, vortexed briefly, and centrifuged at 7,500 x g for 5 minutes, at 4°C. The ethanol supernatant was removed gently and the RNA pellets were dried briefly at room temperature. RNA was re-suspended in ddH2O by pipetting and the concentration was determined using a NanoDrop® ND-1000 Spectrophotometer. All RNA samples were stored at -80°C. RNA quality was assessed by checking for intact 28S and 18S rRNA bands after agarose gel electrophoresis.

cDNA was synthesized using the Tetro cDNA Synthesis Kit, as recommended by the manufacturer. Master mix was prepared on ice and 9µl aliquoted into individual PCR tubes (Table 17). 11µl of sample containing between 500ng to 2µg of RNA was added to each tube. RNA concentrations added were kept constant between biological triplicates and controls within an experiment. Both random hexamer and oligo $(dT)_{18}$ priming were used concurrently. Samples were mixed gently by pipetting and incubated at 25°C for 10 minutes, 45°C for 30 minutes and the reaction was terminated by incubation at 85°C for 5 minutes. Samples were chilled on ice and diluted 1 in 2 with ddH2O. Samples were either kept at 4°C for short term or -20°C for long term storage.

Table 2.17: Tetro cDNA synthesis reaction.

Component	Volume
RNA	500ng to 2µg
10mM dNTP mix	1µl
Random Hexamer mix	1µl
Oligo $(dT)_{18}$ mix	1µl
5X RT Buffer	4µl
RiboSafe RNase Inhibitor	1µl
Tetro Reverse Transcriptase (200u/µl)	1µl
DEPC-treated water	To 20µl

Quantitative RT-PCR

Quantitative RT-PCR analysis was performed using IDT PrimeTime qPCR probe-based assays, with all predesigned assay IDs listed in the materials sections (Table 3). 10µl reactions were set up containing 1µl of 10X probe-primer mix, 2µl of HOT FIREPol Probe qPCR Mix Plus (ROX) polymerase, 2-3µl of cDNA and made up to 10µl with ddH2O. Each biological triplicate was measured in duplicate reactions, in a 96 well plate on the AB7300 Real- Time PCR cycler. All IDT Probe/primer assays were validated with a custom IDT gBlock titration. Expression of each gene was normalized to NoNo expression which is a validated reference gene for qPCR analysis for 3T3-L1 cells [167] and relative mRNA expression was calculated using the 2(-delta delta C(T)) method.

Western Blotting

Cell lysates were prepared as follows: 3T3-L1, 3T3 NIH or MEF cells were washed with PBS and scraped into lysis buffer (2% SDS, 62.5mM Tris-HCL; pH 6.8, 10% glycerol, 0.01% bromophenol blue, 41.6mM DTT). Lysates were sonicated for approximately 10 seconds and centrifuged at 16,000 x *g* for 20 mins at 4°C, and stored at -80°C. Tris-glycine SDS-Polyacrylamide gels were cast in 1.5mm BIO-RAD casting plates (Table 18, Table 19). For SDS-polyacrylamide gel electrophoresis (PAGE), lysates were boiled for 5 minutes and cooled on ice before being separated on 8-12% polyacrylamide gels, with the EZ-Run^{TM}prestained protein ladder. Electrophoresis was run at 100 volts through the stacking gel, and at 120 volts through the resolving gels in Tris-Glycine buffer, until the tracking dye had diffused into the buffer. Samples were transferred to nitrocellulose membranes (Amersham Protran 0.2µm NC), in transfer buffer at 100 volts for 45-60 minutes, and protein transfer was confirmed by Ponceau staining. Membranes were blocked for 1hr at room temperature and immunoblotted with primary antibodies at 4°C overnight, as recommended by antibody manufacturers (Table 19). Membranes were then washed three times for 5 minutes at room temperature, in wash buffer recommended for each primary antibody (Table 19). Membranes were incubated with HRP-conjugated secondary antibody (1:2000 dilution, 5% milk – Amersham ECL IgG, HRP-linked whole ab, GE Healthcare Life Sciences), for 1hr at room temperature and washed three times again, for 5 minutes, with recommended wash buffer. Signals were detected with

SuperSignal™ West Pico/Femto Chemiluminescent Substrate, and developed on CL-XPosure™ radiography film.

Table 2.18: 5% stacking gel for SDS-PAGE.

Component	Volume (5ml)
30% Polyacrylamide	0.85 ml
1M Tris(pH6.8)	0.625 ml
10% Ammonium persulfate	0.05 ml
10% SDS	0.05 ml
TEMED	5 µl
H_2O	3.4 ml

Table 2.19: Resolving gels for SDS-PAGE.

Component	Volume (10ml)	
	12%	**8%**
30% Polyacrylamide	4 ml	2.7 ml
1.5M Tris(pH8.8)	2.5 ml	2.5 ml
10% Ammonium persulfate	0.1 ml	0.1 ml
10% SDS	0.1 ml	0.1 ml
TEMED	4 µl	6 µl
H_2O	3.3 ml	4.6 ml

Table 2.20: Primary antibody recommended buffers.

Antibody	Blocking buffer	Primary AB incubation	Washing buffer
Anti-Flag	5% Milk in TBS	5% Milk in TBS	TBS
THE™ DYKDDDDK Tag antibody	5% Milk in PBS	1%BSA in PBST	PBST
Anti-PPARγ	5% Milk in TBST	5%BSA in TBST	TBST
Anti-Lamin A/C (2032)	5% Milk in TBST	5%BSA in TBST	TBST
Anti-ITM2A (14407)	5% Milk in TBST	5%Milk in TBST	TBST
Anti-B-actin	5% Milk in TBST	5%Milk in TBST	TBST
Anti-α-tubulin	5% Milk in TBST	5%Milk in TBST	TBST

Table 2.21: Antibody dilutions.

Antibody	Dilution	Dilution for secondary antibody
Anti-Flag	1:1000	Anti-Mouse 1:2000
THE™ DYKDDDDK Tag antibody	1:1000	Anti-Mouse 1:2000
Anti-PPARγ	1:1000	Anti-Rabbit 1:2000

Anti-Lamin A/C (2032)	1:1000	Anti-Rabbit 1:2000
Anti-ITM2A (14407)	1:1500	Anti-Rabbit 1:2000
Anti-B-actin	1:2000	Anti-Mouse 1:2000
Anti-α-tubulin	1:2000	Anti-Mouse 1:2000

Table 2.22: Western Blotting buffer compositions.

Component	Final Concentration
Tris-Glycine buffer for SDS-PAGE	
Tris Base	25mM
Glycine	192mM
SDS	0.1% (wt/vol)
Transfer Buffer	
Tris Base	25mM
Glycine	192mM
Methanol	20% (vol/vol)

Protein precipitation

Trichloroacetic acid (TCA) and acetone protein precipitation were carried out to concentrate secreted proteins in 3T3-L1 and 3T3-NIH medium. Briefly, 1 volume of TCA was added to 4 volumes of media sample and incubated at 4°C for 10 minutes. Samples were centrifuged at 12,000 rpm for 5 minutes, and the supernatant removed. Protein pellets were washed with 200µl cold acetone and centrifuged at 12,000 rpm for 5 minutes, twice. Protein pellets were then dried for 2-3 minutes on a 95°C heat block to remove acetone. For SDS-PAGE 1X lysis buffer (described in western blotting section) was added to the protein pellets, and the samples boiled for 10 minutes before separating on a 12% polyacrylamide gel.

Luciferase reporter assay

3T3-L1 cells were stably transfected (as described above) and seeded in triplicate for each differentiation treatment (MDI/DI/D, LiCL, and testosterone) in 12 well plates. Cells were grown to confluence, and induced to differentiate as described above. Small aliquots of media (30 µl) were taken at 24 h intervals post media changes and stored at - 20°C until assayed for luciferase activity. Samples (10µl) were assayed for *Gaussia* secreted luciferase activity with 1.43µM coelenterazine (NanoLight Technology) substrate in PBS on the Veritas Microplate Luminometer (Turner

Biosystems) as previously described (58). The luciferase activity directed by each stably transfected ITM2A/IGFBP5 promoter fragment was normalized to that of the pGluc(PB)basic empty vector construct to account for the weak promoter activity of the piggyBac transposable arms in the vector backbone (57).

CHAPTER 3: ITM2A SILENCING RESCUES LMNA MEDIATED INHIBITION OF 3T3-L1 ADIPOCYTE DIFFERENTIATION

INTRODUCTION

ITM2A was first identified as a novel marker for chondro-osteogenesis in a cDNA library screen generated from mouse mandibular condyle explant cultures [168]. This type II membrane protein belongs to a family of integral membrane proteins that includes ITM2B and ITM2C, all of which are part of a BRICHOS superfamily. ITM2 proteins are composed of four defined regions; a hydrophobic, linker, extracellular BRICHOS and the intracellular C-terminal domains. There is a high degree of conservation between the ITM2 proteins as well as between mammalian homologues [169].

Although the exact function of ITM2A is unclear, a number of studies have described a regulatory role in chondrogenic and myogenic differentiation, as well as thymocyte development [170–172]. ITM2A expression is low during the early stages of chondrogenesis and then strongly up-regulated as cells progress through the chondrogenic differentiation programme. Bi-potential C3H10T1/2 cells overexpressing ITM2A show similar levels of adipogenesis and osteogenesis as control cells, when induced to differentiate towards these respective lineages. ITM2A over-expression does however appear to inhibit the chondrogenic differentiation of this cell line. In addition, ITM2A was identified as differentially expressed between ASC and MSC with distinct chondrogenic potentials; ASC have a reduced capacity to differentiate into chondrocytes when compared to MSC, and display higher endogenous levels of ITM2A [170,173]. This may account for the reduced potential of ASC to undergo chondrogenesis.

ITM2A has been identified as a PAX3, GATA3 and PKA CREB target in diverse systems [171,172,174]. In the C2C12 myoblast cell line, endogenous ITM2A expression is increased during cell differentiation and over-expression leads to enhanced myotube formation. ITM2A expression is detected at sites of myogenesis in mice and PAX3 mutant embryos display reduced ITM2A [171,175]. ITM2A was described as a GATA3 target in mouse thymocytes and reported to be down-regulated in GATA3 knockout thymocytes when compared to control [172]. Recently a novel role for ITM2A has been

reported in autophagy. It is described as a PKA-CREB signalling target, and when over-expressed appears to interfere with autophagic flux, leading to the accumulation of autophagosomes and a block in the formation of autolysosomes. ITM2A silencing was also seen to obstruct autophagy, with the formation of large agglomerations within the cell [174]. These reports highlight the importance of ITM2A in the differentiation of a number of cell types, however the exact molecular function of the protein remains to be described. ITM2A knock-out mice have been produced independently by two different groups [171,172] neither of which have reported a specific altered phenotype.

This study aims to investigate the relationship between ITM2A, adipogenesis and inhibition of adipogenesis by LMNA.

RESULTS

Method development and vector construction

Extensive work was carried out in this thesis aimed at developing a system that facilitated the generation of a diverse number of gene constructs and robust analysis of transfected gene activity in the adipocyte differentiation 3T3-L1 cell model. In the early stages of this work, significant difficulties were encountered with standard methods. In particular, transient transfection of LMNA proved problematic as a) the 3T3-L1 cell line is difficult to transfect with common methods yielding low transfection efficiencies, b) following transfection, differentiation of the cells into adipocytes takes approximately ten days during which time significant loss of transiently transfected constructs occur, c) selection for stable transfectants proved to have very variable success rates and influenced the downstream differentiation potential of these cells, and d) stable transfection with dual constructs was not feasible. To overcome these and other limitations, the piggyBac transposon system was utilised. This flexible system was adapted and proved sufficiently robust for use as a central method in this thesis. Full details of the development of the piggyBac system and the extensive vector construction carried out in this thesis are described in detail in the methods section.

LMNA over-expression inhibits 3T3-L1 adipogenesis and increases ITM2A expression

Exogenous expression of human LMNA (WT and R482W mutant) has previously been shown to inhibit in vitro differentiation of mouse 3T3-L1 preadipocytes [20]. In order to investigate the effects of LMNA on the transcriptional profile of these cells during the early stages of terminal differentiation 3T3-L1 preadipocytes were successfully stably transfected with human LMNA over-expression constructs (pCDNA3-LMNA-WT and pCDNA3-LMNA-R482W) and differentiation was induced. At 36 h post application of the induction cocktail RNA was extracted from the stably transfected cells and RNA-Seq analysis was performed. Altered expression of over 200 genes was detected in comparison to control, including ITM2A, with a 16 and 8 fold increase in expression observed in response to LMNA-WT and LMNA-R482W mutant respectively.

To confirm the effects of LMNA on ITM2A expression 3T3-L1 preadipocytes were stably transfected with human pCMV(PB)-Flag-LMNA-WT and pCMV(PB)-Flag-LMNA-R482W using a piggyBac transposable system. These preadipocytes were then induced to differentiate, adipogenesis was assessed at day 8 through Oil Red O staining of intracellular lipid droplets (Figure 3.1A) and LMNA over-expression was assessed at the mRNA level using quantitative real-time PCR (qPCR) and at the protein level by western blotting (Figure 3.1B, C). Cells transfected with EV control differentiated well, while cells expressing both WT and R482W mutant LMNA accumulated significantly less lipid droplets, confirmed by Oil Red O quantification (Figure 3.1A).

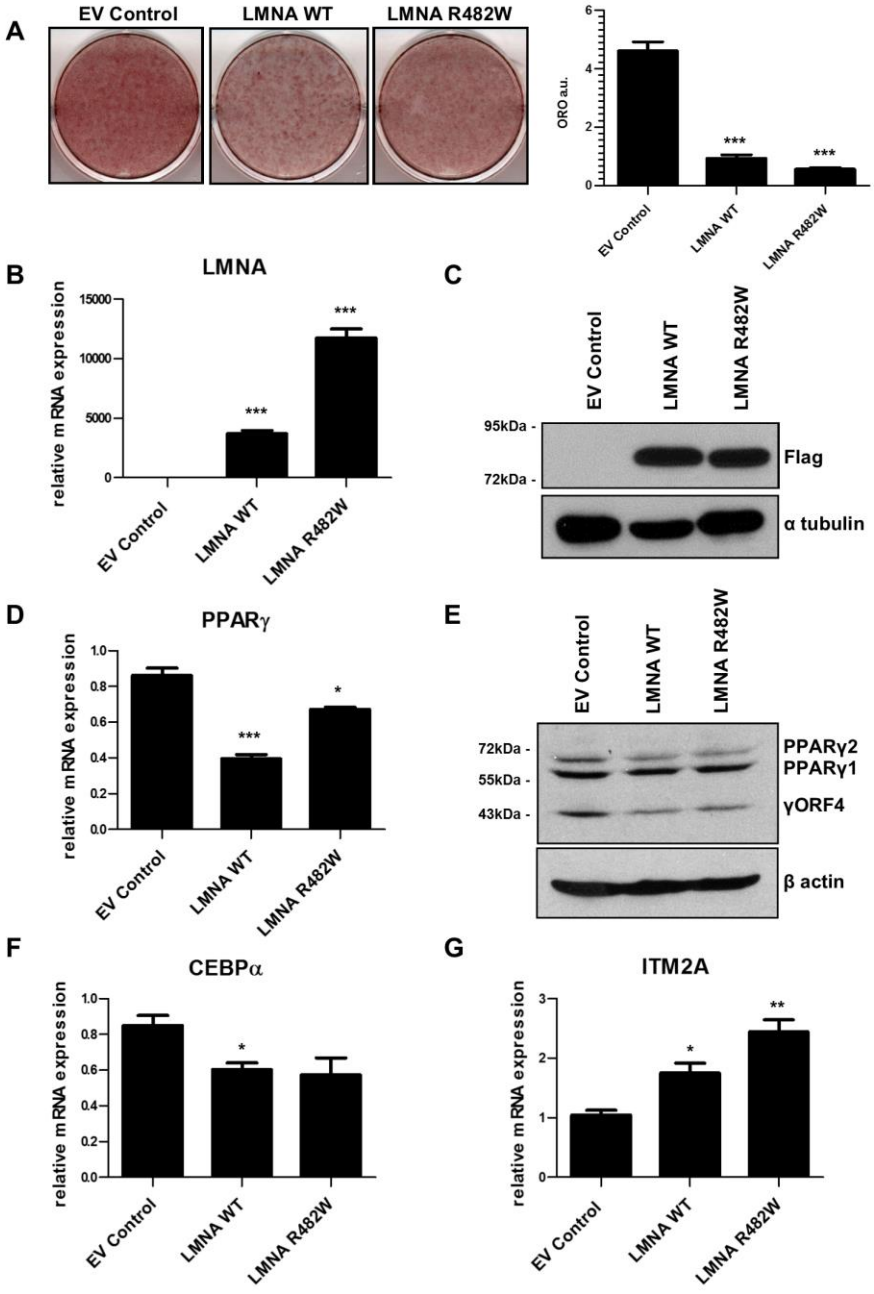

Figure 3.1: LMNA inhibits differentiation of 3T3-L1 cells and increases ITM2A mRNA expression. 3T3-L1 preadipocytes were stably transfected with pCMV(PB)-Flag-LMNA-WT, pCMV(PB)-Flag-LMNA-R482W or empty vector (EV) control pCMV(PB) and induced to differentiate into adipocytes. (A) Adipogenesis was assessed at day 8 post induction; cells were stained for lipid droplet accumulation with Oil Red O. Oil Red O quantification was carried out using ImageJ and expressed as Oil red O absorbance units (ORO a.u.). (B) Total RNA was isolated at day -2 of

differentiation from the stably transfected 3T3-L1 preadipocytes and LMNA expression measured by qPCR using primers specific for human LMNA. (C) Immunoblot analysis of flag-LMNA WT and R482W mutant at day -2. (D, F) Total RNA was isolated at day 4 post induction and the expression of PPARγ and CEBPα was analysed by qPCR. (E) Immunoblot analysis of PPARγ at day 4 post induction. (G) ITM2A expression was analysed at day -2 by qPCR. Student's *t*-test (two-tailed, assuming equal variance) was used to calculate statistical significance compared to empty vector control cells, indicated as follows: *=P<0.05;**=P<0.01; ***=P<0.001.

Previously, several reports have shown that LMNA over-expression reduces PPARγ2 expression in adipogenesis; over-expression of WT and mutant LMNA in 3T3-L1 cells [20] and in MSCs [176] produced this effect while reduction of PPARγ2 expression was also observed when LMNA over-expression was driven from an adipose specific promoter in transgenic mice (55). To determine the effects of LMNA on specific adipogenic markers, PPARγ2 and CEBPα expression was measured at day 4 in differentiating 3T3-L1 cells expressing WT or R482W mutant LMNA and the expression of both markers was reduced in these cells in comparison with the control (Figure 3.1D, F). Immunoblot analysis of PPARγ at day 4 of differentiation revealed the presence of 3 PPARγ isoforms of ~60, ~55 and ~45 kDa respectively (Figure 3.1E). The two larger isoforms PPARγ2 and PPARγ1, are produced through the use of alternative promoters and have differential abilities to promote adipogenesis. PPARγ2 has an additional 28 N terminal amino acids and is exclusively expressed in adipose tissue, where it functions as a master regulator of adipogenesis [123–125]. A number of studies have identified a smaller PPARγ isoform, known as γORF4, which does not contain the ligand-binding domain of PPARγ1 and 2 and displays dominant negative activity towards PPARγ [125,153]. It is likely, although not confirmed, that the 45kDA protein detected here is the previously described γORF4. Interestingly, ectopic expression of WT and R482W mutant LMNA appears not only to reduce PPARγ2 as expected, but also γORF4, while having little to no effect on PPARγ1 (Figure 3.1E).

Having confirmed LMNA over expression and the resulting inhibition of adipogenic differentiation, ITM2A expression levels were assessed in the stably transfected 3T3-L1 preadipocytes. Both WT and R482W mutant LMNA increased endogenous ITM2A expression levels (Figure 3.1G).

Endogenous ITM2A expression and promoter activity in 3T3-L1 differentiation

ITM2A expression has previously been characterised in chondrogenic and myogenic differentiation where it is up-regulated at distinct stages of each of the respective differentiation programmes [170,171]. Microarray analysis of gene expression in 3T3-L1 differentiation has reported relatively low levels of ITM2A expression throughout differentiation with little variation observed across the adipogenic programme [178]. ITM2A expression was profiled during 3T3-L1 differentiation and similar to the microarray data previously described relatively low expression of ITM2A was observed, however a significant down-regulation of gene expression at day 2 was detected (Figure 3.2), approximately 48 h post application of the induction cocktail. This reduction in ITM2A expression was consistently observed at this specific stage of cell differentiation. Expression levels consistently reverted back to pre-induction levels by 96 h.

The in-vitro differentiation of 3T3-L1 preadipocytes involves the growth of these cells to confluence (day-2) where they undergo growth arrest. Induction of differentiation (day 0) is triggered by the application of an induction cocktail that activates insulin growth factor (Insulin), cAMP (IBMX) and glucocorticoid (dexamethasone) signalling pathways. Approximately 16 to 20 h post induction, the cells re-enter the cell cycle and undergo MCE, after which point they exit the cell cycle and terminally differentiate. The adipogenic transcription factors; CEBPα and PPARγ, are up-regulated post MCE and proceed to drive the adipogenic programme (101,88).

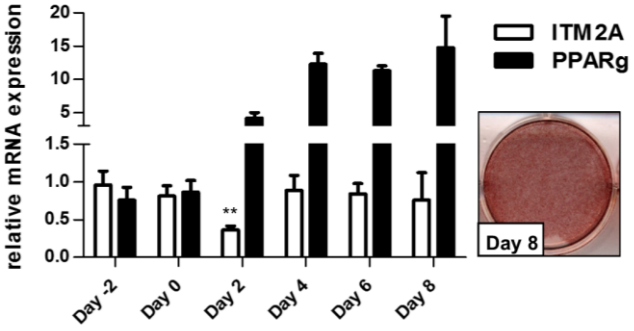

Figure 3.2: Endogenous ITM2A expression in 3T3-L1 differentiation. 3T3-L1 preadipocytes were grown to confluence (day-2) and two days later induction media was applied (day 0). A further two days later cells were supplemented with fresh media containing insulin (day 2). Following this, fresh media was applied every two days until day 8. Adipogenesis was assessed at day 8 when cells were stained for lipid droplet accumulation with Oil Red O. Total RNA was isolated at the indicated time points during 3T3-L1 differentiation. ITM2A and PPARγ expression was analysed by qPCR. Transcript expression at the various time points is shown relative to expression at day 0. A Student's *t*-test (two-tailed, assuming equal variance) was used to calculate statistical significance at day 2 is in comparison to transcript levels at day 0, indicated as follows: *=P<0.05;**=P<0.01; ***=P<0.001.

In order to explore the relationship between these induction components and the observed reduction in ITM2A expression we constructed a piggyBac transposable luciferase reporter plasmids containing a 2kb fragments of the mouse ITM2A proximal promoter (Figure 3.3A) and analysed its activity in response to full (MDI) and sub-maximal (DI or D) induction media. 3T3-L1 preadipocytes were stably transfected with the luciferase construct, grown to confluence, and induced to differentiate. Oil-Red-O staining of lipid droplets at day 8 showed reduced adiposity of cells treated with the sub-maximal induction cocktail (DI or D). Luciferase activity was measured throughout cell differentiation and the ITM2A reporter construct displayed similar activity to that of the endogenous promoter, with reduced luciferase activity observed at day 2 of differentiation, in response to the full induction mix (MDI) when compared to limited induction with DI or D (Figure 3.3B). These results are in agreement with previously detected endogenous down-regulation of ITM2A mRNA at day 2 of differentiation, and indicate that full induction of adipogenesis is associated with a reduction of ITM2A promoter activity in the early stages of differentiation. To identify elements within the 2kb promoter responsible for this down-regulation, deletion analysis was carried out in which a series of smaller piggyBac transposable luciferase reporter plasmids were constructed containing 1.5kb, 1kb and 0.5kb fragments of the ITM2A promoter (Figure 3.3A). Luciferase activity was assessed during 3T3-L1 differentiation in response to full (MDI) and submaximal induction (DI or D), and similar results were observed with these smaller promoter constructs (Figure 3.3B). Although the 1kb promoter was found to behave slightly differently in that pre-induction expression levels of luciferase were observed at day 4 – somewhat earlier than the other constructs.

This luciferase data indicates that the M (IBMX) component of the MDI leads to a reduction in ITM2A promoter activity and the region of the promoter governing the reduction is in the 500bp immediately upstream of the ITM2A gene. This is most likely to be mediated by CREB interaction with the CRE binding site on the ITM2A promoter as forskolin like IBMX is known to raise cellular cAMP levels and activate the cAMP-PKA-CREB signalling pathway in adipogenesis. These two agents lead to similar levels of 3T3-L1 and MEF cell differentiation when used in an adipogenic induction cocktail [180,181]. In this scenario, CREB could function as a repressor of ITM2a expression, activated through forskolin or IBMX stimulation of the cAMP-

PKA-CREB signalling pathway. In contrast to the observed situation in adipogenesis it has been reported that forskolin mediated PKA-CREB activation leads to increased human ITM2A promoter activity through a conserved CRE site in transfected HEK293 cells [174]. This indicates that regulation of the ITM2A promoter is likely to differ in different cell contexts with CREB signalling resulting in ITM2A down-regulation during 3T3-L1 cell differentiation and up-regulation in HEK293 cells. As the focus of this thesis was on aspects of adipogenesis influenced by LMNA, the role of CREB in ITM2A regulation was not pursued here, as there have been no reports of LMNA interaction with CREB to date.

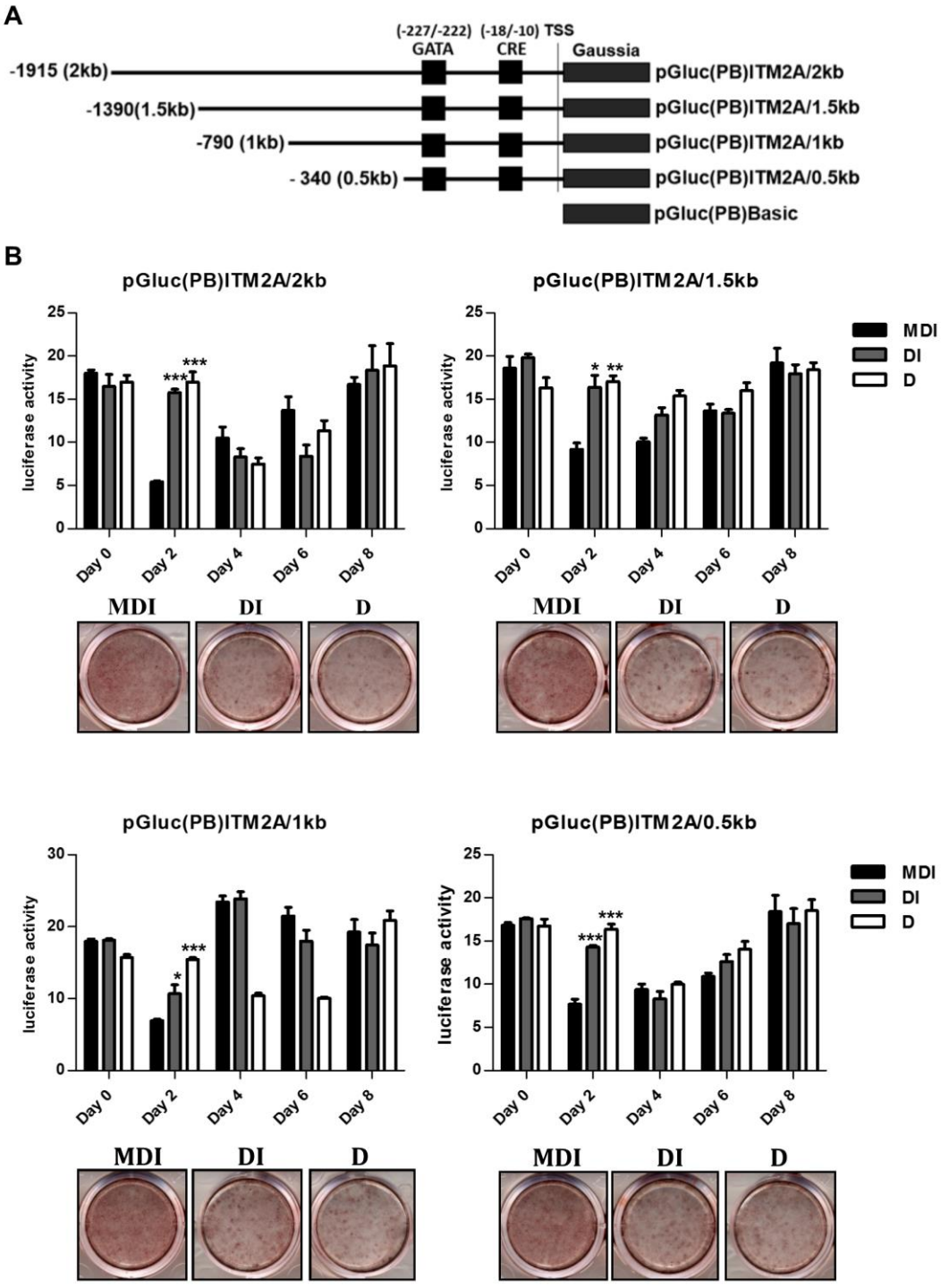

Figure 3.3: ITM2A promoter activity during 3T3-L1 differentiation (A) Schematic depiction of ITM2A promoter luciferase constructs generated. 2kb, 1.5kb, 1kb and 0.5kb promoter fragment were cloned upstream of *Gaussia* luciferase in pGluc(PB) basic vector. The distance (-1915, -1390, -790 and -340) from the transcriptional start site (TSS) and previously predicted GATA and CRE binding sites are shown. (B) Luciferase activity (secreted) in 3T3-L1 cells stably transfected with

pGluc(PB)ITM2A/2kb, pGluc(PB)ITM2A/1.5kb, pGluc(PB)ITM2A/1kb or pGluc(PB)ITM2A/0.5kb throughout differentiation. Cells were induced to differentiate using full differentiation media (MDI– methylisobutylxanthine, dexamethasone and insulin), sub-maximal media (DI– dexamethasone and insulin) or D (dexamethasone) as indicated. Adipogenesis was assessed at day 8 when cells were stained for lipid droplet accumulation with Oil Red O. Luciferase activity is normalised to the pGluc(PB)basic empty vector control. Student's *t*-test (two-tailed, assuming equal variance) was used to calculate statistical significance compared to MDI induced cells, indicated as follows: *=P<0.05;**=P<0.01; ***=P<0.001.

As previously mentioned ITM2A has been described as a GATA3 target in mouse thymocytes where it was identified as one of the most down-regulated genes in a gene chip analysis comparison of GATA3 knockout versus WT cells. Subsequently a GATA binding site was identified in the proximal ITM2A promoter and GATA3 overexpression was shown to activate a 2kb ITM2A promoter reporter construct in the GATA3 deficient M12 mouse cell line [172].

The role of specific GATA transcription factors in adipogenesis has previously been described in a number of studies. GATA2 and GATA3 are expressed in preadipocytes and are down-regulated as the cells progress through the adipogenic programme [182]. GATA3 over-expression has been shown to inhibit 3T3-L1 differentiation by binding directly to the PPARγ promoter and down-regulating PPARγ expression [182,183], as well as by modulating CEBP activity through protein-protein interactions [182].

Recently, GATA3 has been identified as a Wnt/β-catenin signalling target in adipogenesis. Canonical Wnt/β-catenin signalling is a well characterised modulator of adipogenesis. Much like the GATA transcription factors, specific Wnt glycoproteins (WNT10a, WNT10b, WNT6) are down-regulated during adipogenesis as they are potent inhibitors of adipocyte terminal differentiation (88,183). Wang and Di (2015) [183] showed that β-catenin up-regulates GATA3 expression which leads to the inhibition of 3T3-L1 cell differentiation. LiCl treatment is known to activate Wnt/β-catenin signalling and increase cellular β-catenin [185]. Wang and Di (2015) demonstrated that LiCl activation of Wnt/β-catenin signalling leads to a marked increase in GATA3 expression, increased GATA3 binding to the PPARγ promoter and a resulting decrease in PPARγ expression.

Considering that a) the RNA-Seq analysis indicates that overexpressed WT or R482W mutant LMNA increases expression of Wnt6, b) Wnt/β-catenin signalling can up-regulate GATA3 expression leading to the inhibition of 3T3-L1 cell differentiation [183], and c) previous reports that describe both increased and decreased β-catenin activity in response to LMNA over-expression and mutation, respectively [176,186], it was of interest to explore the role of the GATA binding site in the ITM2A promoter.

Two additional luciferase reporter constructs were generated for this purpose. As the GATA transcription factors are important modulators of adipogenesis, the previously described GATA3 binding site (-222 to -227) was mutated in the 0.5kb ITM2A promoter construct, and a smaller 0.35kb reporter construct was generated to completely exclude the GATA site (Figure 3.4A). 3T3-L1 preadipocytes were stably transfected with these luciferase constructs, grown to confluence, and induced to differentiate. Luciferase activity was measured throughout cell differentiation. Both the GATA mutant and 0.35kb reporter constructs displayed similar activity to the 0.5kb ITM2A construct, with a significant down-regulation of promoter activity at day 2 of differentiation (Figure 3.4B). Therefore, the GATA element in the ITM2A promoter does not play a role in ITM2A down-regulation during early 3T3-L1 differentiation.

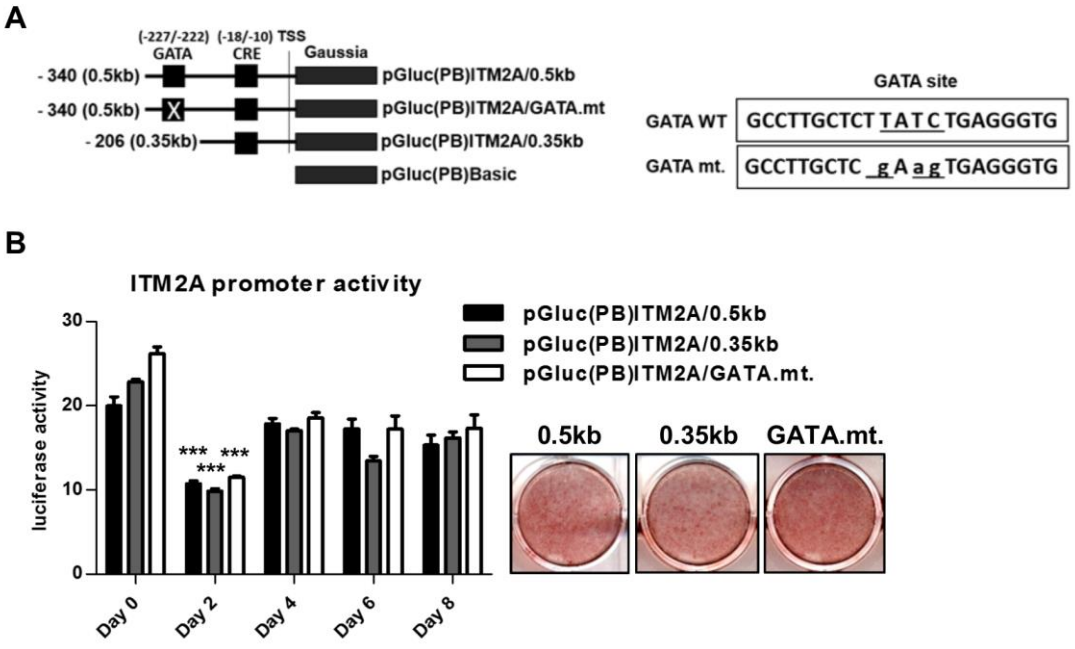

Figure 3.4: GATA mutation of the ITM2A promoter in 3T3-L1 differentiation. (A) Schematic depiction of ITM2A promoter luciferase constructs generated. 0.5kb GATA mutant and 0.35kb promoter fragments were cloned upstream of *Gaussia* luciferase in pGluc(PB) basic vector. WT and mutant GATA sequences are shown. (B) Luciferase activity (secreted) in 3T3-L1 cells stably transfected with pGluc(PB)ITM2A/0.5kb, pGluc(PB)ITM2A/GATA.mt, and pGluc(PB)ITM2A/0.35kb during differentiation. Cells were induced to differentiate using full differentiation media (MDI). Adipogenesis was assessed at day 8 when cells were stained for lipid droplet accumulation with Oil Red O. Luciferase activity is normalised to the pGluc(PB)basic empty vector control. Student's *t*-test (two-tailed, assuming equal variance) was used to calculate statistical significance at day 2 in comparison to luciferase activity at day 0, indicated as follows: *=P<0.05;**=P<0.01; ***=P<0.001.

To investigate the possibility of ITM2A as a downstream target of Wnt/β-catenin signalling in the context of adipogenesis, 3T3-L1 preadipocytes were grown to confluence and induced to differentiate with a 20mM LiCl treatment or vehicle control. Oil-Red-O staining of lipid droplets at day 8 of differentiation showed complete inhibition of adipogenesis in cells treated with LiCl (Figure 3.5A). To verify that the reduced lipid droplet accumulation observed in response to LiCl was not due

to cell death or reduced cell viability, an MTT assay was carried out with varying concentrations of LiCl applied to 3T3-L1 cells, and a 20mM treatment was seen to have no effect on cell viability (Figure 3.5D). PPARγ and CEBPα expression was assessed by qPCR in treated and control cells, and as expected the expression of both adipogenic factors was significantly reduced by LiCl mediated inhibition of cell differentiation (Figure 3.5B). Analysis of ITM2A expression in these cells, showed that LiCl had no effect on ITM2A expression at days 2, 4 or 6 of differentiation (Figure 3.5A). This suggests that ITM2A expression is unaffected by a β-catenin mediated increase in GATA3 during 3T3-L1 differentiation, and does not contribute to the LiCl mediated inhibition of adipogenesis. Interestingly, analysis of luciferase activity during 3T3-L1 differentiation in cells transfected with the 0.5kb, 0.35kb and GATA mutant reporter constructs during 3T3-L1 differentiation in response to LiCl treatment showed an increase in the luciferase activity in all transfected cells (Figure 3.5C). LiCl appeared to increase ITM2A promoter driven luciferase activity at days 4 and 6 of cell differentiation despite having no effect on endogenous mRNA expression at these same time points. It is unclear why LiCl led to increased ITM2A promoter driven luciferase activity in this system, one possible mechanisms could be that the LiCl treatment somehow increased the stability of the secreted *Gaussia* protein, thus leading to an increase in luciferase signal.

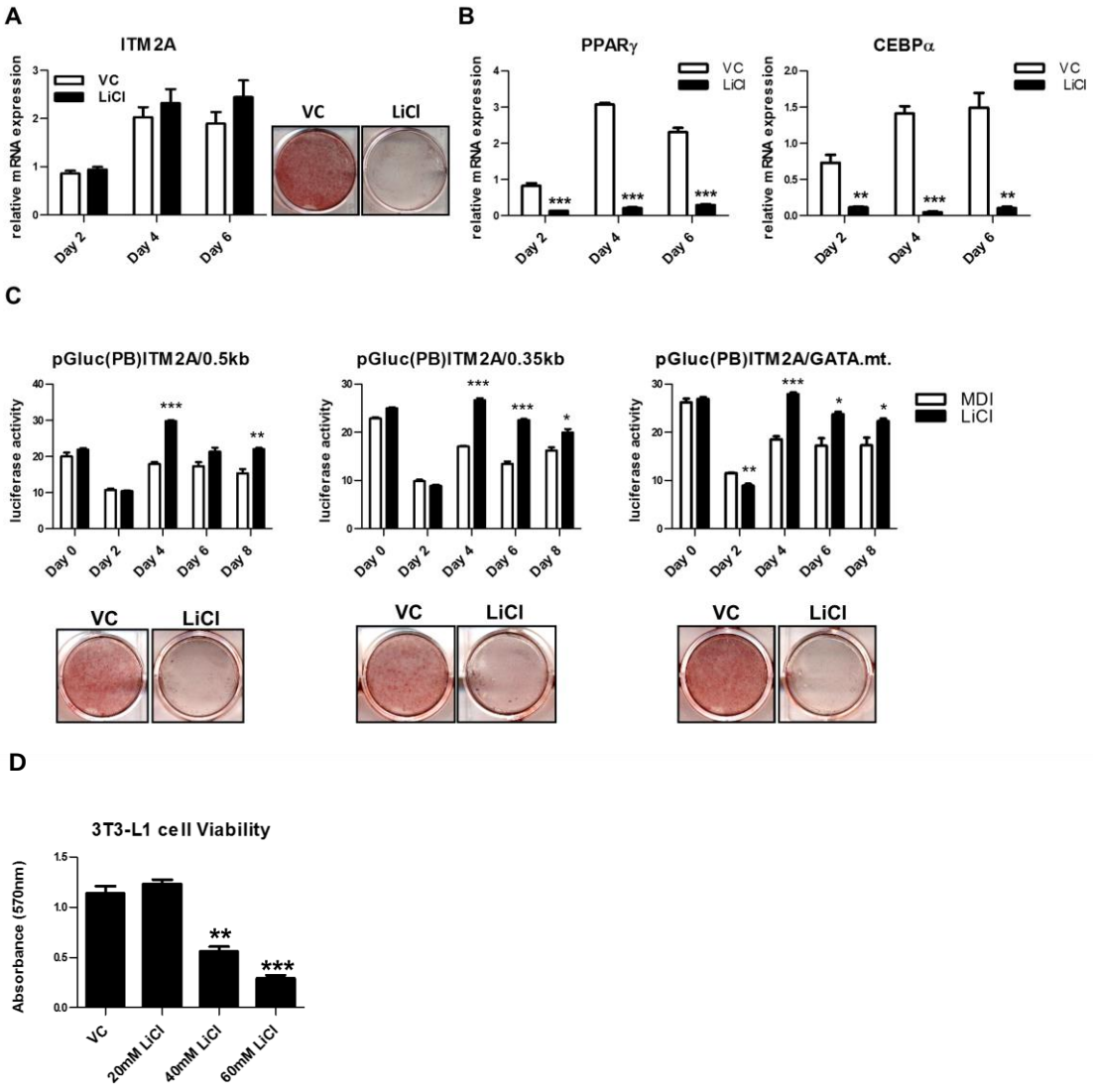

Figure 3.5: LiCl treatment does not affect ITM2A mRNA expression in 3T3-L1 differentiation. 3T3-L1 preadipocytes were grown to confluence and induced to differentiate with a 20mM LiCl treatment or a vehicle control. (A) qPCR analysis of ITM2A expression in LiCl and vehicle control treated cells during cell differentiation. Oil Red O staining was carried out at day 8 (B) qPCR analysis of PPARγ and CEBPα in LiCl and vehicle control treated cells. (C) Luciferase activity (secreted) in 3T3-L1 cells stably transfected with pGluc(PB)ITM2A/0.5kb, pGluc(PB)ITM2A/GATA.mt, and pGluc(PB)ITM2A/0.35kb during differentiation. Cells were induced to differentiate using full differentiation media (MDI) and treated with 20mM LiCl treatment or a vehicle control. (D) 3T3-L1 preadipocytes were treated with increasing concentrations (20mM, 40mM, 60mM) of LiCl for 48hrs and an MTT assay was performed to assess cell viability. A Student's *t*-test (two-tailed, assuming equal

variance) was used to calculate statistical significance between LiCl and vehicle control treated cells, indicated as follows: *=P<0.05;**=P<0.01; ***=P<0.001.

The effect of LMNA on ITM2A promoter

In an attempt to investigate the effects of LMNA expression on the ITM2A promoter we carried out a series of transient co-transfections in both 3T3-L1 and 3T3-NIH cells. 3T3-NIH cells were used as they exhibit a much higher transfection efficiency when compared to that observed for 3T3-L1 cells, which would allow for more sensitive detection of LMNA mediated effects on ITM2A promoter activity. In all instances LMNA overexpression affected the expression of luciferase from the internal transfection control preventing data normalisation. This phenomenon was observed with all three constitutive promoters commonly used in standard control luciferase constructs (CMV, SV40 and HSV-TK promoters). Figure 3.6 shows LMNA mediates reduction in SV40 driven firefly luciferase.

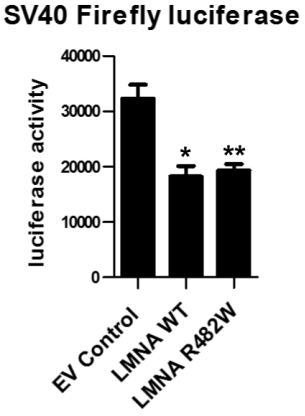

Figure 3.6: LMNA effect on SV40 driven firefly luciferase. 3T3-NIH cells were transiently transfected with a constitutively expressed SV40-Firefly luciferase and LMNA over-expression constructs (WT and R482W mutant) or EV control. A Student's *t*-test (two-tailed, assuming equal variance) was used to calculate statistical significance compared to empty vector control transfected cells, indicated as follows: *=P<0.05;**=P<0.01; ***=P<0.001.

In order to circumvent this issue we made LMNA/ITM2A reporter stable 3T3-L1 lines using a two-step transfection and selection approach; 3T3-L1 preadipocytes were stably transfected with the 2kb, 1.5kb, 1kb and 0.5kb ITM2A promoter reporter constructs (G418 selection) and subsequently stably transfected with LMNA WT or R482W over-expression constructs (puromycin selection). This method eliminates variation caused by differences in transfection efficiencies and allows for the exclusion of an internal control luciferase. These LMNA/ITM2A reporter stable lines cells were grown to confluence and induced to differentiate. Luciferase activity was measured at various time points throughout differentiation and Oil-Red-O staining of lipid droplets at day 8 showed LMNA mediated inhibition of adipogenesis (Figure 3.7A, B).

Figure 3.7 (A) shows the effect of LMNA on the 2kb, 1.5kb, 1kb and 0.5kb ITM2A promoter fragments. Both WT and R482W mutant LMNA significantly increased luciferase activity driven by all four promoters at day 4 of differentiation while WT LMNA over-expression also led to increased activity from the 2kb promoter fragment at day -2. Analysis of ITM2A mRNA expression at day 4 of differentiation in LMNA transfected cells identified an increase in ITM2A expression in response to both WT and R482W mutant LMNA (Figure 3.7B).

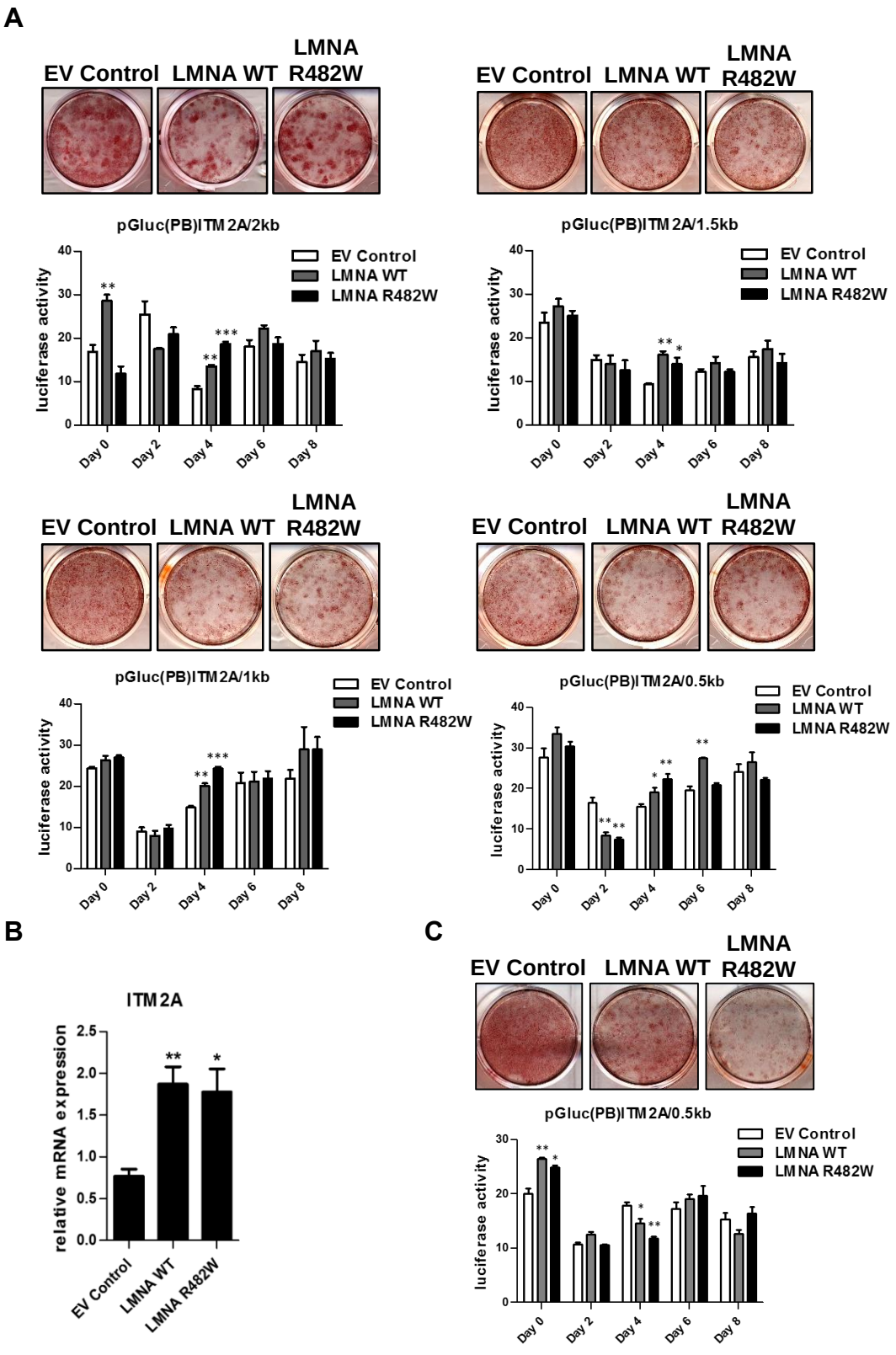

Figure 3.7: LMNA effect on ITM2A promoter activity in 3T3-L1 differentiation. (A) Luciferase activity (secreted) in 3T3-L1 cells stably transfected with pGluc(PB)ITM2A/2kb, pGluc(PB)ITM2A/1.5kb, pGluc(PB)ITM2A/1kb or

pGluc(PB)ITM2A/0.5kb and LMNA over-expression constructs (WT and R482W mutant) or EV control. (B) 3T3-L1 cells were stably transfected with pCDNA3-LMNA-WT, pCDNA3-LMNA-R482W or pCDNA3.EV and induced to differentiate. ITM2A expression was assessed at day 4 of differentiation by qPCR. (C) Luciferase activity in 3T3-L1 cells stably transfected with pGluc(PB)ITM2A/0.5kb and LMNA over-expression constructs (WT and R482W mutant) or EV control. Adipogenesis was assessed at day 8 when cells were stained for lipid droplet accumulation with Oil Red O. Luciferase activity is normalised to the pGluc(PB)basic empty vector control. Student's *t*-test (two-tailed, assuming equal variance) was used to calculate statistical significance compared to EV control, indicated as follows: *=P<0.05;**=P<0.01; ***=P<0.001.

Figure 3.7 (A) demonstrates a significant LMNA effect on the ITM2A promoter in the four independently established stably transfected cell lines. Figure 3.7 (B) shows that WT and R482W mutant LMNA in an independent experiment increases expression of endogenous ITM2A at day 4 and is consistent with the result shown in Figure 3.7 (A). However, it should be noted that consistency was an issue with respect to reproducibility in these experiments. For example, when this experiment was repeated with the 0.5kb reporter construct (Figure 3.7C), the opposite effect was observed at day 4, with LMNA reducing promoter activity in comparison to the empty vector control. However, in this case, LMNA increased 0.5kb promoter activity at day-2, an effect which was not observed in the previous experiment. These results indicate that significant variation occurs between cell differentiations and the underlying reason for this is unclear. In our experience transfection and selection of 3T3-L1 cells can sporadically affect the adipogenic potential of these cells. We observed a large degree of variation in the ability of dual transfected/selected cells to differentiate as well as disparity in the ability of LMNA to inhibit differentiation in this context. The data shown here represents differentiations in which LMNA was seen to reduce adipogenesis, as assessed by Oil-Red-O staining at day 8 of differentiation. Although it is well established here and in prior literature that LMNA over expression inhibits adipogenesis in 3T3-L1 cells, a significant number of 3T3-L1 differentiations were observed where over expressed LMNA did not effectively inhibit differentiation. The reason for this is also unclear. One possibility is that LMNA inhibitory effects may be restricted to a limited time period in differentiation with effective inhibitory

concentrations being reached at different times in different differentiations. In such a scenario, achievement of an effective inhibitory concentration early in differentiation or in the period preceding differentiation may affect gene expression at an earlier time point than achieving an effective inhibitory concentration later in differentiation. This could account for the differences observed between Figure 3.7 (A) vs. 3.7 (C). The lack of inhibition of differentiation by LMNA that is observed in some cases may indicate that LMNA did not achieve an effective inhibitory concentration during the active time period. High resolution measurement of LMNA with respect to time and abundance will be required to test such an idea.

In addition, it is important to note that although LMNA was seen to inhibit differentiation in all five of the Oil Red O cell images included in figure 3.7, variation is observed in the quantities of lipid droplet accumulation between empty vector controls as well as variation in the degree of inhibition mediated by LMNA overexpression. It is possible that this variation could contribute to the inconsistencies observed in the luciferase data obtained from these cells.

ITM2A over-expression inhibits 3T3-L1 differentiation

To investigate the role of ITM2A in adipogenesis we stably transfected 3T3-L1 preadipocytes with a piggyBac transposable ITM2A over-expression construct (pMSCV(PB)ITM2A) or empty vector control (pMSCV(PB)) and induced the cells to differentiate. Oil Red O staining at day 8 showed that 3T3-L1 differentiation was inhibited to a moderate but significant degree in the ITM2A expressing cells in comparison to EV control (Figure 3.8A). QPCR analysis of ITM2A expression at various time points in these differentiating cells confirmed maintenance of ITM2A over-expression throughout adipogenesis (Figure 3.8B).

PPARγ expression appeared to be unaltered by increased ITM2A expression; qPCR analysis showed no significant difference in PPARγ expression throughout differentiation in comparison to EV control (Figure 3.8C) and PPARγ protein isoforms were equally unaffected (Figure 3.8D, E). CEBPα expression was also assessed through qPCR analysis, and although small variations were observed, overall no significant differences between ITM2A over expressing cells and EV control were observed (Figure 3.8F).

Detection of ectopic ITM2A protein in 3T3-L1 cells was attempted using both a Flag antibody and a commercially available ITM2A antibody, but was unsuccessful presumably due to limited over expression. Similar results were reported in a previous study [170] where detection of ITM2A protein in the bipotential C3H10T1/2 cell line proved difficult. The mechanism underlying the difficulty in overexpressing ITM2A to high levels in 3T3-L1 cells is unclear. In the experiment described, the overall levels of ITM2A mRNA over-expression in 3T3-L1 cells were approximately 8 fold higher than control. Attempts were made to over-express ITM2A at a higher level by placing the gene under the control of a strong CMV promoter to see if adipogenesis could be inhibited further by higher ITM2A expression levels and to facilitate ITM2A protein detection. However, expression levels of ITM2A gene under the CMV promoter (pCMV(PB)ITM2A), were similar to the levels observed with the MSCV promoter.

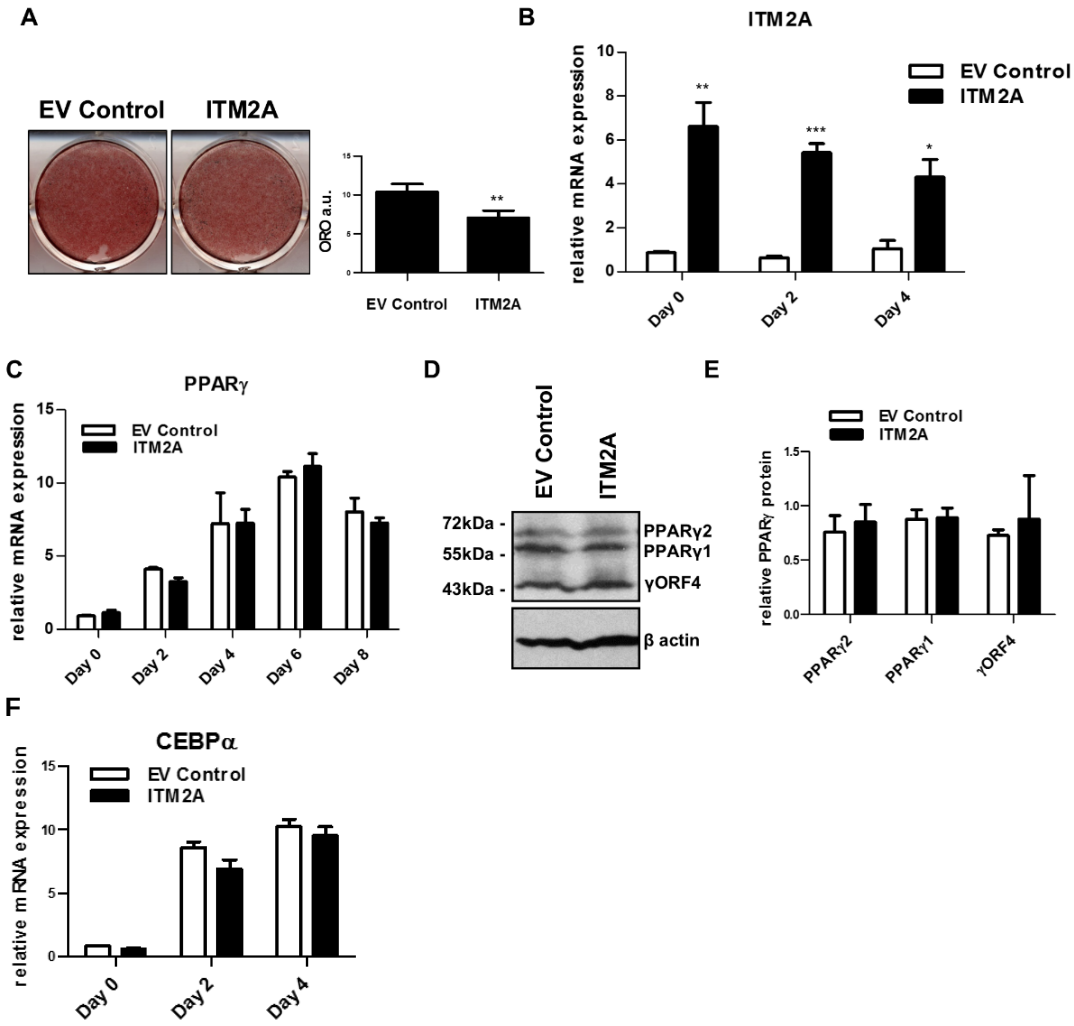

Figure 3.8: ITM2A over-expression in 3T3-L1 differentiation. 3T3-L1 preadipocytes were stably transfected with pMSCV(PB)-ITM2A or empty vector control pMSCV(PB) plasmid and induced to differentiate into adipocytes. (A) Adipogenesis was assessed at day 8 post induction by staining with Oil Red O and quantification was performed using ImageJ and expressed as Oil red O absorbance units (ORO a.u.). (B,C,F) qPCR analysis of ITM2A,PPARγ and CEBPα expression during differentiation of stably transfected 3T3-L1 cells. (D) Immunoblot analysis of PPARγ at day 4 post induction. (E) Quantification of PPARγ protein relative to β-actin, with mean and standard deviations determined by densitometry from two biological replicates. A Student's *t*-test (two-tailed, assuming equal variance) was used to calculate statistical significance compared to empty vector control cells, indicated as follows: *=P<0.05;**=P<0.01; ***=P<0.001.

Knockdown of ITM2A enhances 3T3-L1 adipogenesis

The role of endogenous ITM2A in 3T3-L1 cell differentiation was explored by silencing ITM2A expression. Initially 3T3-L1 preadipocytes were stably transfected with pRFP.shITM2A(1,2,3 and 4) or scramble control pRFP.shControl and induced to differentiate. A stimulatory effect on adipogenesis was observed with 3 (shITM2A-1, -2 and -3) out of 4 different shITM2A constructs assayed when compared to the scramble control (Figure 3.9A). QPCR analysis of ITM2A expression confirmed the knockdown of endogenous ITM2A by shITM2A-1, -2 and -3 at various time points across differentiation (Figure 3.9B) and shITM2A-1 was selected as the most potent knockdown agent.

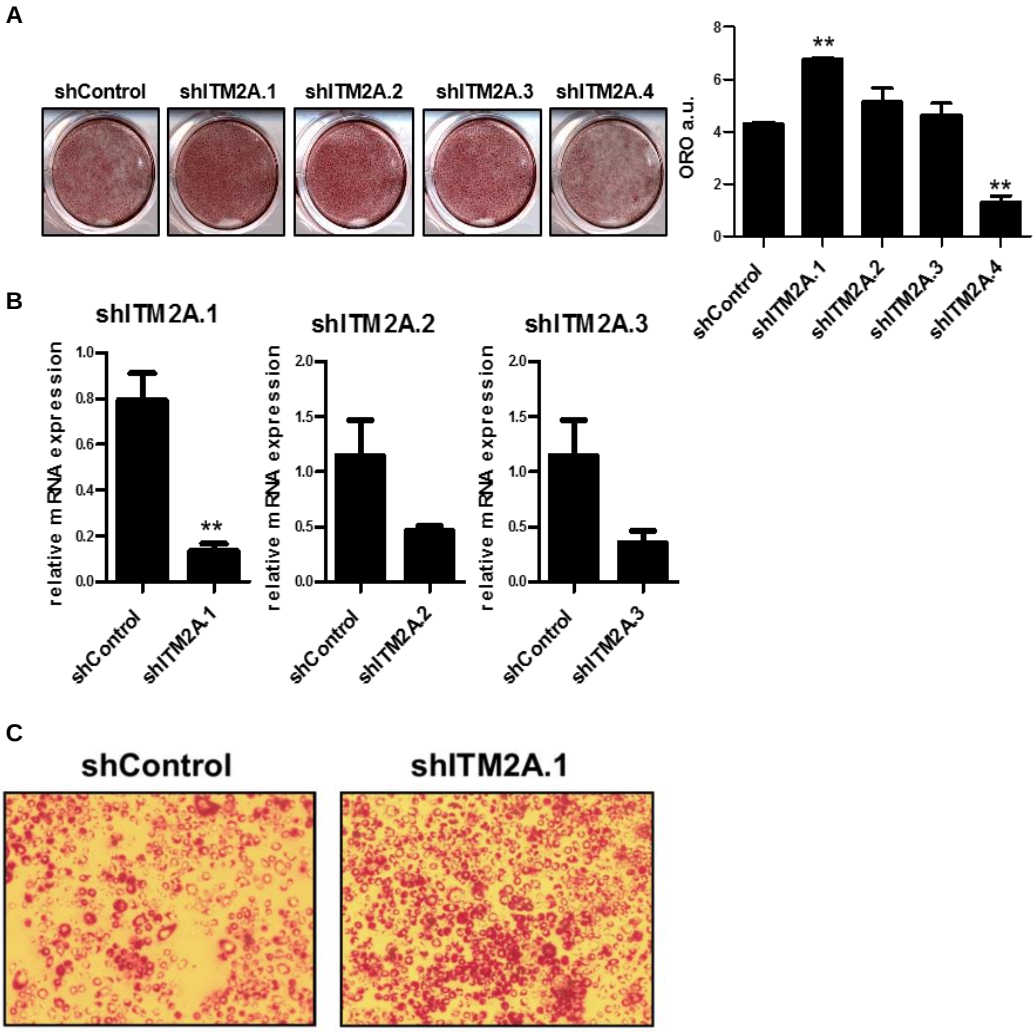

Figure 3.9: shRNA mediated knockdown of ITM2A in 3T3-L1 differentiation. (A) 3T3-L1 preadipocytes were stably transfected with pRFP(PB).shITM2A(1,2,3 and 4) or scramble control pRFP(PB).shControl and induced to differentiate. Adipogenesis

was assessed at day 8 post induction by staining with Oil Red O; quantification was carried out using ImageJ and expressed as Oil Red O absorbance units (ORO a.u.). (B) qPCR analysis of ITM2A expression at day 2 during 3T3-L1 differentiation. (C) 20X microscope image depicting Oil red O staining of shControl and shITM2A.1 transfected cells (Leica DM IL). Statistical significance compared to scramble control cells indicated as follows: *=P<0.05;**=P<0.01; ***=P<0.001.

3T3-L1 preadipocytes were stably transfected with a piggyBac transposable ITM2A shRNA knockdown construct, pRFP(PB).shITM2A.1 or scramble control pRFP(PB).shControl and induced to differentiate. Knockdown of endogenous ITM2A appeared to enhance adipogenesis in comparison to control cells (Figure 3.10A). The stably transfected cells were induced to differentiate using full induction media MDI, sub-maximal media DI or D alone. Enhanced adipogenesis was observed in response to the full MDI induction media while a significant difference was not observed with DI or D alone (Figure 3.10A). QPCR analysis of ITM2A expression confirmed the knockdown of endogenous ITM2A at various time points across differentiation (Figure 3.10B). Similarly to the difficulty encountered with detection of ectopically expressed ITM2A, detection of the endogenous ITM2A protein in 3T3-L1 cells using the commercial ITM2A antibody was unsuccessful. In contrast, ITM2A over-expression was detectible in transfected 3T3-NIH mouse fibroblasts. Thus, validation of shRNA mediated ITM2A knockdown at the protein level was performed in these cells. 3T3-NIH cells were transfected with pCMV.ITM2A and either pRFP(PB).shITM2A or scramble control pRFP(PB).shControl. ITM2A protein knockdown was analysed by immunoblot with ITM2A and Flag antibodies (Figure 3.10C) and a number of ITM2A protein species were detected.

To date, there is a limited amount of data published on the murine ITM2A protein. The predicted molecular weight of the 263 amino acid protein is 30kDa [168], however immunoblot detection has previously reported a 45kDa protein in mouse brain tissue and two protein species of 45kDa and 43kDa in the EL4 T lymphocyte cell line [187,188]. An N-linked glycosylation site is predicted at amino acid 166 [168], and protein de-glycosylation in the EL4 T lymphocytes was seen to convert the 45kDa and 43kDa proteins to a smaller 39kDa protein [188]. Proteolytic processing of the ITM2A related

protein ITM2B (human) has been characterized in HEK293TR cells, and a number of cleavage events identified. Firstly, a propeptide is released from the C-terminal of the protein through furin-mediated cleavage, followed by shedding of the extracellular BRICHOS domain via ADAM10 processing. Finally, the residual N-terminal fragment undergoes intramembrane proteolysis by a signal peptide peptidase-like 2 (SPPL2) protease, to produce an intracellular domain [189,190]. As protein structure is highly conserved within the ITM2 family [169], it is likely that ITM2A is also processed in a similar fashion.

A number of protein species were detected when ITM2A was over-expressed in 3T3-NIH cells. A 90kDa protein was detected using both ITM2A and FLAG antibodies (Figure 3.10C) and its expression was inhibited by shITM2A. Although much larger than the predicted ITM2A size, it could represent a heavily glycosylated form of the protein. We consistently detected a 20kDa protein, which was eliminated by shITM2A expression. This protein could potentially represent an ITM2A N-terminal fraction produced by cleavage similar to that described for ITM2B. ITM2A is Flag-tagged at the C terminal and in support of our cleavage theory, the Flag antibody was unable to detect the 20kDa protein. A 40 kDa protein was also detected using the FLAG antibody which was partially knocked down by the shITM2A. Finally, the ITM2A antibody was seen to bind a 20kDa protein in the cell culture media, which could potentially represent the cleaved and secreted BRICHOS domain (Figure 3.10H).
PPARγ and CEBPα expression in transfected cells was analysed by qPCR during differentiation. No differences were observed in the expression of either transcription factor in response to ITM2A knockdown (Figure 3.10D). Surprisingly, when PPARγ protein levels were measured in these cells, an increase in all three PPARγ isoforms was observed at day 2 and 4 of differentiation in comparison with control cells (Figure 3.10E, F). Increased PPARγ1 protein was also observed at day 0 (Figure 3.10E, F) before induction of the adipose specific PPARγ2 isoform. Densitometry performed across biological replicates (Figure 3.10G) confirmed a significant increase in PPARγ1 and PPARγ2 protein isoforms, while elevated γORF4 was less consistent. The observation that there was no difference in PPARγ mRNA expression between shITM2A and shControl transfected cells indicates that ITM2A knockdown is likely to influence PPARγ protein stability. An increase in PPARγ2 protein stability during

adipogenic differentiation would be expected to promote adipogenesis and could account for the observed increase of lipid droplet accumulation in cells transfected with shITM2A.

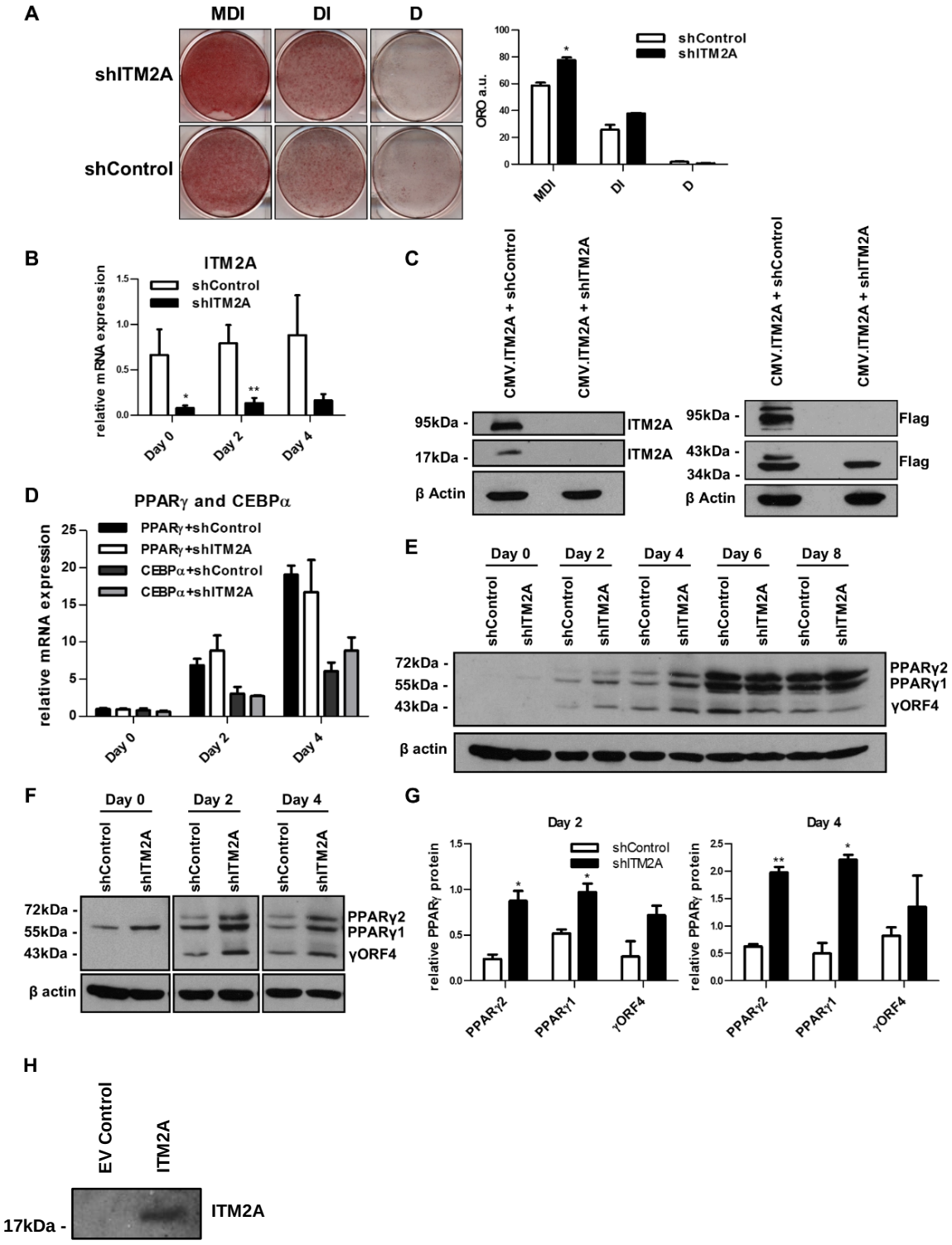

Figure 3.10: shRNA mediated knockdown of ITM2A enhances 3T3-L1 differentiation and increases PPARγ protein. 3T3-L1 preadipocytes were stably transfected with pRFP(PB).shITM2A or scramble control pRFP(PB).shControl and induced to differentiate using full induction media MDI (methylisobutylxanthine,

dexamethasone and insulin), sub-maximal media DI (dexamethasone and insulin) or D (dexamethasone) as indicated. (A) Adipogenesis was assessed at day 8 post induction by staining with Oil Red O; quantification was carried out using ImageJ and expressed as Oil Red O absorbance units (ORO a.u.). (B, D) qPCR analysis of ITM2A, PPARγ and CEBPα and immunoblot analysis of PPARγ (E, F) expression during differentiation of 3T3-L1 cells stably transfected with pRFP(PB).shITM2A or scramble control pRFP(PB). (C) Immunoblot analysis of ITM2A knockdown in 3T3-NIH cells dual transfected with pCMV.ITM2A and pRFP(PB).shITM2A or pRFP(PB).sh.Control. (G) Quantification of PPARγ protein isoforms relative to β-actin, with mean and standard deviations determined by densitometry from two biological replicates. (H) Immunoblot analysis of ITM2A in 3T3-L1 culture media. Statistical significance compared to scramble control cells indicated as follows: *=P<0.05;**=P<0.01; ***=P<0.001.

ITM2A knockdown rescues LMNA inhibition of adipogenesis in 3T3-L1 differentiation

The observation that LMNA increases ITM2A expression and knockdown of ITM2A enhances adipogenesis led us to consider whether ITM2A knockdown could ameliorate LMNA inhibition of adipogenesis. To investigate this idea we generated a series of six dual constructs that contained either LMNA WT, LMNA R482W or empty vector (EV) with shITM2A or shControl. The constructs created were pCMV(PB)-Flag-LMNA-WT.shITM2A, pCMV(PB)-Flag-LMNA-WT.shControl, pCMV(PB)-Flag-LMNA-R482W.shITM2A, pCMV(PB)-Flag-LMNA-R482W.shControl, pCMV(PB).shITM2A and pCMV(PB).shControl. 3T3-L1 preadipocytes were stably transfected with these constructs and induced to differentiate. Figure 3.11(A) shows that ITM2A knockdown rescued inhibition of adipogenesis mediated by both LMNA-WT and LMNA-R482W. Moreover, ITM2A knockdown in the LMNA expressing 3T3-L1 cells enhanced adipogenesis to the same extent as ITM2A knockdown enhanced adipogenesis in the EV control cells. LMNA over-expression was assessed at the mRNA and protein levels (Figure 3.11B, C). Interestingly, increased amounts of LMNA protein were observed when ITM2A expression was reduced (Figure 3.11C), lending support to the notion that ITM2A knockdown somehow influences protein stability in 3T3-L1 cells.

As previously mentioned ITM2A knockdown does not appear to alter PPARγ expression in comparison to shControl (Figure 3.10D). Figure (3.11D) reiterates this, with ITM2A knockdown having no effect on PPARγ mRNA levels at day 4 of differentiation when cells were stably transfected with pCMV(PB).shITM2A or pCMV(PB).shControl. ITM2A knockdown was however able to rescue the LMNA mediated reduction of PPARγ mRNA, and restore it to EV control expression levels. PPARγ was assessed at the protein level and as previously observed LMNA (WT and R482W) over-expression was seen to reduce PPARγ2 while ITM2A knockdown increased the protein levels of all three PPARγ isoforms (Figure 3.11E) This significant increase in PPARγ2 protein, presumably mediated by increased stability, is most likely the driving force behind the enhanced adipogenesis observed in shITM2A transfected cells. The increase in PPARγ2 protein arising from ITM2A knockdown is able to enhance adipogenesis despite the LMNA mediated reduction in

PPARγ transcription and expression. Thus, ITM2A knockdown not only rescues but also overrides LMNA inhibition of adipogenesis.

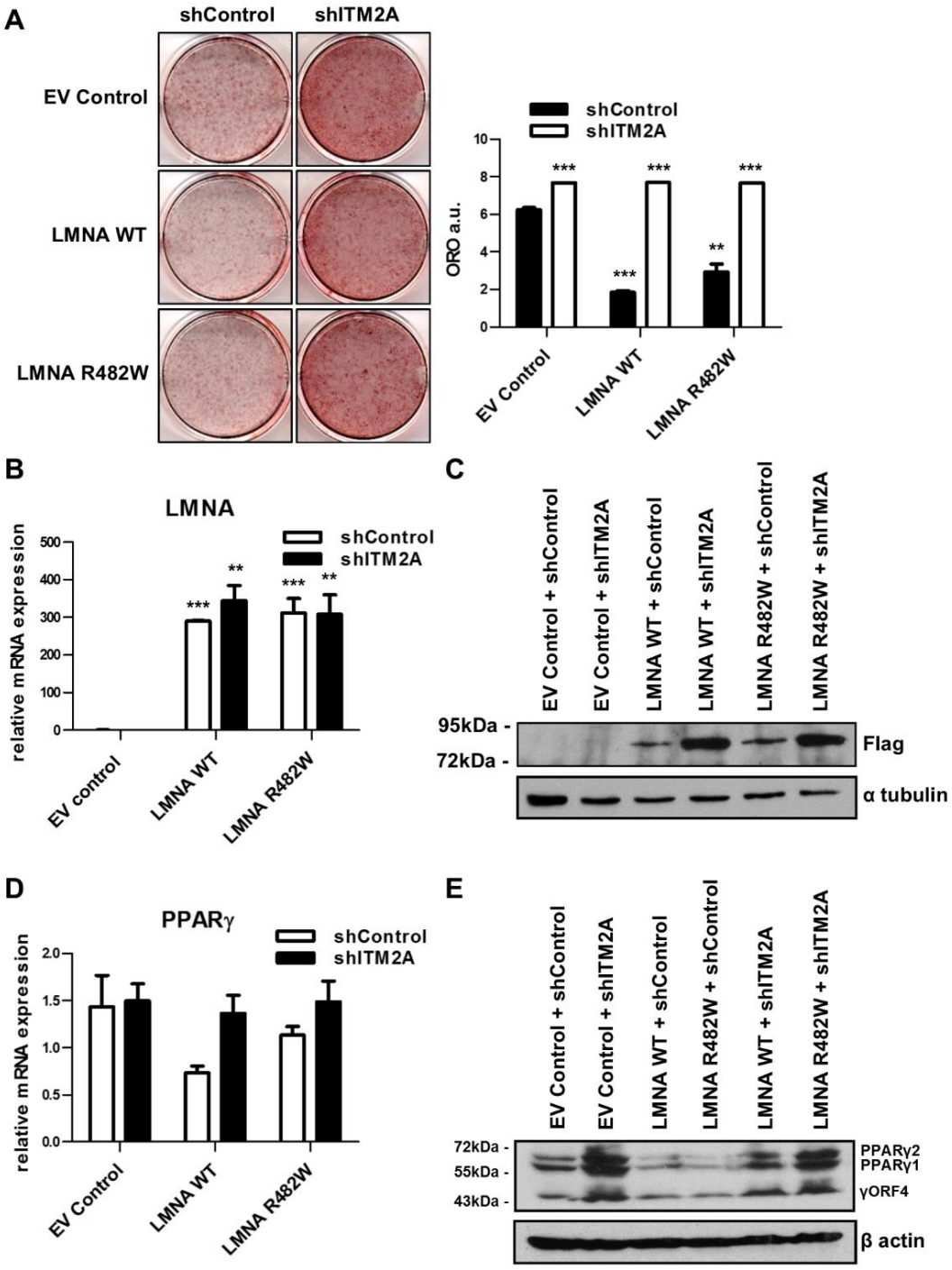

Fig 3.11: shRNA mediated knockdown of ITM2A rescues LMNA inhibition of 3T3-L1 differentiation. 3T3-L1 preadipocytes were stably transfected with pCMV(PB)-Flag-LMNA-WT.shITM2A, pCMV(PB)-Flag-LMNA-WT.shControl, pCMV(PB)-Flag-LMNA-R482W.shITM2A, pCMV(PB)-Flag-LMNA-R482W.shControl or empty vector control pCMV(PB).shITM2A and pCMV(PB).shControl dual constructs. The cells were induced to differentiate. (A)

Adipogenesis was assessed at day 8 post induction by staining with Oil Red O; quantification was carried out using ImageJ and expressed as Oil red O absorbance units (ORO a.u.). (B) Total RNA was isolated at day -2 of differentiation from the stably transfected 3T3-L1 preadipocytes and LMNA expression measured by qPCR using primers specific for human LMNA. (C) Immunoblot analysis of flag-LMNA WT and R482W mutant at day -2. (D) Total RNA was isolated at day 4 post induction and the expression of PPARγ was analysed by qPCR. (E) Immunoblot analysis of PPARγ at day 4 post induction. Student's *t*-tests (two-tailed, assuming equal variance) were used to calculate statistical significance compared to empty vector control cells, indicated as follows: *=P<0.05;**=P<0.01; ***=P<0.001.

ITM2A expression in LMNA wild type and KO MEFs

To further elucidate the relationship between LMNA and ITM2A we investigated the endogenous levels of ITM2A expression in wild type and LMNA knockout mouse embryonic fibroblasts (MEFs). Previously generated LMNA -/- MEFS were grown as described and LMNA knockout was confirmed at the protein level in these cells (Figure 3.12A). Measurement of ITM2A expression in the LMNA KO MEFs showed that ITM2A was significantly reduced in these cells in comparison with wild type MEFs (Figure 3.12B), supporting the theory that LMNA increases or modulates ITM2A expression in some way.

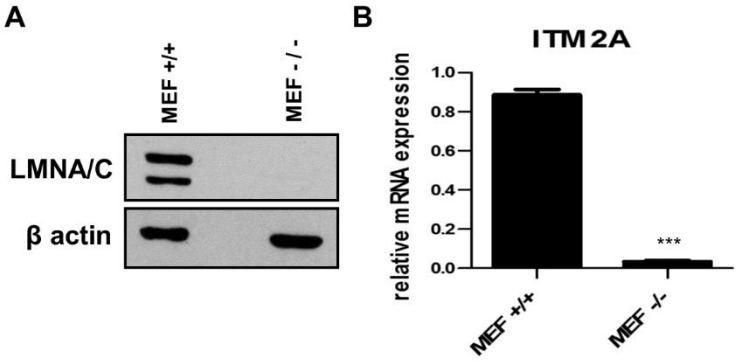

Figure 3.12: ITM2A expression is down-regulated in LMNA KO MEFs. (A) Total RNA was isolated from LMNA wild type (+/+) and knockout (-/-) MEFs and the expression of ITM2A was analysed by qPCR. (B) Immunoblot analysis of mouse LMNA in WT and KO MEFs. Student's *t*-test (two-tailed, assuming equal variance) was used to calculate statistical significance compared to LMNA WT control cells, indicated as follows: *=P<0.05;**=P<0.01; ***=P<0.001.

DISCUSSION

While significant advances have been made in understanding the pathophysiology of FPLD2, the molecular aetiology of the disease remains to be confirmed. Previous reports have described pleiotropic effects of LMNA on gene regulation and interaction of LMNA with multiple proteins. Both of these aspects are altered by mutations in the LMNA gene (151,152,154,155). In the case of FPLD2, there is a clear impact of LMNA mutations on adipogenesis and a number of studies have proposed altered LMNA-SREBP1 interactions as the driving force of the disease phenotype [145,151,152,191]. Here, we investigated the effect of LMNA in the early stages of adipogenesis though the exploring genes identified using RNA-Seq which indicated that ITM2A regulation is altered by LMNA over-expression. This led us to explore the relationship between ITM2A expression and adipogenesis as well as the modulatory relationship between LMNA and ITM2A within this context.

ITM2A in adipogenesis

Characterisation of ITM2A activity during 3T3-L1 differentiation identified a distinct expression profile for this gene in adipogenesis and showed that endogenous ITM2A is transiently down-regulated in early cell differentiation. This transient down-regulation has not been reported previously even though global gene expression has been profiled during 3T3-L1 adipogenesis [178]. Our work here indicates that ITM2A is a lowly expressed gene/protein in 3T3-L1 cells and that it's expression is only altered for a specific period, around day 2 of adipogenesis (Figure 3.2). Investigation of cells stably transfected with a 2kb, 1.5kb, 1kb or 0.5kb ITM2A promoter reporter constructs confirmed that ITM2A promoter activity is reduced in 3T3-L1 cells when adipogenesis is fully induced using MDI, while a reduction in promoter activity is not observed under limiting induction conditions with DI or D alone (Figure 3.3B). Thus, full induction of adipogenesis is associated with reduced ITM2A promoter activity in the early stages of differentiation.

Investigation of the role of ITM2A in adipogenesis showed that ectopic expression of ITM2A moderately but significantly inhibited the differentiation of 3T3-L1 cells (Figure 3.8). However, the mechanism of this inhibition is unclear as there were no obvious effects on the mRNA or protein levels of the key adipogenic transcription

factors PPARγ and CEBPα in ITM2A over-expressing cells. Knockdown of endogenous ITM2A had the opposite effect to over-expression and enhanced adipogenesis in comparison to control cells. Similar to ITM2A over-expression, knockdown of ITM2A did not effect PPARγ and CEBPα mRNA levels. In contrast, a significant increase in PPARγ1 and PPARγ2 protein isoforms was observed and although not significant, a similar trend was observed for the γORF4 isoform (Figure 3.10 D, E). These observations suggest that ITM2A knockdown enhances PPARγ protein stability. Such an enhancement could explain the effect of ITM2A knockdown on adipogenesis as an increase in PPARγ2 protein stability would be expected to promote adipogenesis.

In the rescue experiment (Figure 3.11) ITM2A knockdown was seen to increase or rescue PPARγ expression in LMNA transfected cells as well as increase PPARγ2 protein levels. This is the only context in which we observed an effect of ITM2A silencing on PPARγ expression, as ITM2A knockdown or over-expression alone were not seen to alter its expression in comparison to controls. The mechanism of action underlying the effect of ITM2A on PPARγ expression in LMNA transfected cells is unclear. However, as PPARγ and CEBPα are known to cross-activate each other [88,104], it is possible that increased PPARγ protein activity may influence its own expression by up-regulating CEBPα, which can in turn up-regulate PPARγ expression through a C/EBP regulatory element in the PPARγ promoter [106]. However, similar to PPARγ expression, we did not observe any differences in CEBPα expression in response to 3T3-L1 cells transfected with shITM2A.1 vs. scrambled shControl (Figure 3.10D). This suggest that ITM2A knockdown only influences the expression of these transcription factors (possibly through PPARγ protein stabilization) under the inhibitory conditions of LMNA overexpression.

Adipogenesis and autophagy

While the mechanisms underlying enhanced PPARγ protein stability in ITM2A knock down cells are unclear, altered regulation of autophagy during cell differentiation may be involved.

Autophagy is an evolutionarily conserved catabolic pathway in which cytoplasmic components are degraded through the formation of double membrane vesicles (autophagosomes) that fuse with lysosomes (autolysosomes) to facilitate the breakdown of the vesicle contents [193]. Recent studies have described the regulatory role of autophagy in adipogenesis in a number of different contexts. Silencing of autophagy genes Atg5 and Atg7 in 3T3-L1 and MEF cells have been shown to inhibit cell differentiation while the adipose specific knockout of Atg7 in mice generates a lean phenotype with impaired white adipose tissue development [194,195]. In addition increased autophagy activity has been reported in the adipose tissue of obese patients [196]. During 3T3-L1 differentiation autophagy is up-regulated upon the addition of the induction cocktail, during the early phase of adipogenic differentiation (day 0 to 4) [197–199]. Guo et al., (2013) [198] have demonstrated that CEBPβ activation of autophagy genes and autophagic degradation of adipogenic inhibitors are necessary for cell differentiation. Finally, Zhang et al., (2013) [199] recently proposed a model in which autophagy activation functions to stabilize PPARγ2 in 3T3-L1 differentiation through the repression of proteasome-dependent PPARγ2 degradation.

As previously described, ITM2A is reported to regulate autophagic flux by interacting with specific v-ATPases, the proton pumps that mediate lysosome acidification [174,200]. In HEK293 human embryonic kidney cells ITM2A overexpression is seen to interfere with autophagic flux in a similar way to BafA1, an autophagy inhibitor that blocks the formation of mature autolysosomes. Silencing of ITM2A in Hela cells appears to block starvation induced autophagy as well as reduce BafA1 driven autophagosome accumulation [174]. Although it is clear that ITM2A is involved in the regulation of autophagic flux, the exact consequences of ITM2A silencing are unclear.

We observed that endogenous ITM2A expression is transiently down-regulated during 3T3-L1 differentiation. This reduction in ITM2A expression coincides with activation of autophagy in adipogenesis [197,198]. It is therefore possible that ITM2A down-regulation is involved in autophagic activation or flux, and that ITM2A silencing somehow enhances this process, leading to enhanced adipogenesis. When we

investigated the effects of ITM2A knockdown on markers of adipogenesis we observed a significant increase in PPARγ protein at the beginning of cell differentiation (day 0 to Day 4), around the same time as autophagy activation. We propose a model in which ITM2A knockdown functions to modulate autophagy and promote 3T3-L1 differentiation. We suggest that the reduced ITM2A expression observed at day 2 in normal 3T3-L1 differentiation may play a role in the endogenous up-regulation of autophagy observed at this stage of cell differentiation [198,199] and that ITM2A knockdown in the context of differentiation functions to stabilize PPARγ2 through altered regulation of autophagy. Further investigation is required to elucidate the role of ITM2A in adipogenesis and confirm the involvement of autophagy in this process.

LMNA and ITM2A

Consistent with previous reports [20,177], we observed that over-expression of WT and R482W mutant LMNA have an inhibitory effect on 3T3-L1 differentiation. Here we show that endogenous ITM2A expression is up-regulated during adipogenesis in LMNA WT and R482W mutant cells (Figure 3.1G), suggesting that LMNA mediated altered regulation of ITM2A may play a role in LMNA inhibition of adipogenesis. In agreement with this, we detected significantly lower levels of endogenous ITM2A expression in LMNA knockout vs. normal MEFs (Figure 3.12B). Taken together, these data indicate that LMNA has a regulatory role in the control of ITM2A expression.

We attempted to determine if LMNA WT or mutant directly affected the expression of ITM2A using the ITM2A promoter reporter constructs. However, data normalisation proved problematic as transient LMNA over-expression had significant effects on the expression of firefly luciferase from all three constitutive promoters commonly used for normalisation purposes in promoter reporter assays.

This is not surprising given that LMNA is implicated in many different aspects of genome biology through extensive interactions with chromatin [8] and with proteins of the nuclear lamina [3].

Data normalisation issues were overcome by generating LMNA/ITM2A reporter stable 3T3-L1 lines using a two-step transfection and selection approach. Both WT and R482W mutant LMNA significantly increased luciferase activity driven by all four promoters at day 4 of differentiation and this was in agreement with qPCR data

(Figure 3.7). The data indicates that the key element though which LMNA mediates it effects is in the 500bp ITM2A promoter region immediately upstream from the structural gene. Further investigation will be necessary to identify the precise factor(s) in the ITM2A promoter mediating the LMNA effect.

While there were some consistency issues, taken together the data supports a model whereby overexpression of WT or R482W LMNA up-regulate ITM2A expression during adipogenesis and this up-regulation is likely to contribute to LMNA mediated inhibition of adipogenesis. The data presented here combined with previously published data suggests that LMNA over-expression is likely to inhibit adipogenesis through a combination of mechanisms. In addition to previous work showing that LMNA alters SREBP1 and FXR1P function in adipogenesis [191,192] and reduces PPARγ expression [20], our work demonstrates a LMNA effect on ITM2A expression that is likely to have a functional effect on adipogenesis in 3T3-L1 preadipocytes.

It is not clear how LMNA alters ITM2A expression in this context. One plausible mechanism stems from the report by Lund et al., (2013) where they identified 4000 genes that disengage from LMNA during human ASC differentiation. They compared genes present in lamin rich domains or LDRs before (pre-induction: day 0) and after (day 21) differentiation into mature adipocytes and observed that approx. 80% of the genes that lost or gained LMNA association did not exhibit changes in expression. Therefore the effect of ITM2A disassociation on ITM2A expression is unknown. Although this phenomenon has not been confirmed in mouse adipogenesis, it is possible that disengagement of ITM2A from LMNA during adipogenesis may facilitate its transient down-regulation in cell differentiation. LMNA disassociation may allow for the binding of a repressor to the ITM2A promoter, to produce the distinct ITM2A expression profile observed. If follows that LMNA overexpression may prevent this disengagement and thus prevent ITM2A down-regulation in adipogenesis. The impact of this newly described relationship on ITM2A expression and function in an endogenous FPLD2 patient setting is unknown.

LMNA and Autophagy

The observation that knockdown of ITM2A enhances adipogenesis prompted us to explore whether LMNA inhibition of adipogenesis could be rescued by knocking down ITM2A expression. Interestingly the LMNA inhibition was completely rescued by this approach (Figure 3.8A). Moreover, the rescue was effective despite the observation that the ITM2A knockdown enhanced the stability of LMNA. A likely explanation for this is that the increased stability of PPARγ in the ITM2A knockdown cells drives adipogenesis forward and its effects are dominant over the inhibitory effects of the increased LMNA.

The relationship between ITM2A and autophagy and the demonstration that ITM2A knockdown can suppress LMNA inhibition of adipogenesis suggests a potential role for autophagy modulation in the treatment of lamin associated lipodystrophies. A recent study has described autophagy dysregulation in the LMNA H222P driven cardiomyopathy, where increased AKT-mTORC1 signalling is observed in human patients [201]. Treatment of LMNA H222P/H222P mice with the mTOR inhibitor temsirolimus was seen to reactivate autophagy and lead to improved cardiac function in these mice [201]. In addition, the treatment of HGPS patient primary fibroblasts with the mTOR inhibitor rapamycin, was seen to improve the disease phenotype and slow senescence of these cells by stimulating autophagy [202]. Thus, taken together our findings suggest that exploration of therapies that reactivate autophagy are warranted for treatment of FPLD2 and related lipodystrophies such as HAART- associated lipodystrophy.

CHAPTER 4: IGFBP5 IN 3T3-L1 ADIPOGENESIS

INTRODUCTION

The Insulin-like Growth Factor System and Adipogenesis

Insulin, insulin-like growth factors (IGF-I/II) and their receptors play an important role in the regulation of key mammalian processes such as growth, survival and metabolism [203,204]. Insulin is known to promote adipogenesis through IGF-I receptor signalling and is an essential ingredient in the 3T3-L1 cell induction cocktail [92]. IGF-1 present in culture media serum also contributes to the progression of these cells through the differentiation programme [124]. The importance of insulin and IGF-1 signalling in adipogenesis is emphasised in a number of mouse studies in which various components of the system are lost or mutated. Mice deficient in insulin or IGF-1 receptors experience severe growth defects, are underweight and usually die shortly after birth [205,206], while transgenic mice with adipose tissue specific silencing of both insulin and IGF-1 receptors display significant loss of adipose tissue [207]. Loss of the insulin receptor substrate proteins (IRS) is seen to perturb adipogenesis [92,205,206] and other downstream factors involved in the insulin/IGF signalling cascade, such as PI3K, AKT and mTOR, have also been shown to modulate adipogenesis in various contexts [92,206].

Insulin Growth Factor Binding Proteins

Insulin growth factor binding proteins (IGFBPs) function to modulate IGF availability both positively and negatively, as well as having IGF-independent properties [208] . There are six highly conserved binding proteins that are secreted by various cell types in a cell-, tissue- and development stage specific manner. Each of these proteins has unique context-specific functions and characteristics. Of the six binding proteins, IGFBP5 is the most highly conserved in mammals [208,209]. Most IGFs in circulation are IGFBP bound and these binding proteins have a higher affinity for IGF than that of the IGF receptors [210]. There are a number of ways in which IGF and IGFBP interactions are altered or reduced, which leads to important changes in IGF and IGFBP activity. These include IGFBP5 proteolysis, phosphorylation and IGFBP interaction with extracellular matrix (ECM) components [209].

IGFBP5: Structure, interactions and proteolysis

The IGFBP5 protein has a tripartite structure consisting of a C-terminal domain, a mid-region and an N-terminal domain that contains a 20-amino acid signal peptide, which is cleaved to produce the mature secreted IGFBP5 protein (Figure 4.1) [208]. Each of these regions play important roles in IGFBP5 function. The N-terminal contains the primary IGF-binding site [211], the mid-region is where most post-translational modifications occur [208], and the C-terminal domain contains a basic region involved in ECM, ALS and cell membrane interactions [212–214]. The C-terminus also contains a nuclear localisation signal which is involved in the importin-β mediated nuclear import of IGFBP5 [208].

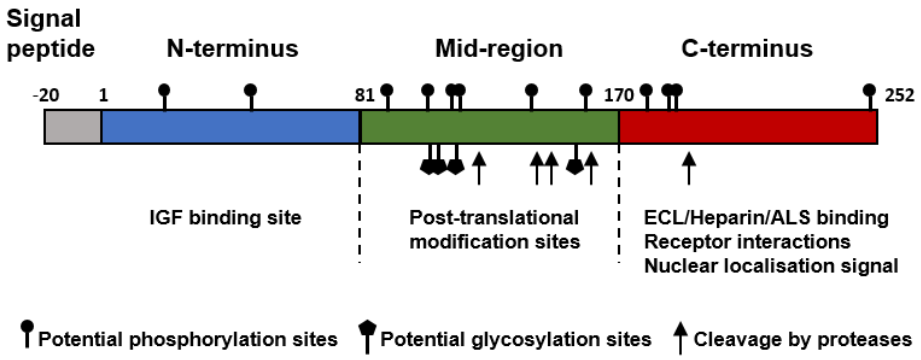

Figure 4.1: Schematic representation of IGFBP5 protein structure. Adapted from Schneider et al., (2002)[208].

IGFBP5 has been shown to directly bind numerous components of the ECM in various cell models, including collagens, fibronectin, laminin, heparin sulphate, vitronectin, thrombosondin-1, and osteopontin [215–217]. These interactions are of biological significance, as they appear to modulate IGF-1-binding, which in turn influences IGF-1 activity [209]. The IGFBP5 mid-region contains specific residues that can be glycosylated [218] or phosphorylated [219], as well as multiple proteolytic cleavage sites. IGFBP5 proteolysis has been reported in many different cell types and is mediated by diverse proteases. This processing plays an integral role in regulating IGFBP5 activity, as it alters the proteins ability to bind IGF-1 [208]. IGFBP5 can be protected from cleavage through interactions with IGF-I [220] or ECM components [221] and it has been suggested that IGFBP5 cleavage products may have associated biological activity [209].

IGFBP5 promoter

Previous studies have identified multiple elements that positively and negatively regulate IGFBP5 transcriptional activity in a cell-type specific manner. These include cell signalling molecules, metabolites, hormones, glucocorticoids, transcription factors and growth factors.

Interestingly, two of the 3T3-L1 induction components, elevated cAMP (IBMX) and dexamethasone, have been shown to modulate IGFBP5 in different cell systems. As previously mentioned forskolin, like IBMX, can be used to increase intracellular cAMP and induce the adipogenic differentiation of 3T3-L1 preadipocytes [180]. Induction of IGFBP5 promoter activity by cAMP has been reported in GM10 fibroblasts, where it was shown that forskolin treatment lead to increased activity through conserved AP-2 elements within the IGFBP5 proximal promoter [222]. In these cells AP-2 was shown to increase IGFBP5 promoter driven luciferase in a biphasic manner; low levels of AP-2 overexpression lead to transactivation of the promoter constructs (-503 to +775) while higher levels of AP-2 did not. This was not observed in other cell lines (HepG2 and A673) where AP-2 was seen to increase IGFBP5 promoter activity in a dose dependent fashion [222]. Similarly, PTH has been shown to increase IGFBP5 mRNA in rat osteosarcoma cells through a cAMP-mediated mechanism [223]. Dexamethasone is reported to decrease IGFBP5 mRNA and secreted protein, which is thought to contribute to dexamethasone mediated inhibition of human osteoblast-like cell differentiation [224].

IGFBP5 promoter analysis in various bone cell lines has reported increased promoter activity in response to progesterone, parathyroid hormone (PTH) and prostaglandin E_2, while reduced promoter activity has been described in response to cortisol and bone morphogenetic protein 7 [225–228]. In addition to AP-2, several other transcription factors or co-activators have been shown to regulate IGFBP5 promoter activity through conserved sequences, including NF1, C/EBP, MN1 and Myb [101,229–232]. Retinoic acid (RA) is reported to up-regulate IGFBP5 promoter activity by reducing C/EBPα/β mediated repression of IGFBP5 in neuroblastoma differentiation [230]. In undifferentiated cells the C/EBP factors mediate a repressive effect through interaction with a C/EBP element in the IGFBP5 promoter. In the same study RA stimulation is also shown to promote C/EBPα induction of IGFBP5 promoter activity through interaction with a conserved TATA box. Therefore, depending on the

differentiation status of these cells and to which promoter element it binds, C/EBPα appears to either inhibit or induce IGFBP5 promoter activity [230]. Testosterone has been shown to activate an IGFBP5 promoter (1278bp) reporter in human androgen responsive fibroblasts and increase IGFBP5 mRNA [233]. Finally, numerous studies have reported increased IGFBP5 mRNA and protein in response to IGF-1 in various cell systems [220,223,233,234].

IGFBP5 in cancer

The IGF axis is known to play an important role in normal and malignant cell growth, proliferation and differentiation [210]. IGFBP5 is expressed in many different tissues, where its expression and distinct functions are modulated by tissue-specific ECM interactions, proteolysis and hormonal regulation [209]. Dysregulation of IGFBP5 expression is a feature of many human cancers, and has been most extensively studied in breast cancers models. Mammary epithelial cells are known to secrete IGFBP5 and a role for this binding protein has been outlined in mammary gland involution, where it functions to inhibit IGF survival signalling in this setting and promote post-lactation involution [235]. IGFBP5 expression and activity have been assessed in a many different breast cancer cell lines where it appears to have conflicting actions; either to promote cell survival or induce apoptosis [236]. In addition to breast cancers, altered IGFBP5 expression has been linked to many other cancer types; overexpression has been reported in prostate [237] ovarian [238], lung [239], pancreatic [240] and thyroid cancers [241], while reduced IGFBP5 expression is associated with squamous cell carcinomas of the head and neck [242,243], as well as cervical carcinomas [244]. The various roles of IGFBP5 in these diverse systems are unclear, however a recurrent theme appears to be that IGFBP5 expression, regulation and function are highly dependent on cellular context.

IGFBP5 and differentiation

IGFBP5 expression and activity have been described in diverse systems. Of relevance to our study, is the characterisation of this secreted protein in the differentiation of various cell types, including myogenesis, osteogenesis, chondrogenesis and neuronal cell differentiation.

Analysis of IGFBP5 expression in C2 myoblasts identified up-regulation of IGFBP5 expression and secretion during the differentiation of these cells [212]. Surprisingly no

other IGFBPs were detected during C2 myoblast differentiation in this study. Subsequently James et al., (1996) [245] investigated the role of IGFBP5 in C2 myogenesis and reported reduced myogenic differentiation in response to IGFBP5 over-expression and enhanced cell differentiation in C2 myoblasts expressing an IGFBP5 antisense transcript. The inhibitory effect of exogenous IGFBP5 expression on myogenesis was rescued by the addition of IGF-1 to the culture media during cell differentiation, suggesting that the action of IGFBP5 in this system is IGF-dependent [245]. In agreement with these findings Cobb et al., (2003) [246] demonstrated that the an IGFBP5 non-IGF binding mutant was unable to inhibit C2 myogenic differentiation. Cobb et al., (2003) also described an IGF-independent anti-apoptotic function of IGFBP5 in these cells.

IGFBP5 has been studied in bone cell proliferation, differentiation and in vivo formation, where it appears to have different effects depending on the experimental method and model system [247]. IGFBP5 treatment or overexpression in various bone cell lines has been shown to either increase [208,248] or decrease [249] osteoblast differentiation. Liu et al., (2015) have recently reported enhanced osteogenic differentiation of MSC in response to IGFBP5 over-expression and reduced osteogenic differentiation in response to IGFBP5 silencing. In vivo IGFBP5 treatment studies have been shown to increase bone formation [248,250] in mice, however differences in effect are observed depending on delivery method which may influence IGFBP5 proteolytic cleavage [247]. IGFBP5 overexpression from an osteoblast specific [251] or β-actin [252] promoter in transgenic mice have also been reported to reduce bone formation. Finally, IGF-independent functions of IGFBP5 have also been proposed in the context of osteogenesis [208,247].

To date, there is little published data on the role of IGFBP5 in chondrogenesis. Sekiya et al., (2001)[253] have reported increased IGFBP5 expression in the differentiation of human adult stem cells isolated from bone marrow stroma, however the function of IGFBP5 during this process is unknown. IGF-1 and IGFBP5 appear to play a role in chondrocyte proliferation, where IGFBP5 enhances the proliferative effect of IGF-1 in these cells and IGF-1 in turn increases IGFBP5 expression through the PI3-kinase signalling [254]. Finally, Samuel et al., (2010) [255] reported substantial IGFBP5 down-

regulation in human retinal pigment epithelial cells during neuronal differentiation. C/EBPβ is thought to mediate this reduction as a downstream regulator of MAPK signalling, through a C/EBPβ response element in the IGFBP5 promoter [255,256]. In contrast to these results, Tanno et al., (2005) [257] observed impaired neuronal differentiation in response to IGFBP5 silencing in a number on neuronal cell lines (LAN-5, SY5Y), which was rescued by treatment with recombinant IGFBP5. In addition, a role for IGF-1 and IGFBP5 has been described in Schwann cell differentiation in which IGF-1 was observed to stimulate differentiation and increase IGFBP5 expression. IGFBP5 overexpression was also seen to promote the differentiation of these cells [258].

IGFBPs and WNT

Recent studies have reported interactions between various IGFBPs and the Wnt/β-catenin signalling pathway in both cancer and cell differentiation settings. The anti-tumoral actions of IGFBP3 has been described in metastatic melanoma cells, where it interacts with GSK-3β to activate cytoplasmic β-catenin degradation [259]. IGFBP5 is reported to be involved in the down-regulation of Wnt/β-catenin signalling in colon cancer cells [260], and the regulation of IGFBP5 itself is modulated by a canonical β-catenin signalling dependent mechanism, in WNT1 driven mammary tumours [261]. IGFBP4 has been shown to induce cardiomyocyte differentiation through inhibition of canonical Wnt/β-catenin signalling in the murine P19CL6 cell model. This IGF-independent action is mediated through direct interactions with the frizzled and LRP5/6 wnt receptors. Endogenous IGFBP4, 3 and 5 expression is up-regulated in P19CL6 cardiomyocyte differentiation and silencing of IGFBP4 is seen to inhibit the differentiation of these cells. IGFBP3 and IGFBP5 knockdown did not affect cardiomyogenesis [262]. In addition, IGFBP4 has been shown to protect the ischemic heart by inhibiting Wnt/β-catenin signalling [263].

IGFBP5 in adipogenesis

The above studies suggest diverse roles for IGFBP5 in the differentiation of numerous cell types. Both IGF-dependent and IGF-independent functions have been described in the various systems, and the experimental model used appears to influence IGFBP5 activity, emphasising the effect of context on IGFBP5 gene function.

IGFBP5 activity and function have yet to be characterised in adipogenesis, however numerous studies have commented on the IGFBP expression of adipose cells in vivo and in vitro. Boney et al., (1994) [264] described IGFBP expression and secretion in 3T3-L1 cells before and after differentiation; up-regulation of IGFBP2, 3, and 4 was observed while IGFBP5 was undetected in this study. IGFBP1 is reported to inhibit adipocyte differentiation [265], and transgenic over-expression of both IGFBP1 and 2 are seen to protect against obesity in mice [266,267]. While the IGFBP1 and 2 effects on adipogenesis are thought to be mediated by IGF-1 sequestration, IGFBP3 has been shown to inhibit adipogenic differentiation in an IGF-independent manner [268]. Studies on 3T3-L1 preadipocytes have demonstrated that IGFBP3 can inhibit insulin stimulated glucose uptake in these cells [269], as well as interfere with PPARγ-RXRα interactions to inhibit their transcriptional activity [270]. Interestingly, Wabitsch et al., (2000) [271] measured an increase in IGF-I and IGFBP3 expression in human adipocytes when compared to preadipocytes isolated from human subcutaneous adipose tissue. It is possible that increased IGFBP3 expression during adipocyte differentiation may be part of a negative feedback mechanism [268].

Conflicting reports of IGFBP5 expression have been reported in porcine adipocytes. High levels of IGF-II and IGFBP5 expression where observed in porcine preadipocytes, both of which were seen to decrease during the in vitro differentiation of these cells, alongside increased expression of adipogenic markers and Insulin, IGF-I and IGF-I receptor genes [272]. In contrast, Hausman et al., (2002) [273] measured high levels of IGFBP5 in mature porcine adipocytes isolated form subcutaneous pig adipose tissue. Recently, characterisation of human adipose depot specific gene expression profiles identified increased IGFBP5 expression in abdominal adipose depots when compared to gluteal fat. In this study, differential endogenous IGFBP5 expression was associated with differences in fat depot methylation patterns [274].

Several transgenic and knockout mouse models have been employed to investigate IGFBP5 function in various settings. Transgenic over-expression of IGFBP5 from the bone specific osteocalcin promoter generated mice with decreased bone volume and impaired osteoblast function [251], while CMV/ß-actin promoter driven expression of IGFBP5 lead to decreased bone density that was dependent on both age and gender [252]. Neither of these studies reported any changes in weight or fat accumulation between transgenic mice and their respective wild type littermates. IGFBP5 over-expression has also been studied in mouse mammary glands, where the mammary specific B-lactoglobulin promoter was used to express the transgene in this environment. These mice experienced impaired mammary gland development [275]. The most severe phenotype was reported in mice that over-expressed IGFBP5 ubiquitously from early development. Reduced female fertility, growth inhibition, decreased body weight and impaired muscle development were observed, suggesting an important role for IGFBP5 in mouse development [252].

IGFBP knockout mouse models are reported to display modest phenotypes, presumably due to compensation by other IGFBPs [252,276]. IGFBP5 null mice develop normally, with no differences observed in general growth, fat pad and organ weight, skeletal muscle, circulating IGF-1 levels and mammary gland development in comparison to wild type littermates. These mice do however show increased levels of IGFBP3 as well as impaired mammary gland involution post weaning [277]. In contrast, triple IGFBP3/4/5 KO mice have significantly reduced growth with smaller fat pads containing smaller adipocytes, reduced circulating IGF-1, increased insulin secretion and enhanced glucose disposal, in comparison to their wild type littermates [276]. These studies suggest congruent roles for IGFBP5 and IGFBP3 in mouse development and growth [276].

RNA-Seq analysis identified a differential decrease in IGFBP5 expression in response to mutant and wild type LMNA. The aim of this study was to characterise IGFBP5 activity and function in 3T3-L1 differentiation, and investigate whether the LMNA mediated changes in IGFBP5 gene expression contribute to the altered adipogenesis observed in the FPLD2 phenotype.

RESULTS

Endogenous IGFBP5 expression in 3T3-L1 differentiation

Microarray analysis of gene expression in 3T3-L1 and hASC differentiation by Mikkelsen et al., (2010) [178] measured relatively constant levels of IGFBP5 expression across 3T3-L1 differentiation, while a dramatic increase was observed in the early differentiation of hASC (day 1-3), with expression levels remaining high in mature human adipocytes (day 14) (Figure 4.2A). IGFBP5 expression was assessed during 3T3-L1 differentiation and in contrast to this microarray data, variable IGFBP5 expression was detected during cell differentiation. A highly specific expression pattern was observed in which IGFBP5 is lowly expressed in preadipocytes (day-2) and then highly up-regulated at day 2, post induction of differentiation. IGFBP5 expression levels were reduced at day 4/6 and then up-regulated again at day 8 of differentiation. Figure 4.2 (B) shows the characteristic induction of PPARγ expression in adipogenesis alongside the distinct IGFBP5 expression profile, which was consistently observed in 3T3-L1 differentiation.

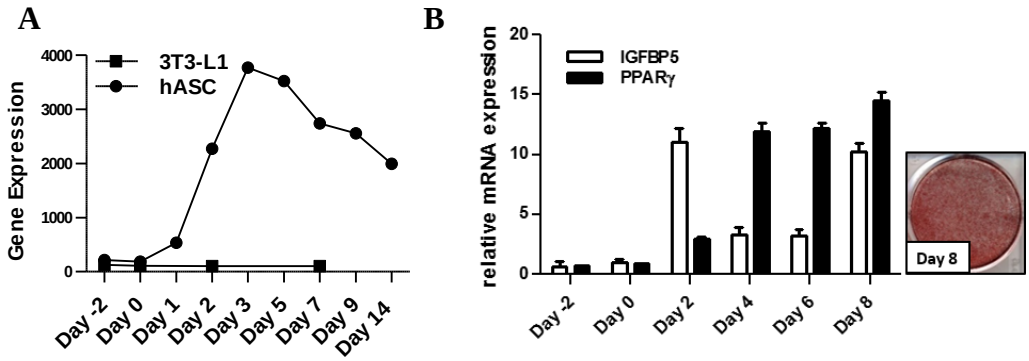

Figure 4.2: Endogenous IGFBP5 expression during 3T3-L1 differentiation. (A) IGFBP5 gene expression in 3T3-L1 and hASC differentiation, as measured by microarray analysis carried out by Mikkelsen et al., (2010). (B) 3T3-L1 preadipocytes were grown to confluence and induced to differentiate. Adipogenesis was assessed at day 8 when cells were stained for lipid droplet accumulation with Oil Red O. Total RNA was isolated at the indicated time points during 3T3-L1 differentiation. IGFBP5 and PPARγ expression was analysed by qPCR. Transcript expression at the various time points is shown relative to expression at day 0.

Originally, qPCR analysis of IGFBP5 expression in 3T3-L1 differentiation was carried out with cDNA in which oligo dT primers were used to prime the cDNA synthesis reaction. In these samples, the dramatic increase in IGFBP5 expression at day 2 of differentiation was not detected. Examination of the mouse (and human) IGFBP5 transcripts shows that it has an extraordinarily long 3' untranslated region (UTR) of approximately 5 kilobases. Figure 4.3 illustrates the distribution of 3'UTR sizes within the human, mouse and rat genomes, highlighting the unusually length of the IGFBP5 3'UTR [278]. As oligo dT priming involves the use of the poly-A tail at the 3' end of mRNA transcripts, the 5' ends of very long mRNAs can be under represented in the resulting cDNA pool. This offers an explanation for the reduced detection of IGFBP5 using qPCR approaches that employ oligo dT priming for cDNA synthesis. When random hexamers were used for priming in cDNA synthesis, detection of IGFBP5 by qPCR was enhanced and a considerable increase in IGFBP5 expression at day 2 of differentiation was observed (Figure 4.2). The expression profile detected in these cells is unusual, in that IGFBP5 expression is low prior to induction of differentiation, increases significantly at day 2, is down-regulated at day 4 and 6 of differentiation and then increased again at day 8. The mechanisms regulating this complex expression profile are unclear and were not pursued here. The large size of the 3' untranslated region of the IGFBP5 is intriguing and one possibility is that this 3' region might affect RNA degradation and stabilization rates that could account for the expression pattern observed. Further investigation is required to elucidate the mechanism governing the complex control of IGFBP5 expression in 3T3-L1 differentiation.

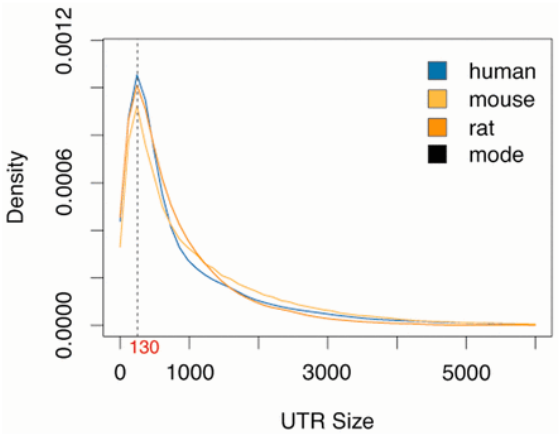

Figure 4.3: Distribution of 3′-UTR sizes in human, mouse and rat genomes. Taken from Andres-Leon et al., 2015 [278].

IGFBP5 overexpression in 3T3-L1 differentiation

To investigate the role of IGFBP5 in adipogenesis 3T3-L1 preadipocytes were stably transfected with a piggyBac transposable IGFBP5 over-expression construct pMSCV(PB)IGFBP5, or empty vector control pMSCV(PB), and induced to differentiate. IGFBP5 over-expression was confirmed by qPCR and did not appear to affect lipid droplet accumulation in comparison to empty vector control (Rep 1) (Figure 4.4A). To assess whether IGFBP5 overexpression influenced adipogenesis during submaximal induction of differentiation, cells were induced to differentiate using full induction media MDI, sub-maximal media DI or D alone. The reduced induction cocktail DI appeared to reveal a slight inhibition of differentiation in response to IGFBP5 overexpression, however when Oil Red O quantification was carried out the observed reduction in lipid droplet accumulation was not found to be statistically significant (Figure 4.4B). Immunoblot detection of over-expressed IGFBP5 using both a Flag and Myc antibody was unsuccessful in these cells.

Interestingly, when this experiment was repeated as part of a larger rescue experiment, over-expression of IGFBP5 was seen to significantly inhibit lipid droplet accumulation in comparison to the empty vector control (Rep. 2) (Figure 4.4C). These cells were dual transfected with either pMSCV(PB) and pCMV(PB) (EV Control) or pMSCV(PB)IGFBP5 and pCMV(PB) (IGFBP5) and selected with both G418 and puromycin as part of a larger experiment designed to investigate the effects of both LMNA and IGFBP5 overexpression on 3T3-L1 differentiation. Although the larger rescue experiment was unsuccessful (LMNA did not inhibit differentiation in this particular experiment) the IGFBP5 overexpression alone appeared to influence cell differentiation. It is unclear why IGFBP5 over-expression produced inconsistent effects on cell differentiation. A possible explanation could be the varying degrees of IGFBP5 over-expression achieved in the respective replicates. QPCR analysis of IGFBP5 expression in the two independent experiments (Figure 4.4A, C) revealed a significant disparity in the levels of exogenous expression, which could potentially account for the distinct impacts on 3T3-L1 differentiation observed. IGFBP5 was over-expressed approximately 200-fold in the first replicate and approximately 5000-fold in the second replicate. Oil Red O staining at day 8 showed that 3T3-L1 differentiation was unaffected by moderate overexpression (Figure 4.4A) while higher levels of overexpression lead to inhibition of adipogenesis (Figure 4.4C) in

comparison to EV control. Oil Red O quantification confirmed a significant reduction in lipid droplet accumulation in response to greater IGFBP5 overexpression (Figure 4.4C).

Again, immunoblot detection of over-expressed IGFBP5 was unsuccessful in these cells. The IGFBP5 protein over-expressed in these experiments contains a C-terminal dual Myc-Flag tag which was undetected by both antibodies. Considering the extensive levels of over-expression achieved in these experiments, this is unusual. Unspecific binding of the Flag antibody was observed at the predicted size of IGFBP5 in both over-expressed and empty vector samples, which may have obstructed IGFBP5 detection, however this was not observed with the Myc antibody. The difficulties experienced in detecting this highly expressed gene at the protein level, could suggest an unusual translational aspect for this protein. Further investigation is required to optimize protein detection in this system.

As IGFBP5 is a secreted factor, the effect of IGFBP5 in 3T3-L1 culture media on cell differentiation was investigated. Conditioned media was harvested from IGFBP5 overexpressing 3T3-L1 preadipocytes or EV control transfected cells and used along with the standard induction cocktail (MDI) to induce differentiation of un-transfected 3T3-L1 preadipocytes. No difference in lipid droplet accumulation was observed in comparison to EV control, as assessed by Oil Red O staining and quantification (Figure 4.4D).

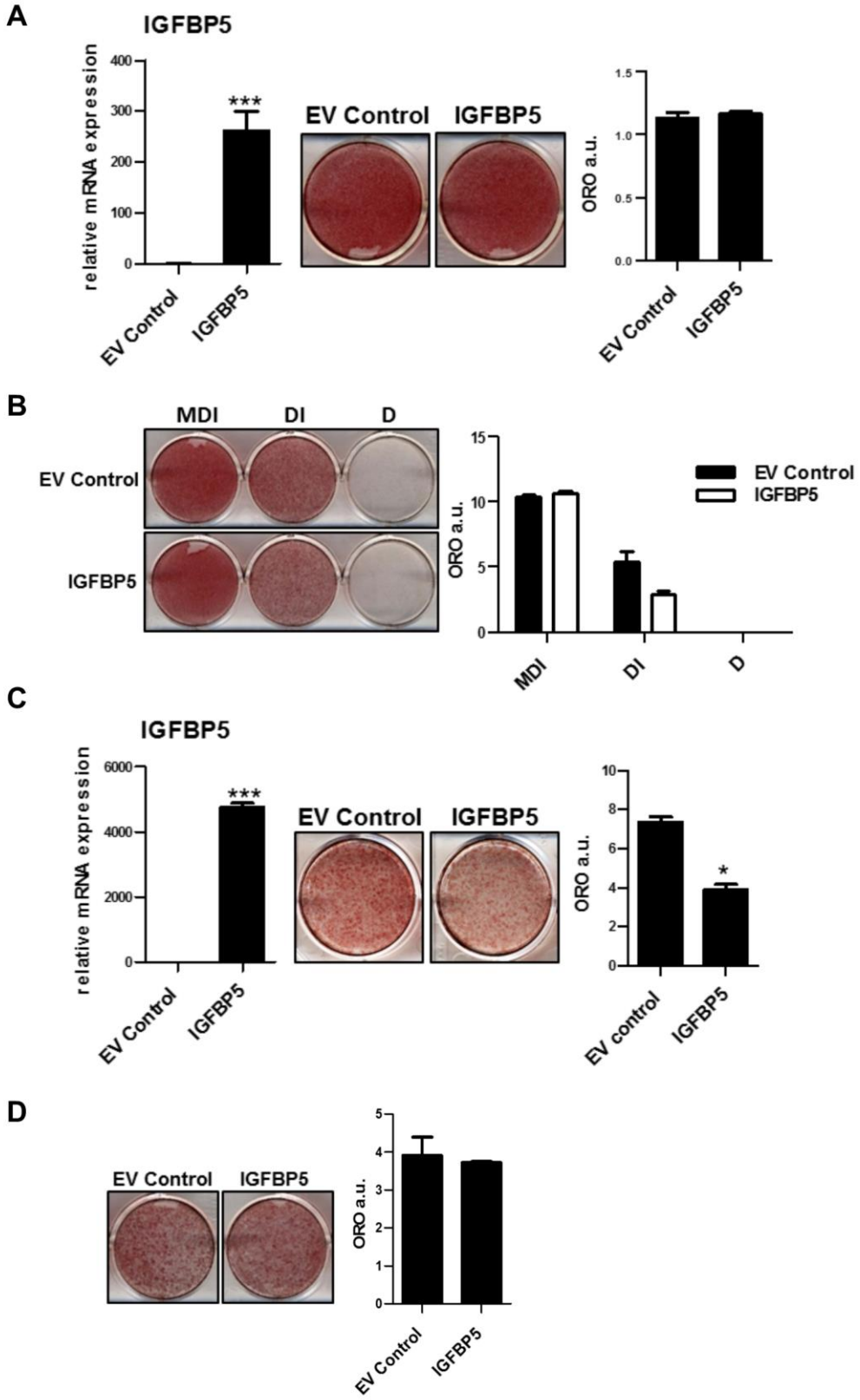

Figure 4.4: IGFBP5 overexpression has varied effects on 3T3-L1 differentiation. (A) 3T3-L1 preadipocytes were stably transfected with pMSCV(PB)-IGFBP5 or empty vector control pMSCV(PB) plasmid and induced to differentiate into

adipocytes. qPCR analysis of ectopic IGFBP5 expression was performed at day -2 of differentiation in stably transfected 3T3-L1 cells. (B) Cells stably transfected with pMSCV(PB)-IGFBP5 or empty vector control pMSCV(PB) plasmid were induced to differentiate using full induction media MDI (methylisobutylxanthine, dexamethasone and insulin), sub-maximal media DI (dexamethasone and insulin) or D (dexamethasone) as indicated. (C) 3T3-L1 preadipocytes were stably transfected with pMSCV(PB)-IGFBP5 and pCMV(PB) (IGFBP5) or empty vector controls pMSCV(PB) and pCMV(PB) (EV Control) and induced to differentiate into adipocytes. qPCR analysis of ectopic IGFBP5 expression was performed at day -2 of differentiation in stably transfected 3T3-L1 cells. (D) Media was harvested from growing 3T3-L1 preadipocytes stably transfected with pMSCV(PB)-IGFBP5 or empty vector control pMSCV(PB). Un-transfected 3T3-L1 preadipocytes were induced to differentiate using the standard MDI induction cocktail in the previously harvested IGFBP5 conditioned medium. The condition medium was used throughout differentiation. Adipogenesis was assessed at day 8 post induction by staining with Oil Red O. Quantification was performed using ImageJ and expressed as Oil Red O absorbance units (ORO a.u.). A Student's t-test (two-tailed, assuming equal variance) was used to calculate statistical significance compared to empty vector control cells, indicated as follows: *=P<0.05; **=P<0.01; ***=P<0.001.

IGFBP5 knockdown in 3T3-L1 differentiation

To investigate the role of endogenous IGFBP5 in 3T3-L1 cell differentiation shRNA constructs were designed to silence IGFBP5 expression. 3T3-L1 preadipocytes were stably transfected with a piggyBac transposable IGFBP5 shRNA knockdown construct, pRFP(PB).shIGFBP5 or scramble control pRFP(PB).shControl and induced to differentiate. Knockdown of endogenous IGFBP5 appeared to enhance adipogenesis in comparison to control cells, as assessed by Oil Red O staining and quantification (Figure 4.5A). QPCR analysis of IGFBP5 expression at day -2, 4 and 8 (Figure 4.5A) showed variable silencing of IGFBP5 expression during differentiation. No knockdown was detected at day -2, a slight reduction in expression levels was observed at day 4, and IGFBP5 was significantly reduced at day 8. It is not clear why the stably transfected shIGFBP5 only appeared to significantly reduce IGFBP5 expression at day 8. It would be of interest to assess the effects of shITM2A at other time points during differentiation. Although there are no reports of alternative splicing for IGFBP5 in the literature, the presence of different IGFBP5 isoforms at different time-points during cell differentiation could account for the time-point specific knockdown of IGFBP5 expression by the shRNA construct. It would be of interest to assess IGFBP5 expression at day 2 of differentiation, as this is the only other time-point during differentiation in which IGFBP5 is highly expressed. This experiment warrants repetition and further analysis to fully elucidate the pattern of IGFBP5 expression in response to shIGFBP5 transfection during cell differentiation. Immunoblot analysis of PPARγ at day 4 of differentiation revealed an increase in PPARγ2 protein in shIGFBP5 transfected cells (Figure 4.5B). This is consistent with the observed increase in lipid droplet accumulation in these cells. The RNA–Seq data indicate that LMNA over expression decreases IGFBP5 expression, raising the possibility that IGFBP5 down regulation plays a role in LMNA mediated adipogenesis inhibition. By contrast, the knockdown of IGFBP5 reported here shows the opposite effect namely that IGFBP5 down regulation enhances adipogenesis. The reason for these incongruous findings is unclear, however, given the complex nature of IGFBP5 and its activity it is possible that knockdown of IGFBP5 in the early stage of adipogenesis has the opposite effect to knockdown of IGFBP5 in the later stages of adipogenesis. Given the findings reported in the previous chapter where ITM2A knockdown can rescue adipogenesis inhibition by LMNA over expression, it would

be interesting to determine whether such inhibition could also be rescued by IGFBP5 knockdown.

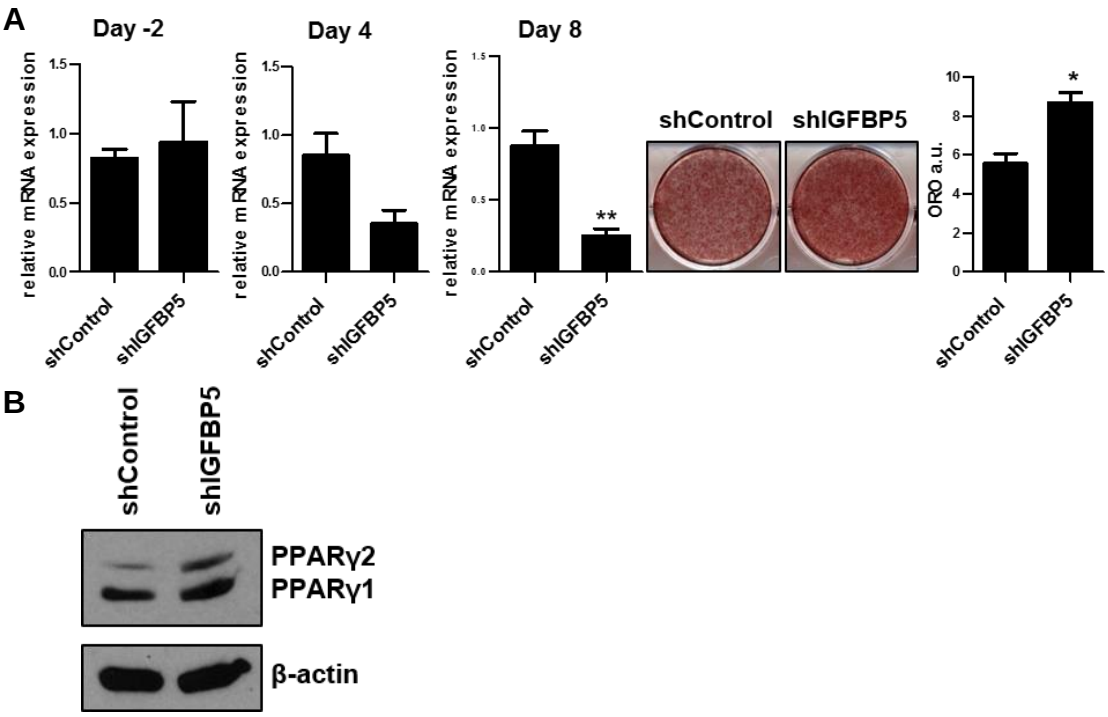

Figure 4.5: shRNA mediated knockdown of IGFBP5 expression in 3T3-L1 differentiation. 3T3-L1 preadipocytes were stably transfected with pRFP(PB).shIGFBP5.1 or scramble control pRFP(PB).shControl and induced to differentiate. (A) qPCR analysis of IGFBP5 expression at the indicated time points during 3T3-L1 cell differentiation. Adipogenesis was assessed at day 8 by staining with Oil Red O; quantification was carried out using ImageJ and expressed as Oil Red O absorbance units (ORO a.u.). (B) Immunoblot analysis of PPARγ at day 4 post induction. Student's t-test (two-tailed, assuming equal variance) was used to calculate statistical significance compared to shControl, indicated as follows: *=P<0.05; **=P<0.01; ***=P<0.001.

IGFBP5 promoter analysis in 3T3-L1 differentiation

As previously described the IGFBP5 promoter has been studied in diverse systems. To characterise IGFBP5 promoter activity in 3T3-L1 differentiation a series of luciferase reporter plasmids were constructed containing fragments of the mouse IGFBP5 promoter (1.2kb and 2.4kb) (Figure 4.6A) and their activity was analysed during differentiation. 3T3-L1 pre-adipocytes were transfected with the luciferase constructs, grown to confluence, and induced to differentiate. The 1.2kb IGFBP5 promoter fragment directed luciferase activity throughout differentiation, while the larger 2.4kb was not active as a promoter and directed less luciferase activity than the empty pGluc control construct (Figure 4.6B). Similar results have been reported in some of the previously described promoter studies, in which larger IGFBP5 promoter constructs failed to direct luciferase activity in comparison to smaller segments [226]. This suggests the presence of an inhibitory element between 1.2 to 2.4 kb upstream of the IGFBP5 gene.

Surprisingly, the 1.2kb promoter activity observed during differentiation did not follow the pattern of endogenous IGFBP5 gene expression described in Figure 4.2B. IGFBP5 promoter activity appeared to be significantly reduced at day 2 of 3T3-L1 differentiation, in stark contrast to the increase observed in the endogenous IGFBP5 mRNA at this same time point when measured by qPCR.

Despite this inconsistency, the effect of LMNA over expression on the 1.2 kb IGFBP5 promoter was examined to determine if LMNA had any effect on the cloned IGFBP5 promoter. As previously mentioned LMNA overexpression appears to affect luciferase activity driven from internal transfection control promoters in standard dual-luciferase transient transfections, preventing data normalisation. Thus, the effects of LMNA on the IGFBP5 promoter were not assessed in this format. Rather, LMNA/IGFBP5 1.2kb reporter stable 3T3-L1 lines were generated using a two-step transfection and selection approach (as previously described in chapter 3). Briefly, 3T3-L1 preadipocytes were transfected with piggyBac transposable reporter constructs and selected with one antibiotic. Once selected, these cells were transfected again with piggyBac LMNA over-expression constructs and selected with a second antibiotic. The 1.2kb IGFBP5 promoter fragment was cloned into a piggyback

transposable pGluc(PB) construct to allow for stable integration and selection in these experiments.

Both WT and R482W mutant LMNA over-expression appeared to increase IGFBP5 promoter activity prior to induction (day 0) and decrease promoter activity after the cells were induced and throughout differentiation (day 4, 6 and 8) (Figure 4.6C). Oil-Red-O staining showed reduced lipid droplet accumulation in R482W mutant LMNA transfected cells, however the WT LMNA did not appear to affect adipogenesis.

Finally, the effects of LiCl and testosterone on IGFBP5 promoter activity were assessed during differentiation. As previously described IGFBPs have been shown to interact with various components of the canonical Wnt/β-catenin signalling pathway in diverse settings. Wnt signalling plays an important inhibitory role in adipogenesis, and its down-regulation is necessary for cells to progress through the differentiation programme (92). LiCl treatment inhibits 3T3-L1 differentiation through activation of Wnt/β-catenin signalling and increased cellular β-catenin. Testosterone has previously been shown to activate the IGFBP5 promoter in androgen responsive fibroblasts and numerous publications have reported testosterone mediated inhibition of adipocyte differentiation [280–282]. To assess the effects of these components on IGFBP5 promoter activity in adipogenesis 3T3-L1 preadipocytes were stably transfected with pGluc(PB)/IGFBP5/1.2kb, grown to confluency and induced to differentiate with full induction media (MDI) including LiCl or testosterone. Oil Red O staining confirmed LiCl inhibition of cell differentiation as these cells did not accumulate any lipid droplets (Figure 4.6D). Testosterone, in contrast to published reports, however did not have any effect on 3T3-L1 differentiation (Figure 4.6D). This was consistently observed across many differentiations and for increased concentrations of testosterone, and will be discussed further in chapter 5. LiCl treatment appeared to reduce IGFBP5 promoter activity significantly at day 2, 6 and 8 of differentiation, while testosterone treatment had very little effect on promoter activity, with a small reduction observed on day 2 of differentiation.

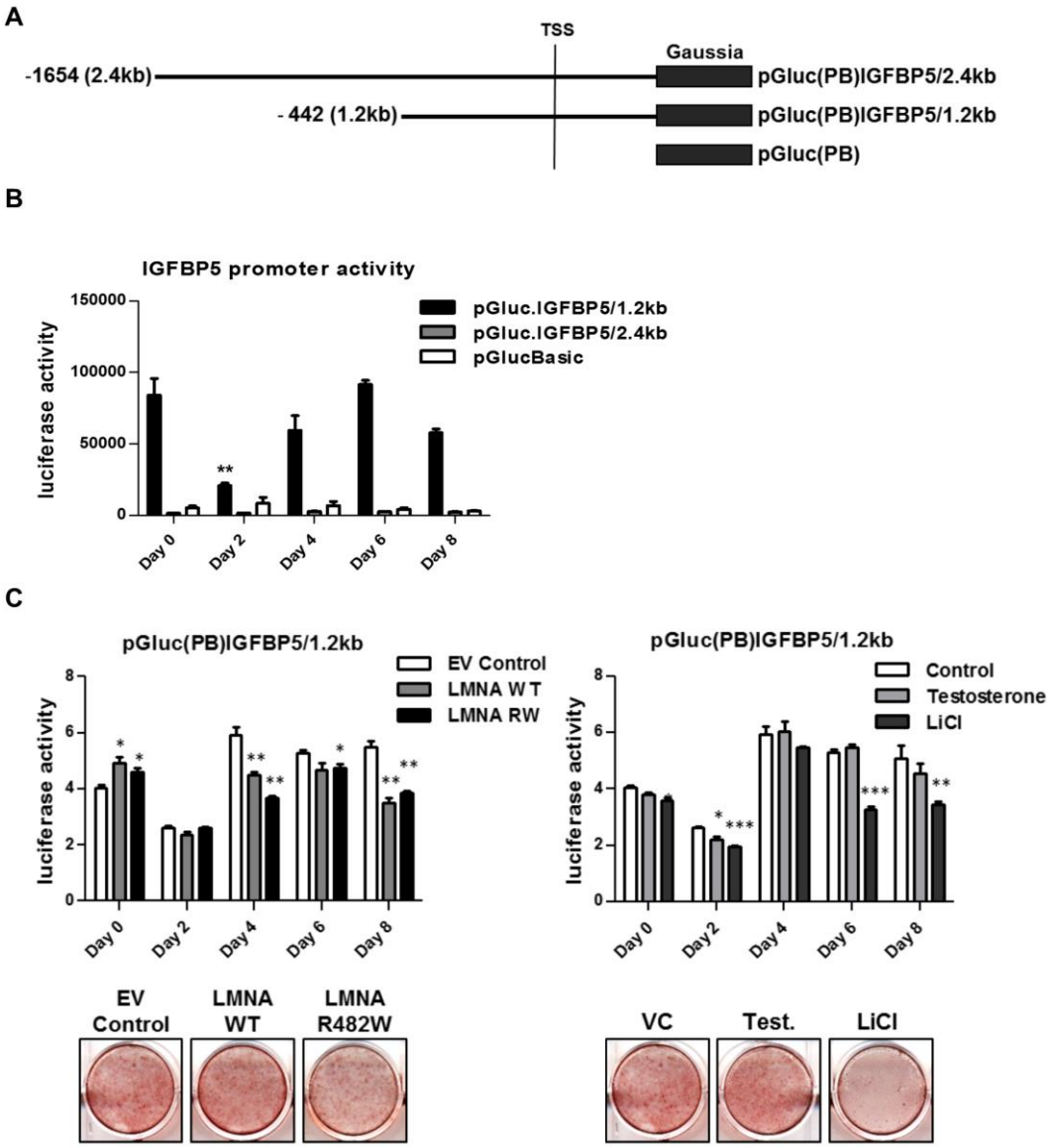

Figure 4.6: IGFBP5 promoter activity in 3T3-L1 differentiation. (A) Schematic depiction of IGFBP5 promoter luciferase constructs bearing a 2.4kb or 1.2kb promoter fragment cloned upstream of *Gaussia* luciferase in the pGluc(PB) basic vector. The distance (-1654, -442) from the transcriptional start site (TSS) is shown. (B) Luciferase activity (secreted) in pGluc/IGFBP5/1.2kb and pGluc/IGFBP5/2.4kb transfected 3T3-L1 cells at various time points throughout differentiation. (C) Luciferase activity in 3T3-L1 cells stably transfected with pGluc(PB)/IGFBP5/1.2kb and LMNA overexpression constructs (WT and R482W mutant) or EV control. Luciferase activity in 3T3-L1 cells stably transfected with pGluc(PB)/IGFBP5/1.2kb and treated with LiCL (20mM) and testosterone (100nM). Adipogenesis was assessed at day 8 by

staining with Oil Red O. Student's t-test (two-tailed, assuming equal variance) was used to calculate statistical significance compared to MDI (B, C), EV Control (D) or vehicle control (D), indicated as follows: *=P<0.05; **=P<0.01; ***=P<0.001.

LMNA overexpression has variable effects on IGFBP5 expression in 3T3-L1 differentiation

The previously described RNA-Seq data identified reduced expression of IGFBP5 36 h post differentiation induction of cells overexpressing WT and R482W mutant LMNA. Interestingly IGFBP5 expression was reduced 50-fold in response to WT LMNA and only 5-fold in response to the R482W mutant.

To confirm these distinct effects of WT and R482W mutant LMNA on IGFBP5 expression, 3T3-L1 preadipocytes were stably transfected with human LMNA overexpression constructs and induced to differentiate. Figure 4.6 shows two separate transfection experiments in which LMNA over-expression inhibited lipid droplet accumulation when compared to empty vector controls, as determined by Oil Red O staining (Figure 4.7A, C). IGFBP5 expression analysis identified conflicting effects of LMNA on IGFBP5 expression between the two replicates. Increased IGFBP5 expression was observed in replicate 1(Figure 4.7B), while reduced IGFBP5 expression was observed in the second replicate (Figure 4.7D). It is important to note that WT and R482W mutant LMNA had distinct effects on IGFBP5 expression in both replicates. In the first replicate, an overall trend of increased IGFBP5 expression was observed in response to both LMNA WT and R482W mutant, although not always significant at each time point. In the second replicate, WT LMNA appeared to significantly reduce IGFBP5 expression at day 2 and 4 of 3T3-L1 differentiation, while the R482W mutant LMNA did not alter IGFBP5 expression at any point. This is a similar trend to the distinct fold reductions measured in the RNA-Seq experiment, where LMNA WT over-expression lead to a much greater decrease in IGFBP5 transcription (50 fold), in comparison to R482W mutant LMNA (5 fold).

The reason for this disparity is unclear and some possible explanations are provided in the discussion.

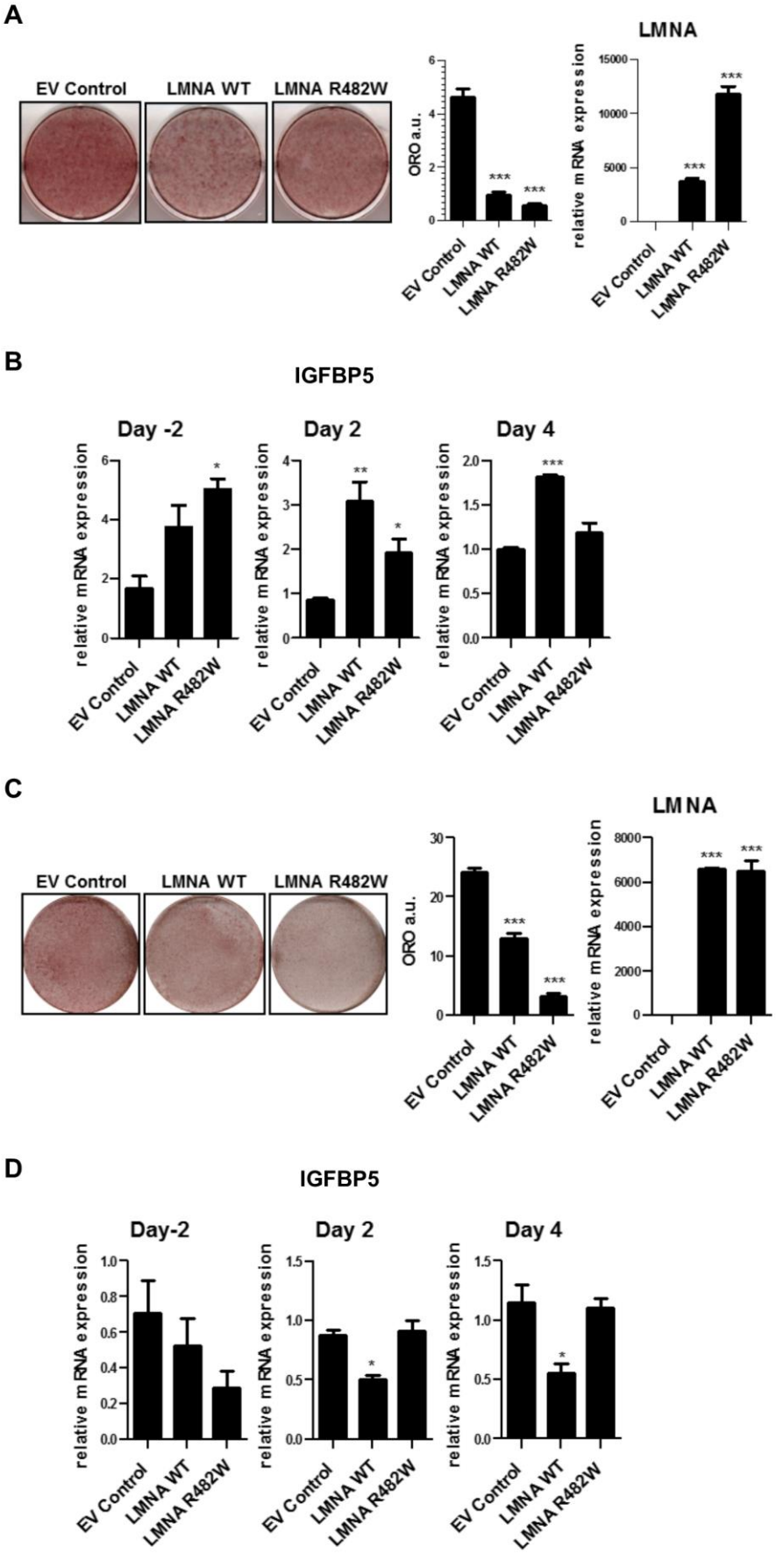
A
EV Control
LMNA WT
LMNA R482W
ORO a.u.
LMNA
relative mRNA expression
B
IGFBP5
Day -2
Day 2
Day 4
C
D
Day-2

Figure 4.7: LMNA over-expression both increases and decreases IGFBP5 expression in 3T3-L1 differentiation. (A, C) 3T3-L1 preadipocytes were stably transfected with pCMV(PB)-Flag-LMNA-WT, pCMV(PB)-Flag-LMNA-R482W or pCMV(PB) in replicate 1 (A) and pcDNA3-Flag-LMNA-WT pcDNA3-Flag-LMNA-R482W or pcDNA3.EV in replicate 2 (C). Adipogenesis was assessed by Oil Red O staining at day 8 of differentiation and ORO quantification was carried out using ImageJ and expressed as Oil Red O absorbance units (ORO a.u.). QPCR analysis of LMNA over-expression was performed at day -2 for each replicate. (B, D) QPCR analysis of IGFBP5 expression in replicate 1 (B) and 2 (D) at day -2, 2 and 4 of differentiation. A Student's t-test (two-tailed, assuming equal variance) was used to calculate statistical significance compared to empty vector control cells, indicated as follows: *=P<0.05; **=P<0.01; ***=P<0.001.

DISCUSSION

IGFBP5 in 3T3-L1 differentiation

The IGF axis plays a critical role in preadipocyte survival, proliferation and differentiation. The adipose organ is known to secrete many bio-active factors that are important in the regulation of metabolism, and has been described as a major source of secreted IGF-1 [283]. IGFBPs have been studied extensively in a variety of systems and display diverse IGF-dependent and independent functions, depending on their environment. As targets of transcriptional and hormonal regulation, the IGFBPs appear to have highly specific expression profiles, and their activities are further regulated by protein interactions and proteolytic degradation.

A previous study in 3T3-L1 preadipocytes failed to detect secreted IGFBP5 in this system [264] and conflicting reports of IGFBP5 expression have been reported in porcine adipocytes [272,273]. In this study, a distinct expression profile for IGFBP5 has been described in 3T3-L1 differentiation. Endogenous IGFBP5 expression is highly up-regulated at day 2 of 3T3-L1 differentiation, 48 h post application of the induction cocktail, and again at day 8 of differentiation, when the cells have accumulated lipid droplets and are considered mature adipocytes (Figure 4.2B). This specific expression pattern has not been observed previously when global gene expression was assessed in 3T3-L1 differentiation (Figure 4.2A), however it does resemble the human IGFBP5 expression profile of differentiating hASC, in which a sharp increase in gene expression is observed following induction of differentiation [178].

Investigation of IGFBP5 promoter activity in this system using a 1.2kb IGFBP5 promoter reporter constructs produced unexpected results. Promoter activity decreased in response to the induction cocktail rather than increase, which was predicted due to the dramatic increase in IGFBP5 mRNA at this stage of differentiation. Previous studies have reported increased IGFBP5 promoter activity in response to cAMP (forskolin) and reduced activity in response to dexamethasone, both ingredients of the 3T3-L1 induction cocktail. It is unclear if either of these induction components are responsible for the decrease observed in this system. A number of the aforementioned studies characterised IGFBP5 promoter activity in various systems using much smaller, yet still highly active promoter fragments in their respective

reporter assays. A much larger or smaller promoter segments might behave differently in the context of 3T3-L1 differentiation. Further analysis of additional promoter regions would be required to elucidate the complicated transcriptional events involved in the control of IGFBP5 expression in 3T3-L1 differentiation. McCarthy et al., (1996) [226] reported that PGE_2 both stimulated IGFBP5 promoter activity and enhanced IGFBP5 mRNA stability in rat osteoblasts. Tardif et al., (2009) [284] identified microRNA regulation of IGFBP5 expression in human osteoarthritic chondrocytes. Over-expression of mir140 in these cells appeared to decrease IGFBP5 expression, with a corresponding decrease in protein production. The large 3' untranslated region in the IGFBP5 transcript contains approximately 13 predicted microRNA binding sites (TargetScan) and it would be of interest to investigate the activity of these microRNA in adipogenesis, with respect to IGFBP5 gene regulation. These studies highlight the complexity of IGFBP5 regulation and suggests that a number of mechanisms may be involved.

Investigation of the role of IGFBP5 in adipogenesis showed that exogenous expression of IGFBP5 could inhibit 3T3-L1 differentiation (Figure 4.3B). Moderate IGFBP5 over-expression (approx. 200-fold) did not appear to affect differentiation (Figure 4.3A), while higher levels of over-expression (approx. 5000-fold) reduced lipid droplet accumulation significantly (Figure 4.3B). Differential effects of IGFBP overexpression have previously been reported to produce distinct phenotypes in IGFBP3 transgenic mice. A study carried out by Silha et al., (2002), [285] reported glucose intolerance and insulin resistance in transgenic mice over-expressing human IGFBP3 from PGK and CMV promoters. Interestingly, the mice expressing IGFBP3 from the CMV promoter showed increased expression of the transgene in their skeletal muscle tissue when compared to PGK driven IGFBP3 and displayed increased adiposity. This difference in phenotype was attributed to variation in tissue levels and timing of IGFBP3 expression between the transgenic mice [285]. It is possible that the varied effects of IGFBP5 on adipogenesis observed here are due to the variation in levels of over-expression.

Addition of IGFBP5 to culture media, using conditioned media harvested from IGFBP5 transfected preadipocytes, did not appear to affect differentiation (Figure 4.3D). Attempts to detect the secreted protein in this conditioned media using a Flag antibody were unsuccessful. Therefore, the quantity or stability of secreted IGFBP5

was not assessed. To accurately examine the modulation of 3T3-L1differentiation by IGFBP5, recombinant IGFBP5 protein could be added to differentiating cells in culture at varying concentrations and at different time points during differentiation. The observation that large amounts of exogenous IGFBP5 reduces cell differentiation suggests that increased IGFBP5 might bind to and sequester IGF-1, thus inhibiting its stimulatory effect on the in vitro differentiation of these cells. Cobb et al., (2003) [246] demonstrated that over-expression of WT IGFBP5 inhibited myogenesis by binding IGF-1 to modulate IGF-1 signalling in this system. It is possible that IGFBP5 over-expression plays a similar role in adipogenesis. An exact function for IGFBP5 in 3T3-L1 differentiation remains to be confirmed and additional experiments would need to be performed to elucidate whether these effects are IGF-dependent or independent.

Knockdown of endogenous IGFBP5 enhanced lipid droplet accumulation in comparison to the scramble control (Figure 4.3A) and increased PPARγ2 protein was observed at day 4 of differentiation in these cells. This effect is consistent with the model that IGFBP5 inhibits IGF-1 stimulation of 3T3-L1 differentiation, as reduced IGFBP5 protein would result in an increase of IGF-1 available to bind IGF-1 receptors. A few technical issues were encountered when attempting to generate IGFBP5 shRNA constructs. Originally a synthetic Gibson assembly approach was employed, where shRNA sequences were purchased as ultramer oligonucleotides (long oligonucleotides of up to 200 bases) from IDT, PCR amplified with Gibson overlap primers and cloned into the pRFP(PB) backbone. High levels of recombination were observed using this technique with frequent deletion of nucleotides within the shRNA 29 mer sequence. A traditional cloning approach was then employed to reduce recombination and one of the three attempted shIGFBP5 constructs was cloned successfully. To confirm the effect of IGFBP5 silencing on 3T3-L1 differentiation additional shRNA constructs would need to be assayed to eliminate the possibility of off target effects. Alternatively, considering the distinct IGFBP5 expression pattern during 3T3-L1 differentiation, it would of interest to investigate the effects of siRNA mediated IGFBP5 knockdown at specific time points during differentiation i.e. from day 0 to day 2. As IGFBP5 expression appears to be up-regulated in response to 3T3-L1 induction it would be interesting to see if blocking this up-regulation had an impact on cell differentiation.

The sharp up-regulation of IGFBP5 during early adipogenic differentiation is reminiscent of the dramatic increase in IGFBP5 observed in mammary gland involution. This hormonally induced stimulation of IGFBP5 expression functions to block IGF-1 survival signalling and induce epithelial cell apoptosis in the involuting mammary gland [275]. The mechanism behind IGFBP5 up-regulation as well as the subsequent function of IGFBP5 protein in early 3T3-L1 differentiation are unclear. Some studies have described enhanced IGF-1 signalling through ECM-associated IGFBP5 [215], where extracellular bound IGFBP5 potentiates the stimulatory growth effects of IGF-1 potentially by acting as some sort of IGF-1 transport and delivery system [275]. If IGFBP5 were to behave in such a manner during 3T3-L1 adipogenesis it could play a role in augmenting specific IGF-1 action in these differentiation cells. To define IGFBP5 action in adipogenesis, multiple factors need to be addressed, including IGF-1 binding, ECM component interactions, IGFBP5 protein stability and proteolytic degradation. As well as modulating IGF-1 activity in this system, IGFBP5 could be affecting differentiation through IGF-1 independent actions. Assessing the effects of an IGFBP5 mutant, unable to bind IGF-1, on 3T3-L1 differentiation could help elucidate the IGFBP5 mechanism of action.

IGFBP5 and LMNA

To investigate the relationship between LMNA and IGFBP5 indicated by the RNA-Seq analysis, 3T3-L1 preadipocytes were stably transfected with human WT and R482W mutant LMNA overexpression constructs and IGFBP5 expression was assessed during cell differentiation (Figure 4.6). Conflicting results were obtained as LMNA over-expression appeared to both increase (Replicate 1) and decrease (replicate 2) IGFBP5 expression during differentiation. In the second experimental replicate, a decrease in IGFBP5 expression was observed in response to WT LMNA in comparison to the null effect of the R482W mutant. This mirrors the variation observed in our RNA-Seq data. Finally, the effect of LMNA on IGFBP5 expression was investigated using a 1.2kb IGFBP5 promoter reporter construct (Figure 4.5C). LMNA appeared to enhance IGFBP5 promoter activity prior to induction and reduce promoter activity during differentiation. However, this method proved problematic

and it was not possible to demonstrate a direct effect of LMNA on the IGFBP5 promoter activity during differentiation.

The effects of LMNA on IGFBP5 in this system are unclear as considerable variation was observed in all lines of enquiry. A number of experimental factors may be responsible for the issues observed in reproducibility. While cell culture conditions were kept as consistent as possible, the complex nature of IGFBP5 regulation might call for tighter controls in this system. During 3T3-L1 cell differentiation, cell confluency is judged by eye prior to induction. It is possible that small variations in cell confluency, passage number and time points during differentiation may have contributed to the inconsistencies observed. In addition, different LMNA over-expression constructs were used in the replicates described in figure 4.6. Although both constructs contained a CMV promoter, G418 selection cassette and the same LMNA cDNA sequence, variable effects of LMNA on IGFBP5 were observed. This could be due to the handling of the cells, and relate to the complex control of IGFBP5 expression in this system.

Another consideration is that IGFBP5 null mice develop normally whereas triple knockouts for IGFBP3, 4 and 5 have smaller fat pads. This suggest that the relationship between LMNA inhibition of adipogenesis and the IGFBPs should consider the combined response of these three IGFBPs in relation to LMNA WT and R482W over expression. Interestingly, the RNA-Seq data suggest that minimally IGFBP3 should be analysed in combination with IGFBP5 as the expression of IGFBP3 is altered (albeit at a lower magnitude than IGFBP5) in the opposite direction to IGFBP5 (Table 1, Chapter 1).

A substantial limitation in this study is the level of intrinsic variation observed in 3T3-L1 transfection and differentiation. The lack of precision in degrees of overexpression of IGFBP5 leads to difficulties in data reproduction and interpretation. Accurate manipulate of IGFBP5 in this system calls for a better understanding on its regulation in adipogenesis.

The initial incentive in studying IGFBP5 was to identify factors that might promote adipogenesis and could potentially be used in novel FPLD2 therapy. Due to the

complicated nature of IGFBP5 regulation in this system, it is not a good therapeutic lead. As LMNA overexpression lead to a reduction in IGFBP5 expression in the RNA-Seq analysis, it was postulated that IGFBP5 overexpression might have a stimulatory effect during adipogenesis. However this was not the case, and the opposite was observed where IGFBP5 over-expression either had no effect or reduced adipogenesis while shRNA mediate IGFBP5 knockdown enhanced adipogenesis. In addition, proximal promoter activity was not in keeping with the mRNA expression profile during adipogenesis. Previously, the study of ITM2A in this system produced robust and reproducible data, and while the reasons behind the observed variability in the study of IGFBP5 are unclear, they are most likely related to the highly regulated and differential expression of IGFBP5 during the process of adipogenesis. An alternative approach might be to assess endogenous IGFBP5 expression and secretion profiles in FPLD2 patient samples or laminopathy/lipodystrophy mouse models.

CHAPTER 5: PRELIMINARY INVESTIGATIONS OF PTPRQ, WNT6 AND TESTOSTERONE IN 3T3-L1 DIFFERENTIATION

SECTION 1: PTPRQ

INTRODUCTION

The phosphorylation and de-phosphorylation of protein tyrosine residues, by protein tyrosine kinases (PTKs) and protein tyrosine phosphatases (PTPs) respectively, plays an important role in cellular signalling transduction systems involved in numerous processes such as cell growth, metabolism and differentiation [286]. The PTP enzyme superfamily are a large group of hydrolytic enzymes that can be divided into three main sub-groups including classical PTPs, low molecular weight PTPs and dual-specificity PTPs [287]. PTPRQ was first identified in rat mesangial cells where it is dramatically up-regulated following renal injury (Wright et al., 1998), and is classified as a type–III receptor PTPase with a single catalytic domain and 18 fibronectin type III domains (FN3) [288].

Relatively little research has been carried out on PTPRQ with only 25 article published on PTPRQ gene function to date. The majority of published work centres on the role of PTPRQ in cochlear hair bundle integrity in the inner ear. A number of PTPRQ mutations have been reported in cases of autosomal recessive non-syndromic hearing impairment (arNSHI), where either nonsense or missense mutations lead to hearing loss and vestibular dysfunction [289,290]. PTPRQ is essential for the formation of shaft connectors in mouse hair bundles, and for the normal development of cochlear hair bundles [291,292]. It has been suggested that there may be multiple PTPRQ isoforms expressed in these hair bundles [293], and a number of alternatively spliced mRNAs have been identified in human tissues, leading to protein isoforms differing in FN3 domain number [289].

Previous studies have identified distinct PTPRQ isoforms that are expressed in a tissue specific manner. PTPRQ is detected in a large receptor-like form or as a smaller cytoplasmic protein in different cell types. Seifert et al., (2002), [288] reported expression of the larger PTPRQ transcript in human kidney and lung tissues, while smaller transcripts were detected in the brain and testis. Both alternative splicing [289,294] and

the use of alternative promoters have been described as mechanisms responsible for the distinct PTPRQ isoforms [294]. In addition, alternative promoters are reported to generate receptor-like and cytoplasmic isoforms of various other PTPases [295,296]. Figure 5.1.1 illustrates the different transcripts detected by Seifert et al., (2002)[294] in various human tissues.

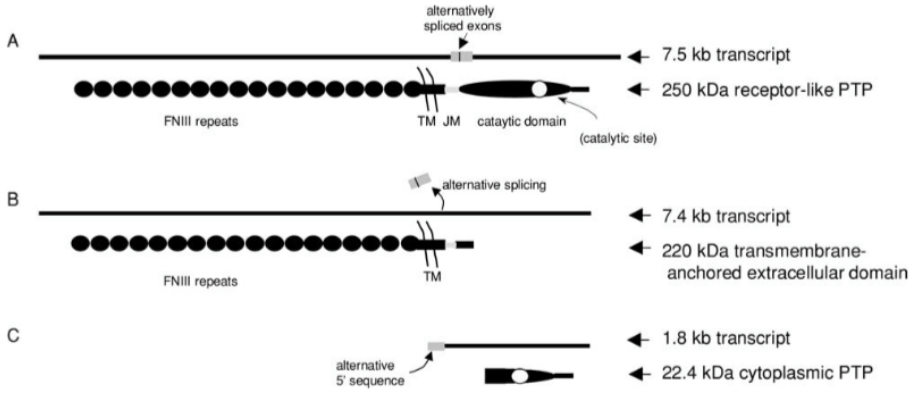

Figure 5.1.1: Alternative PTPRQ transcripts and protein forms. Three PTPRQ transcripts are detected in human tissues; 7.5kb, 7.4kb and 1.8kb. (A) The 7.5kb transcript predicts a 250kDa receptor like protein that has an extracellular domain composed of 18 FN3 repeats, a transmembrane domain (TM) and a catalytic domain that are separated by a small juxtamembrane (JM) segment. The catalytic domain contains the PTP active site. (B) Alternative splicing can lead to the generation of protein lacking a catalytic domain. (C) Alternative promoter usage leads to the generation of a 1.8kb transcript that encodes a truncated catalytic domain, predicted at 22 kDa. Taken from Seifert et al., (2002) [294].

Numerous studies have reported that PTPRQ exhibits low levels of PTPase activity in comparison to other PTP enzymes, and that its predominant activity is as a phosphatidylinositol phosphatase (PIPase) against a broad range of phosphatidylinositol phosphates (PIPs)[297–299]. The PTPRQ catalytic domain contains a Glu residue in place of an Asp that is essential for PTPase activity, and highly conserved in other PTPases, suggesting that PTPRQ may not favour phosphotyrosine as a substrate [297]. PIPase enzymes function to inhibit signalling through PI(3,4,5)P3 activated pathways, preventing downstream AKT/PKB phosphorylation [294]. Oganesian et al., (2003) [297] demonstrated that overexpression of the rat PTPRQ cytoplasmic region (from the first amino acid inside the TM domain) in human

glioblastoma cell lines (U87MG, U373MG) that do not express PTEN (a well characterised PIPase), leads to a decrease in phosphorylated AKT/PKB and significantly reduced rates of proliferation, mediated by PIPase activity. In addition, Yu et al., (2013) [299] have demonstrated that the PTPRQ catalytic loop adopts a flat active-site pocket conformation, making it suitable for de-phosphorylation of larger PI substrates.

In chapter 4 the role of insulin and IGF-1 signalling in adipogenesis was discussed and the phenotypes of multiple mouse models lacking insulin/IGF-1 signalling components were described. As downstream elements of the insulin/IGF-1 signalling cascade phosphatidylinositol-3 kinase (PI3K) and AKT1/protein kinase B (PKB) or AKT2/PKB are essential for adipogenesis. AKT1/AKT2 double knockout mice display severe growth defects with impaired development of bone and skin tissues, skeletal muscle atrophy and a block in adipocyte differentiation [300]. AKT1/AKT2 double KO MEFs fail to differentiate in-vitro as PPARγ up-regulation is blocked in these cells. It has since been shown that insulin stimulates AKT/PKB mediated phosphorylation and nuclear exclusion of the PPARγ repressor, FOXO1 [92,301]. In addition, PI3K inhibitors and rapamycin mediated inhibition of mTOR have been shown to inhibit 3T3-L1 differentiation [302,303]. Figure 5.1.2 illustrates the activity of various extracellular signalling factors during the process of adipogenesis, where insulin and IGF-1 activation of the PI3K/AKT signalling pathway is shown to be involved in the downstream up-regulation of pro-adipogenic factors.

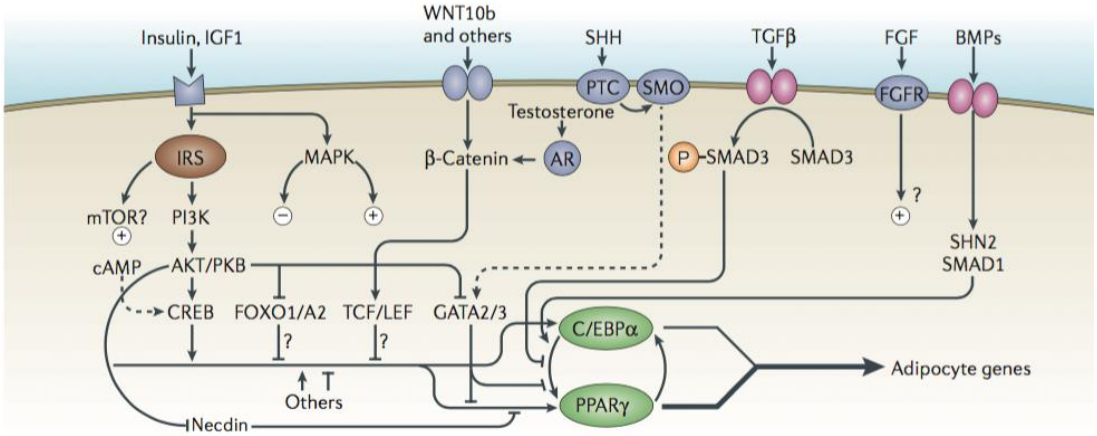

Figure 5.1.2: Extracellular factors involved in the regulation of adipogenesis. Taken from Rosen and MacDougald (2006) [92].

PTPRQ activity and function have previously been described in the context of in-vitro adipogenesis. Jung et al., (2009) [298] reported PTPRQ down-regulation during the adipogenic differentiation of both MSCs and 3T3-L1 preadipocytes. In their study over-expression of the human PTPRQ cytoplasmic region was seen to reduce lipid droplet accumulation in both cell types by reducing AKT/PKB phosphorylation. PTPRQ mutants inactive against just phosphatidylinositol phosphates or both phosphatidylinositol phosphates and phosphotyrosine did not inhibit cell differentiation indicating that wild type PTPRQ reduces intracellular PIP3, which in turn leads to reduced AKT/PKB phosphorylation and inhibition of adipogenesis [298].

The previously described RNA-Seq analysis identified a 4-, and 10-fold increase in PTPRQ mRNA in response to WT and R482W mutant LMNA, respectively. Since previous studies have reported PTPRQ mediated inhibition of 3T3-L1 adipogenesis, the relationship between LMNA and PTPRQ was investigated. An additional incentive for the investigation of PTPRQ in adipogenesis is the recent development of novel PTPRQ phosphatase inhibitors [304]. If a LMNA mediated increase in PTPRQ expression contributed to the inhibition of adipogenesis, then PTPRQ inhibition could potentially rescue adipogenesis in this system.

RESULTS

PTPRQ expression is down-regulated during 3T3-L1 differentiation

Consistent with previous reports [298], endogenous PTPRQ expression was down-regulated during 3T3-L1 differentiation. QPCR analysis revealed low levels of PTPRQ in pre-adipocytes that were further reduced as the cells progressed through the differentiation programme (Figure 5.1.3A). The highest PTPRQ expression was detected at day -2, after which expression levels dropped significantly. PTPRQ was undetected at day 4 and 6 and minimal detection was observed at day 6 and 8. PTPRQ was consistently detectable at day -2 and 0, however it was not detected at day 6 and 8 in all 3T3-L1 differentiation replicates.

PTPRQ silencing in 3T3-L1 differentiation

To investigate the role of endogenous PTPRQ in 3T3-L1 cell differentiation, three shRNA constructs were designed to silence PTPRQ expression as described in materials and methods. 3T3-L1 preadipocytes were stably transfected with piggyBac transposable PTPRQ shRNA knockdown constructs, pRFP(PB).shPTPRQ.1,2 and 3, or scramble control pRFP(PB).shControl and induced to differentiate. One out of the three knockdown constructs, shPRPTQ.3, was seen to moderately inhibit lipid droplet accumulation in these cells (Figure 5.1.3C) and when PTPRQ expression was assessed only shPRPTQ.3 appeared to have reduced endogenous PTPRQ expression, in comparison to the scramble control (Figure 5.1.3B). The two remaining constructs, shPTPRQ.1 and 2 did not have a significant effect on either differentiation (Figure 5.1.3C) or PTPRQ mRNA expression (Figure 5.1.3B) in comparison to the scramble control. It is not clear why some of the KD constructs were unsuccessful in reducing PTPRQ expression. All three constructs contained 29mer shRNA sequences directed at the last 1000bp of the mouse PTPRQ gene, in order to target the catalytic domain.

PTPRQ expression in response to LMNA overexpression

To investigate the effects of WT and R482W mutant LMNA on PTPRQ expression reported in the RNA-Seq analysis, 3T3-L1 preadipocytes were stably transfected with human LMNA overexpression constructs and induced to differentiate. PTPRQ expression was assessed at day -2 of differentiation and no significant changes in

expression were observed in response to LMNA overexpression (Figure 5.1.3D). LMNA overexpression data for replicate one and two is shown in chapter 4 figure 4.7.

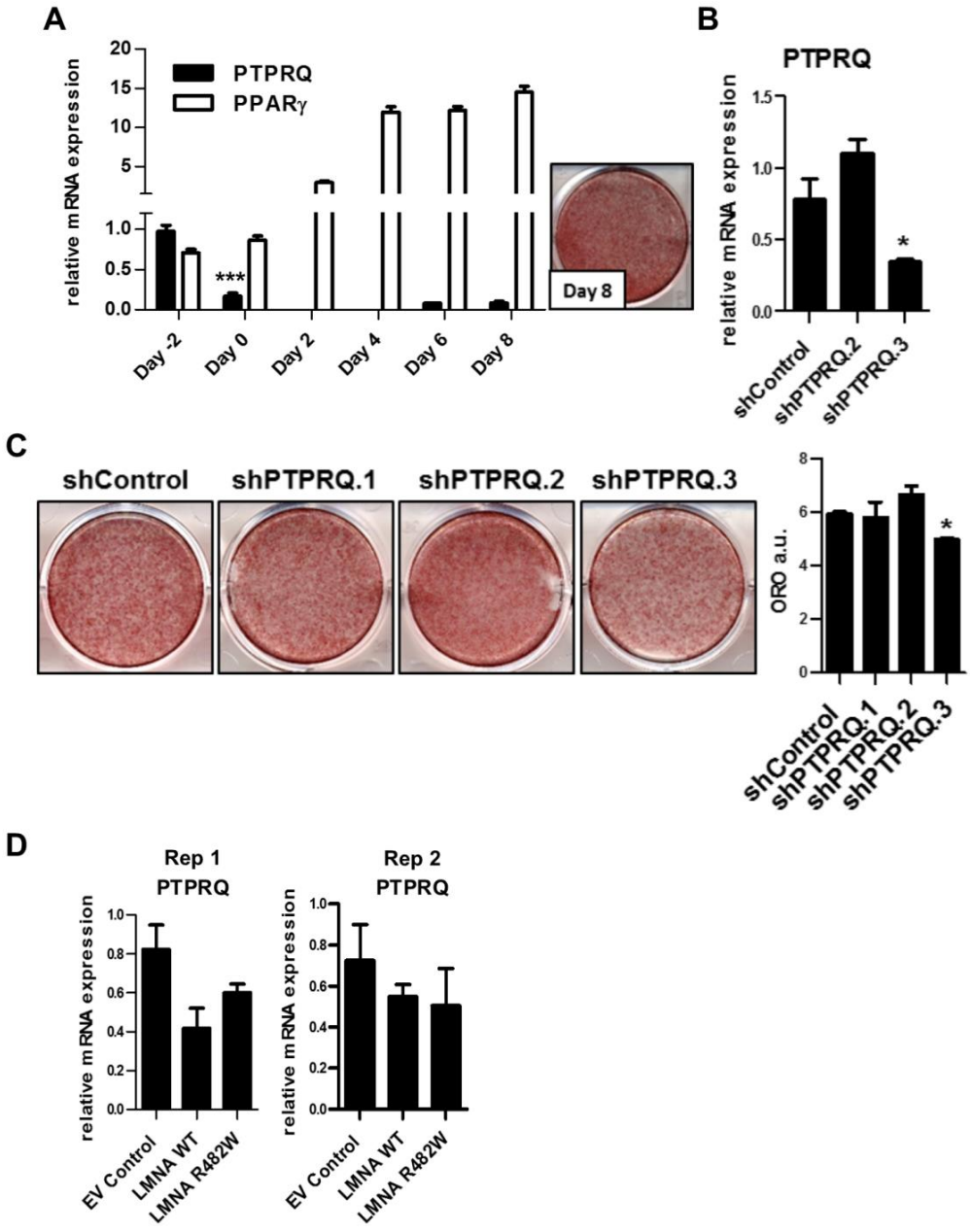

Figure 5.1.3: PTPRQ in 3T3-L1 differentiation and in response to LMNA. (A) 3T3-L1 preadipocytes were differentiated as previously described and adipogenesis was assessed at day 8 by staining with Oil Red O. Total RNA was isolated at the indicated time points during 3T3-L1 differentiation. PTPRQ and PPARγ expression was analysed by qPCR. Transcript expression at the various time points is shown relative to expression at day -2. (B) 3T3-L1 preadipocytes were stably transfected

with pRFP(PB).shPTPRQ.1,2 and 3 or scramble control pRFP(PB).shControl and induced to differentiate. PTPRQ expression was assessed by qPCR analysis at day-2. (C) Adipogenesis was assessed at day 8 post induction by staining with Oil Red O; quantification was carried out using ImageJ and expressed as Oil Red O absorbance units (ORO a.u.). (D) 3T3-L1 preadipocytes were stably transfected with pCMV(PB)-Flag-LMNA-WT, pCMV(PB)-Flag-LMNA-R482W or pCMV(PB) in replicate 1 and pcDNA3-Flag-LMNA-WT pcDNA3-Flag-LMNA-R482W or pcDNA3.EV in replicate 2 (ORO images and expression data shown in Figure 4.7, chapter 4). PTPRQ expression was analysed by qPCR at day -2 of differentiation for each replicate. A Student's t-test (two-tailed, assuming equal variance) was used to calculate statistical significance compared to empty vector control cells or LMNA WT (+/+) MEFs (E), indicated as follows: *=P<0.05; **=P<0.01; ***=P<0.001.

DISCUSSION

The role of insulin/IGF-1 activated PI3K/AKT signalling in adipogenesis has been extensively studied in numerous in-vitro and in-vivo settings. The importance of this system in whole body metabolism is emphasised by the severe lipodystrophic phenotype observed in the previously described AKT1/AKT2 double KO mouse. In addition, severe insulin resistance and type 2 diabetes mellitus have been reported in a family with an inherited mutation in the catalytic domain of AKT2/PKBβ [80]. In the context of adipogenesis, PTPRQ PIPase activity has been shown to reduce Akt/PKB phosphorylation, down-regulating this signalling cascade and inhibiting the in-vitro differentiation of 3T3-L1 and human MSCs [298]. RNA-Seq analysis of the gene expression profile in differentiating 3T3-L1 cells transfected with human WT and R482W LMNA, identified an increase in PTPRQ mRNA in response to LMNA over-expression. Since cytoplasmic PTPRQ over-expression is known to inhibit the differentiation of these cells, it was postulated that the observed increase in PTPRQ could contribute to the LMNA mediated block in adipogenesis.

Investigation of the role of PTPRQ in 3T3-L1 differentiation identified very low levels of expression in pre-adipocytes, which were further down-regulated during differentiation (Figure 5.1.3A). PTPRQ expression was not detected at day 2 or 4 of differentiation in any of the experimental replicates. This is in keeping with previous reports, where Jung et al., (2009) [298] observed that PTPRQ expression was low in 3T3-L1 cells, specifically in comparison to expression levels observed in human MSCs.

To explore the role of endogenous PTPRQ in 3T3-L1 differentiation, cells were stably transfected with shPTPRQ constructs and the effects of PTPRQ silencing on differentiation were assessed (Figure 5.1.2B,C). Although three different KD constructs were designed and constructed, only one of these appeared to reduce PTPRQ expression in these cells (sh.PTPRQ.3), and surprisingly this was seen to reduce lipid droplet accumulation in comparison to the scramble control (Figure 5.1.3C). As cytoplasmic PTPRQ over-expression inhibits 3T3-L1 differentiation, it was predicted that PTPRQ KD might lead to enhanced adipogenesis through increased AKT/PKB phosphorylation and enhanced downstream signalling. It is unclear why this in not the case. Further analysis of the effects of PTPRQ silencing is required to

elucidate the mechanism by which it leads to reduced cell differentiation. As only one of the three shRNA constructs generated produced a significant reduction in PTPRQ expression, additional shRNA constructs would need to be assayed to confirm inhibition of adipogenesis and eliminate the possibility of off target effects. Next, analysis of phosphorylated AKT/PKB and intracellular PIP_3 would be essential to elucidate the impact of PTPRQ knockdown on the PI3K/AKT signalling pathway in these cells.

Finally, PTPRQ expression was assessed in response to LMNA over-expression in 3T3-L1 differentiation and LMNA KO in MEFs. In contrast to the increased PTPRQ mRNA observed in the RNA-Seq analysis, both WT and R482W mutant LMNA failed to significantly alter PTPRQ expression in repeated experimental replicates (Figure 5.1.3D). Previous studies have identified distinct PTPRQ isoforms that are expressed in a tissue specific manner. This complex system of regulation suggests that PTPRQ function and activity may be controlled by cellular localisation and is highly specific to cell type [294]. PTPRQ isoform expression as well as factors effecting PTPRQ expression in adipogenesis have yet to be established. The shRNA constructs and qPCR probes used in this study were directed towards the later exons in the PTPRQ gene (qPCR probes – exon 41), however it is possible that isoforms may exist in mouse adipocytes that are unaffected by the KD constructs used here or undetected by the qPCR probes. A significant limitation in this study was the endogenously low levels of PTPRQ expression detected in these cells. The RNA-Seq analysis was carried out at 36 h post induction of differentiation in this cell system, however in the LMNA over-expression experiments performed to confirm this result, PTPRQ was undetected past day 0 of differentiation. Thus, the effect of LMNA on PTPRQ was assessed at day -2 when the endogenous expression was detectable. This variation in experimental approach may be responsible for the discrepancies observed in LMNA effect on PTPRQ.

This preliminary investigation of PTPRQ activity and function in adipogenesis has brought to light various limitations in this system. Very low levels of endogenous PTPRQ transcripts in these cells make it difficult to measure changes in response to LMNA or other factors. These difficulties in PTPRQ detection may have contributed to the observed variation in experimental results. In keeping with our results, PTPRQ

was undetected in microarray analysis of gene expression in 3T3-L1 and hASC differentiation [178]. As higher levels of PTPRQ expression have been reported in human MSCs [298], a practical solution would be to study the effects of PTPRQ on adipogenesis in this alternative cell system. Finally, it is important to consider the complexity of PTPRQ regulation that has been reported in various cell types [294], as it suggests distinct cell-type specific PTPRQ function and control mechanisms, neither of which have previously been addressed in the context of adipogenesis.

SECTION 2: WNT6

INTRODUCTION

The wingless-type MMTV integration site (Wnt) family members are a group of 19, highly conserved, secreted glycoproteins that activate diverse intracellular signalling pathways to regulate developmental processes, such as cell proliferation and differentiation [305]. Of the numerous pathways activated by Wnt proteins, including Jun N-terminal kinase (JNK) and calcium signalling pathways, the canonical Wnt/β-catenin signalling system is the most well-characterised [306]. Figure 5.2.1 depicts this signalling cascade in which Wnt ligands bind to the frizzled (FZD) receptor and lipoprotein-receptor-related protein-5 or -6 (LRP5/6) co-receptor, and leads to the stabilisation of cytoplasmic β-catenin. Once stabilised, this multi-functional protein is translocated to the nucleus where it binds the T-cell factor/Lymphoid enhancer factor (TCF/LEF) family of transcription factors to regulate Wnt/β-catenin target genes [307].

MSCs have the potential to differentiate into multiple cell types including adipocytes, osteoblasts, myocytes and chondrocytes [308]. Canonical Wnt signalling has been identified as a regulator of MSC fate. MSC adipogenic differentiation is a complex process that involves two main stages, lineage commitment and terminal differentiation. Wnt/β-catenin signalling has been implicated in both stages of the adipose development programme, functioning as an activator of lineage commitment [96] and an inhibitor of adipocyte terminal differentiation [184]. Wnt signalling has been shown to repress adipogenesis through the inhibition of C/EBPα and PPARγ induction [95].

Numerous studies have characterised the activity of certain Wnt ligands in adipogenesis. Endogenous expression of Wnt10a, Wnt10b and Wnt6 is down-regulated during in vitro adipogenic differentiation of 3T3-L1 and bi-potential ST2 cells [184]. Ectopic over-expression of specific Wnt ligands (Wnt1, Wnt10b, Wnt10a and Wnt6) has been shown to block adipogenesis in 3T3-L1 preadipocytes and promote osteogenesis in ST2 cells. Conversely, the knockdown of Wnt expression is seen to enhance adipogenesis and repress osteogenesis [95,184]. Similarly, transgenic mice expressing Wnt10b from an adipose-specific FABP4 promoter display a significant decrease in white adipose tissue, total loss of brown adipose tissue and increased bone

mass, and are resistant to diet induced obesity [309]. Furthermore, it has been established that these effects are mediated through the Wnt/β-catenin signalling pathway, as β-catenin knockdown is seen to abrogate the effects of altered Wnt expression on both osteogenesis and adipogenesis [184,309].

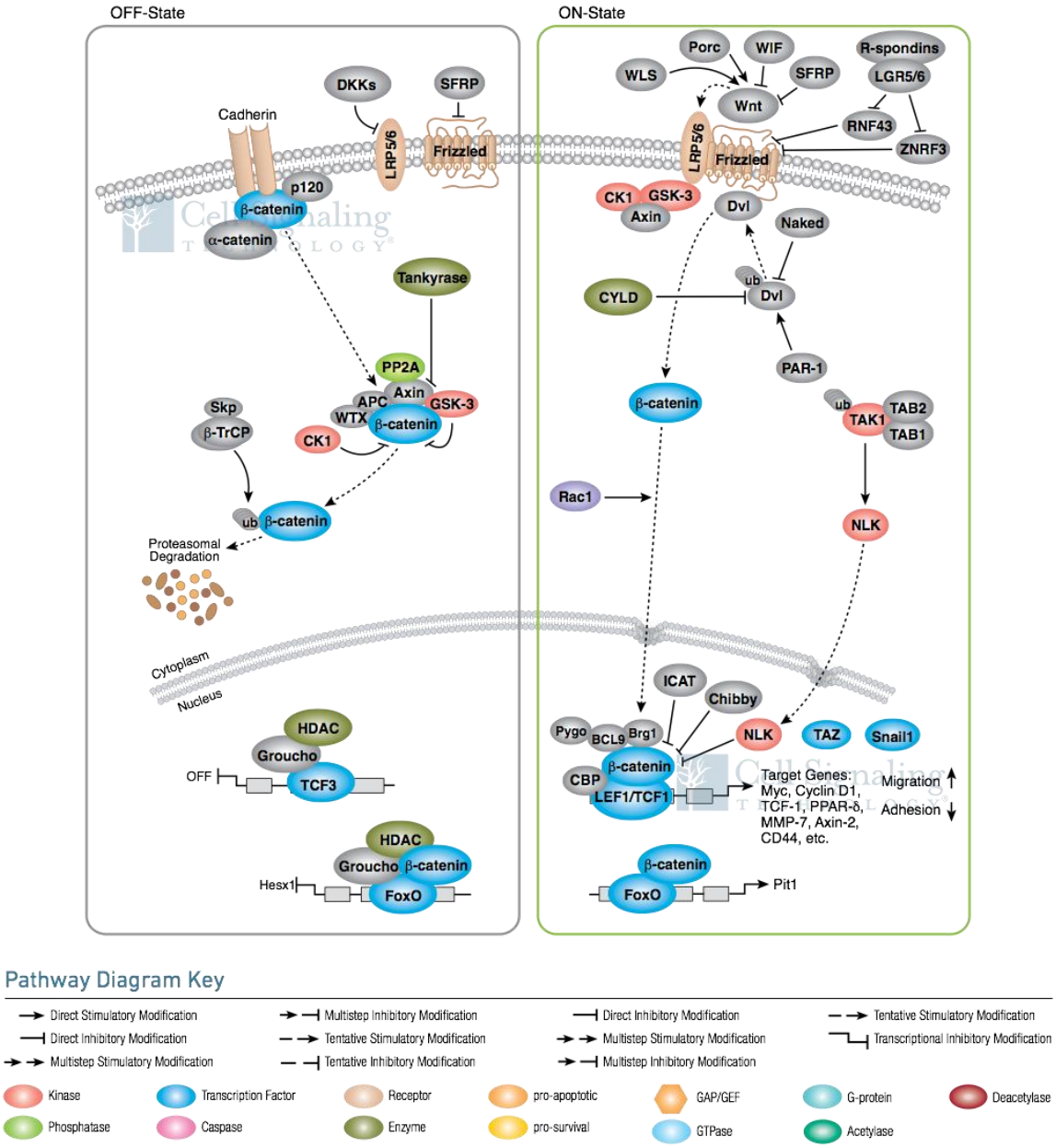

Figure 5.2.1: Canonical Wnt/β-catenin signalling pathway (Cell Signalling Technology (2016)).

RNA-Seq analysis identified an 8-, and 6-fold increase in Wnt6 expression in response to WT and R482W mutant LMNA, respectively. As a well characterised inhibitor of adipogenesis, this study aimed to explore the relationship between Wnt6 and LMNA in the context of adipogenesis and determine whether increased Wnt6 expression was responsible for the LMNA mediated block in 3T3-L1 differentiation. A final aim of this study was to investigate if Wnt6 silencing could rescue LMNA mediated inhibition of adipogenesis.

RESULTS

Wnt6 expression is down-regulated during 3T3-L1 differentiation

Endogenous Wnt6 expression was assessed during 3T3-L1 differentiation as in agreement with previously published results [184], Wnt6 was significantly down-regulated during adipogenesis (Figure 5.2.2).

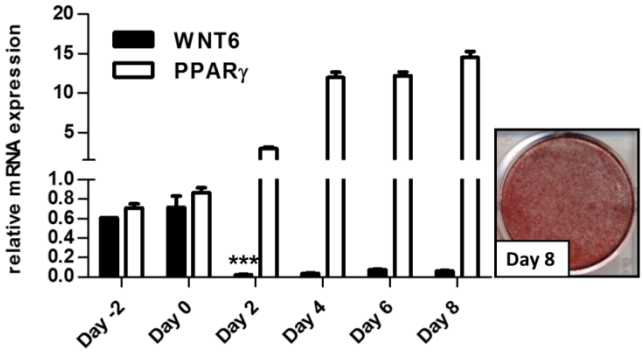

Figure 5.2.2: WNT6 expression in 3T3-L1 differentiation. 3T3-l1 cells were differentiated as previously described and adipogenesis was assessed at day 8 by staining with Oil Red O. Total RNA was isolated at the indicated time points during 3T3-L1 differentiation. WNT6 and PPARγ expression was analysed by qPCR. Transcript expression at the various time points is shown relative to expression at day -2. A Student's t-test (two-tailed, assuming equal variance) was used to calculate statistical significance compared to day 0, indicated as follows: *=P<0.05; **=P<0.01; ***=P<0.001.

Wnt6 silencing in 3T3-L1 differentiation

Cawthorn et al., (2011) [184] have previously demonstrated enhanced 3T3-L1 differentiation in response to shRNA mediated silencing of Wnt6 expression. 3T3-L1 preadipocytes were stably transfected with a piggyBac transposable Wnt6 shRNA knockdown construct, pRFP(PB).sh.WNT6 or scramble control pRFP(PB).shControl and induced to differentiate using full induction media MDI, and sub-maximal media DI or D as indicated (Figure 5.2.3A). Knockdown of endogenous Wnt6 significantly enhanced adipogenesis in comparison to control cells in all differentiation conditions, as assessed by Oil Red O staining and quantification (Figure 5.2.3A). However, qPCR

analysis of Wnt6 expression at day 0, 2 and 4 (Figure 5.2.3B) did not detect a reduction in Wnt6 expression in pRFP(PB).sh.WNT6 transfected ells. Interestingly, Cawthorn et al., (2011)[184] have previously described a similar phenomenon in which they had difficulty detecting Wnt knockdown in the ST2 cell line. Wnt6 knockdown was only detectable in these cells when qPCR primers flanking the shRNA target site were used. Thus, Wnt6 custom primers (CP) were designed flanking the shWNT6 target site and qPCR analysis of Wnt6 expression at day 0, 2 and 4 was repeated with these primers (Figure 5.2.3 – CP). However, Wnt6 expression levels were unaffected by pRFP(PB).sh.WNT6 transfection regardless of the qPCR primer location. The enhanced adipogenesis of pRFP(PB).sh.WNT6 transfected cells suggests a reduction in Wnt/β-catenin signalling, but whether Wnt6 expression is affected by the shRNA is unclear.

Cawthorn et al., (2011)[184] also reported cross-regulation of Wnt ligands, in that Wnt10b expression was also reduced in shWNT6 transfected cells. Therefore, it would be of interest to assess the expression of other Wnt ligands such as Wnt10a and Wnt10b to identify possible down-regulation that might lead to the observed increase in adipogenesis. It would also be of use to measure total β-catenin in the cells, as any reduction in Wnt ligand expression would lead to reduced β-catenin. Alternatively, additional shRNA constructs could be assayed with flanking qPCR primers for successful detection of Wnt6 knockdown.

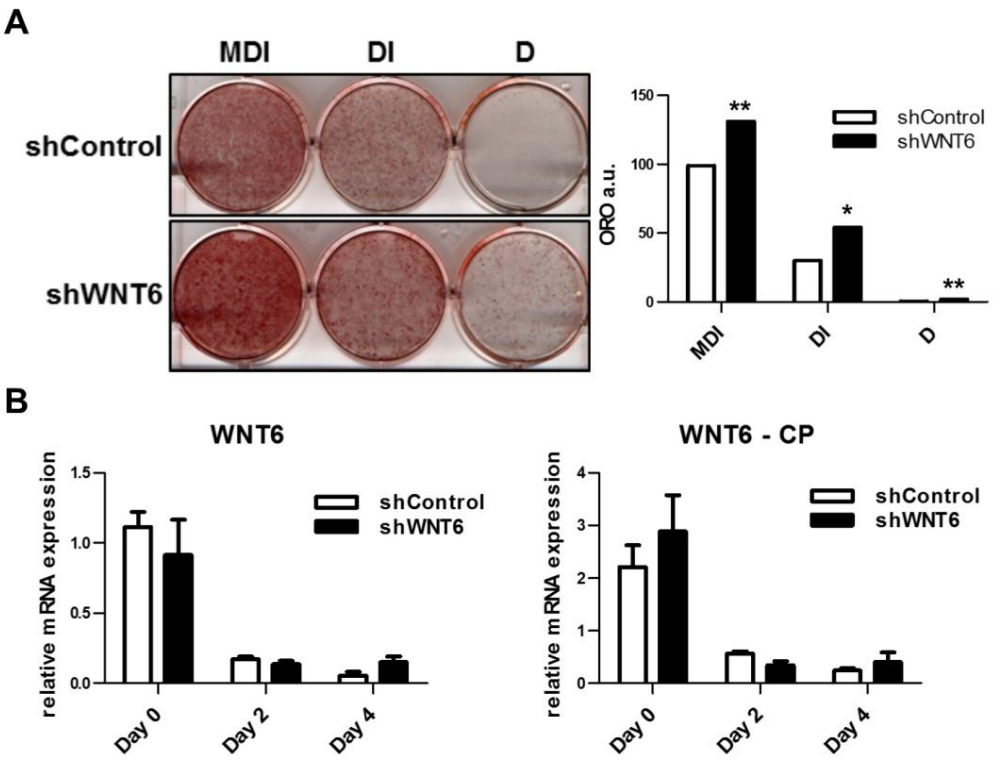

Figure 5.2.3: WNT6 silencing in 3T3-L1 differentiation. (A) 3T3-L1 preadipocytes were stably transfected with pRFP(PB).shWNT6 or scramble control pRFP(PB).shControl and induced to differentiate. Adipogenesis was assessed at day 8 post induction by staining with Oil Red O; quantification was carried out using ImageJ and expressed as Oil Red O absorbance units (ORO a.u.) (B) WNT6 expression was assessed by qPCR analysis at day 0, 2 and 4 with a predesigned WNT6 primers and custom primers (CP). A Student's t-test (two-tailed, assuming equal variance) was used to calculate statistical significance compared to scramble control, indicated as follows: *=P<0.05; **=P<0.01; ***=P<0.001.

As previously mentioned in chapter 4, technical difficulties were encountered when cloning the various shRNA constructs employed in this thesis. High levels of recombination were observed with frequent deletion of nucleotides within the shRNA 29 mer sequence. Sequencing of the shWNT6 construct used here identified a 10-nucleotide deletion in one of the 29mer arms. Hairpin formation of the modified sequence was assessed using the IDT OligoAnalyzer tool and formation of a hairpin of similar structure to the original sequence was predicted, suggesting the deletion might not influence shRNA function. If shWNT6 efficiency is affected by this deletion, it could explain the difficulties experienced in detecting Wnt6 knockdown.

None the less, the enhanced adipogenic phenotype suggests modulation of gene expression to some extent. In order to confirm accurate shWNT6 action and eliminate the possibility of off target effects, a Wnt6 specific antibody should be employed to detect endogenous Wnt6 in this system.

Wnt6 expression in response to LMNA overexpression

To investigate the LMNA mediated increase in WNT6 expression detected in the RNA-Seq analysis, 3T3-L1 preadipocytes were stably transfected with human LMNA overexpression constructs and induced to differentiate. Wnt6 expression was assessed at day -2 and 2 of differentiation (Figure 5.2.4 A, B) in two independent experimental replicates. A significant increase in Wnt6 expression in response to LMNA WT overexpression was detected at day -2 in the second replicate (Figure 5.2.4B) but was not reproducible. Mutant LMNA did not appear to affect Wnt6 expression at any of the time points assessed in either of the replicates. In both experiments LMNA (WT and R482W) was seen to significantly reduce lipid droplet accumulation in comparison to empty vector control (Chapter 4, Figure 4.7). As difficulties were experienced in detecting WNT6 knockdown using qPCR, as described above, it would be of interest to confirm the effects of LMNA over-expression on wnt6 at the protein level.

To investigate whether the increase in adipogenesis in response to pRFP(PB).shWNT6 transfection could rescue LMNA mediated inhibition of adipogenesis, dual constructs similar to those described in chapter 4 were generated; pCMV(PB)-Flag-LMNA-WT.shWNT6, pCMV(PB)-Flag-LMNA-WT.shControl, pCMV(PB)-Flag-LMNA-R482W.shWNT6, pCMV(PB)-Flag-LMNA-R482W.shControl, pCMV(PB).shWNT6 and pCMV(PB).shControl. 3T3-L1 preadipocytes were stably transfected and induced to differentiate, however LMNA did not appear to inhibit differentiation in this experiment and therefore these results have not been included. It would be of interest to repeat this rescue experiment with an alternative shRNA sequence, without mutation and with which the Wnt6 silencing is detectable.

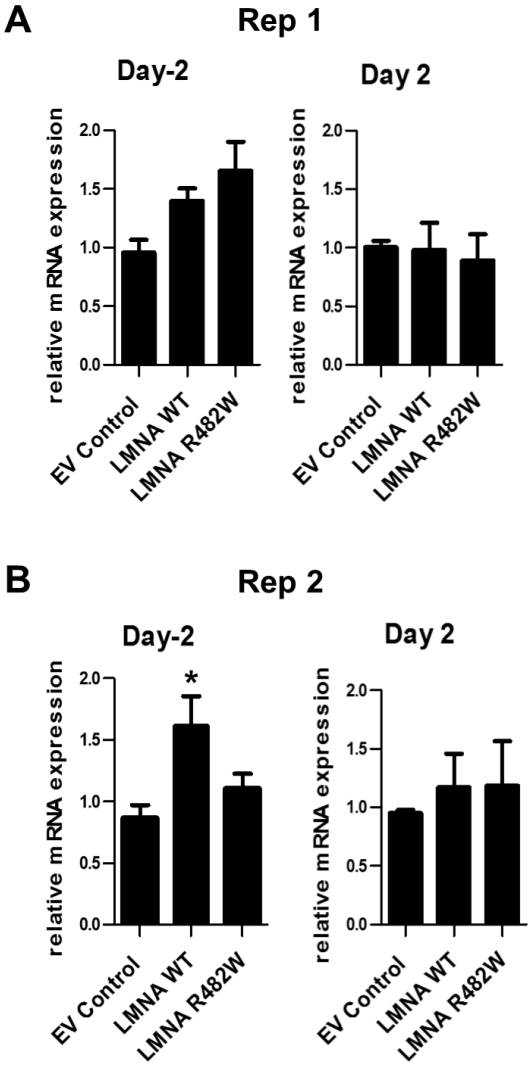

Figure 5.2.4: WNT6 expression in response to LMNA over-expression. (A) 3T3-L1 preadipocytes were stably transfected with pCMV(PB)-Flag-LMNA-WT, pCMV(PB)-Flag-LMNA-R482W or pCMV(PB) and induced to differentiate. WNT6 expression was analysed by qPCR at day -2 and day 2 of cell differentiation. (B) 3T3-L1 preadipocytes were stably transfected with pcDNA3-Flag-LMNA-WT, pcDNA3-Flag-LMNA-R482W or pcDNA3.EV and induced to differentiate. WNT6 expression was analysed by qPCR at day -2, 2 and 4 of cell differentiation. (ORO images and expression data shown in Figure 4.7, chapter 4). A Student's t-test (two-tailed, assuming equal variance) was used to calculate statistical significance compared to empty vector control cells, indicated as follows: *=P<0.05; **=P<0.01; ***=P<0.001.

DISCUSSION

Wnt proteins are important regulators of adipogenesis. The role of canonical Wnt/β-catenin signalling has been extensively studied in this context and endogenous Wnt ligands that activate this pathway are down-regulated during the process of in vitro cell differentiation. Of the 19 secreted glycoproteins, Wnt1 [95], Wnt 3a [310], Wnt10a, Wnt10b and Wnt6 [184] have all been shown to inhibit adipogenesis through β-catenin signalling. Interestingly, various other Wnts, including Wnt5a, Wnt4 [311] and Wnt5b [312], have been shown to enhance adipogenesis. These proteins appear to act through alternative signalling pathways to inhibit canonical Wnt/β-catenin signalling and promote cell differentiation, once again emphasising the importance of the canonical pathway in the control of adipogenesis.

The aim of this study was to investigate the relationship between Wnt6 and LMNA and to determine whether the stimulatory action of Wnt6 silencing could rescue LMNA mediated inhibition of 3T3-L1 differentiation. Previous studies have described LMNA mediated effects on Wnt signalling in diverse systems. LMNA over-expression has been shown to enhance osteoblast differentiation and inhibit the adipogenesis in MSCs, through up-regulation of Wnt7b and Wnt10b as well as other osteogenic genes in these cells. Increased levels of β-catenin were reported in MSCs over-expressing LMNA and reduced β-catenin was seen in response to LMNA KD [176]. Recently, dysregulation of ECM genes and Wnt signalling has been reported in a HGPS mouse model. Hernandez et al., (2010) [186] examined the gene expression profile of LMNAΔ9 (Exon 9 deletion generating a truncated LMNA variant that leads to characteristic HGPS proliferative arrest) MAFs and identified altered expression of cell adhesion and ECM genes. Impaired Wnt/β-catenin signalling was reported in LMNAΔ9 MAFs, caused by reduced TCF/Lef1 activity and cell proliferation was rescued by inhibition of GSK3 (β-catenin degradation) in these cells [186]. Tong et al., (2011) [313] have also described reduced Wnt10b and β-catenin in LMNA -/- mice, along with increased PPARγ and C/EBPα associated with the fat infiltration on muscle and bone tissues in these mice. Similarly, RNA-Seq analysis of 3T3-L1 gene expression during differentiation identified increased Wnt6 expression in response to LMNA WT and R482W overexpression. To confirm the effects of LMNA on Wnt6 expression, 3T3-L1 preadipocytes were stably transfected with human LMNA overexpression

constructs and induced to differentiate. However, qPCR analysis of Wnt6 expression in these cells did not detect a consistent increase in response to LMNA (Figure 5.2.4). RNA-Seq analysis was carried out 36 h post induction of differentiation, while qPCR analysis was carried out at day -2, day 2 (48 h post induction) and day 4 (not shown). The LMNA effect on Wnt6 expression might be specific to early adipogenic induction and should be assessed by qPCR sooner than 48 h post induction (day 2). In addition, it would be of interest to assess the expression of other Wnt proteins and β-catenin in this system as LMNA has previously been reported to affect Wnt10b in various cell types [176,186,313].

While the mechanisms controlling Wnt down-regulation during adipogenesis have yet to be elucidated, numerous factors have been implicated. Various components of the induction cocktail are reported to stimulate the down-regulation of specific Wnt ligands, including insulin, via IRS-1 signalling [314] and cyclic AMP [315]. PPARγ is reported to suppress Wnt/β-catenin signalling in adipogenesis [315] and numerous additional factors such as TZD treatment or obesity are seen to influence Wnt expression in adipose tissue [184,316]. This raises the question of whether LMNA modulates Wnt directly in 3T3-L1 differentiation or through an indirect mechanism. It is possible that LMNA may influence factors involved in adipogenic Wnt regulation to modulate Wnt6 expression rather than affecting its expression directly. Previous studies have reported increased TCF/Lef1 activity in response to LMNA overexpression in MSC [176] and reduced TCF/Lef1 activity in response to LMNAΔ9 in MAFs [186]. Both studies utilized a Topflash luciferase reporter assay to measure β-catenin mediated activation of TCF/Lef1 transcriptional activity. This Topflash system was employed in this work (data not shown) in an attempt to measure an effect of LMNA WT and R482W mutant on TCF/Lef1 transcriptional activity in 3T3-L1 cells. However a number of technical difficulties were experienced. Previously employed dual stable transfection (LMNA and reporter construct) is not appropriate here as basal Topflash activity in these cells was very low, this construct was only seen to direct luciferase activity in response to LiCl treatment, which inhibits 3T3-L1 differentiation as previously shown. The Topflash system does not appear to be sensitive enough to measure altered Wnt/β-catenin signalling in this system. In addition, the activity of various ECM, signalling and transcription factors is highly

regulated during the process of 3T3-L1 differentiation. Measuring the influence of LMNA on any of these factors in pre-adipocytes or other cell models might not reflect the effects observed in the context of cell differentiation.

Technical difficulties were also encountered during attempts to knockdown Wnt6 as well as accurately detect the knockdown in these cells, as outlined in the results section. In addition, a preliminary attempt at the previously outlined rescue experiment was unsuccessful as LMNA failed to inhibit cell differentiation. Due to the large amount of data in the literature supporting a potential role for LMNA in Wnt/ β-catenin regulation during adipogenesis, expansion and optimization of these experiments are warranted.

SECTION 3: TESTOSTERONE

INTRODUCTION

Modulation of various signalling pathways during adipocyte differentiation activates the characteristic transcriptional cascade that leads to a mature adipocyte phenotype. Figure 5.1.2 illustrates numerous pathways that transduce both stimulatory and repressive signals from extracellular components during adipogenesis [92]. Various hormones are known to have important regulatory functions in the process of adipogenesis. Here, the role of testosterone will be considered as it has previously been shown to influence adipocyte function.

Androgen metabolism and action in adipose tissue is highly complex. Sex steroids are thought to contribute to the sexual dimorphism of body fat distribution as they appear to have both depot-specific and sex-specific actions in adipose tissue [317]. Adipose tissue has been identified as a steroid hormone reservoir [318], and androgens are reported to influence key functions of adipose tissue including lipid metabolism (lipolysis and lipogenesis), insulin signalling, adipokine secretion and preadipocyte differentiation [317].

Huang et al., (2013) [319] have described a role for androgen signalling in osteoporosis and obesity, where androgen receptor (AR) deficiency is shown to inhibit osteogenesis and promote adipogenesis. AR KO mice are obese and show abnormal white adipose tissue metabolism [320,321]. AR KO is reported to reduce IGFBP3 expression in bone derived MSCs, leading to Akt activation and stimulation of adipogenesis. IGFBP3 has previously been shown to block IGF-1 driven Akt signalling [269] and Huang et al., (2003) [319] report that AR up-regulates IGFBP3 expression to suppress adipogenesis in this system. These results suggest AR modulation of the IGF-Akt axis as the mechanism by which androgens influences adipogenesis. Androgens have also been reported to impair human ASC commitment to the preadipocyte cell lineage in subcutaneous abdominal adipocytes [282].

The repressive effects of testosterone on 3T3-L1 differentiation are reported to function though AR/β-catenin interaction and translocation to the nucleus, leading to the up-regulation of various Wnt signalling target genes [282]. Testosterone and DHT

treatments were seen to reduce the expression of early adipogenic factors including C/EBPβ,δ, α and PPARγ and induced the translocation of a fraction of cytoplasmic β-catenin into the nucleus. β-catenin was subsequently shown to interact with both AR and TCF4 in the nucleus. Finally, testosterone inhibition of 3T3-L1 differentiation was blocked by over-expression of a dominant negative TCF4, suggesting that testosterone mediated inhibition of adipogenesis might function through the TCF4 signalling pathway [282].

As the FPLD2 adipose specific symptoms are seen to develop post puberty it has been suggested that a hormonal component might be involved in driving this phenotype [33]. Another indicator of the involvement of hormones is the sex dependent aspect of the disease, where symptoms are generally more severe in female patients [48,49]. Finally, the primary symptom of FPLD2 is adipose tissue re-distribution in distinct fat depots in the body, another area in which sex hormones are thought to play a role [317]. If sex hormones were involved in the pathogenesis of FPLD2, the repurposing of androgen deprivation therapy (ADT) could be considered as a potential therapeutic lead.

RESULTS

Throughout this study, the effects of testosterone were investigated on various elements during adipogenesis. Testosterone treatments were applied to 3T3-L1 cells during differentiation at varying concentrations on numerous occasions, however the hormone was not observed to reduce cell differentiation under any circumstances. As this is conflicting with all the published data described above, testosterone treatments were applied to 3T3-L1 cells from alternative sources to investigate the possibility that the lack of inhibition was a cell line specific feature. Previous studies have shown inhibition of lipid droplet accumulation in response to 100nM testosterone treatments [282]. In this study, treatments of up to 200nM testosterone were applied to 3T3-L1 cells from three different sources, repeatedly and with no effect (Figure 5.3.1). In addition, treatments of 500nM testosterone did not appear to influence ZenBio 3T3-L1 differentiation (data not shown). To exclude the possibility that the testosterone used in these experiments was inactive, the more potent androgen DHT was assayed as well. Previous reports have demonstrated inhibition of differentiation with 10nM DHT. DHT treatments up to 250nM were applied to ZenBio 3T3-L1 cells during differentiation, and no effect was observed (Figure 5.3.1). In all instances, testosterone and DHT were solubilized in ethanol as previously described in numerous published studies [282,322].

Previously, the effects of testosterone on IGFBP5 promoter activity during 3T3-L1 differentiation was assessed (chapter 4), as the sex hormone is reported to activate IGFBP5 promoter activity in human androgen responsive fibroblasts [233]. No effect was observed on cell differentiation or promoter activity (Chapter 4 Figure 4.6C). In addition, testosterone was applied to IGFBP5, LMNA WT and LMNA R482W overexpressing cells repeatedly to see if the hormone enhanced or repressed the effects of either on 3T3-L1 differentiation. In all instances, testosterone treatment has no effect.

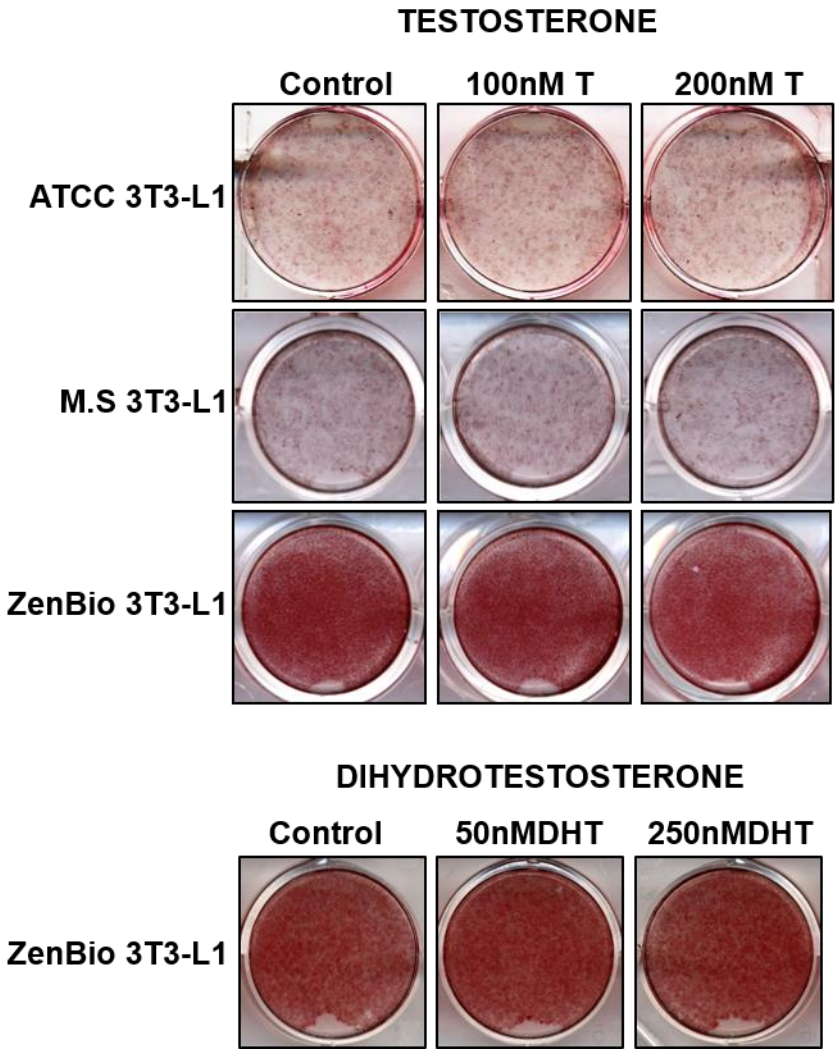

Figure 5.3.1: Testosterone and DHT treatment during 3T3-L1 differentiation. 3T3-L1 preadipocytes were grown to confluency and differentiated with either testosterone or DHT treatments as indicated. Treatments were applied at day -2 and continuously with every media change as described in materials and methods. 3T3-L1 cells from ATCC and ZenBio were assayed, along with cells obtained from Prof. Michael Schupp (MS), Charite, Berlin.

DISCUSSION

Studying the effects of androgens on adipocyte differentiation are of interest considering the puberty induced onset of FPLD2 pathogenesis. It is unclear why neither testosterone nor DHT had an effect on 3T3-L1 differentiation in this study. The volume of data published on androgen action in adipogenesis suggests that this effect is specific to the cells used in this study and it is possible that these cells are not androgen sensitive. In agreement with this, Hartig et al., (2013) [322] found that DHT and a synthetic androgen Metribolone (R1881) had no effect on 3T3-L1 differentiation due to low levels of the androgen receptor (AR) expression in these cells. AR over-expression was shown to sensitise these cells to DHT/R1881 inhibition leading to reduced PPARγ and C/EBPα along with the up-regulation of various osteogenic genes. This is in keeping with the results observed in this study, where testosterone was unable to inhibit 3T3-L1 differentiation, and suggests that the 3T3-L1 cells model is not a suitable for the study of androgen effects on adipogenesis.

GENERAL DISCUSSION

FPLD2 is a rare autosomal dominant disease for which there is no effective therapy. Interest in the development of novel therapeutics for partial lipodystrophies has been accelerated by the increasing prevalence of HAART associated partial lipodystrophies in HIV/AIDS patients [323,324]. While advances have been made in elucidating the molecular mechanisms driving this disease phenotype, the exact aetiology of FPLD2 is unclear.

To date, several studies have described pleiotropic effects of LMNA on gene regulation and interaction of LMNA with multiple proteins in adipogenesis. The majority of published work addressing the FPLD2 mechanism of action, propose reduced protein interaction of mutant LMNA with SREPB1 as the principle factor driving the dysregulation of adipogenesis. Lund et al., (2013)[141] have described the remodelling of sub-nuclear architecture in human ASC differentiation, in which LMNA-promoter interactions are modified thus altering the expression capacity of a subset of genes during this process. Considering the well characterised role of LMNA in the regulation of chromatin organization and gene transcription, it follows that LMNA mutation might lead to the distortion of these processes during the dynamic process of adipogenesis [8].

An investigation into the effects of LMNA on the early stages of adipogenesis though the use of RNA-Seq analysis identified altered expression ITM2A, IGFBP5, WNT6 and PTPRQ transcripts in the 3T3-L1 cell model. Analysis of IGFBP5, WNT6 and PTPRQ in the context of adipogenesis and with respect to LMNA proved challenging. Significant obstacles were encountered in relation to the complex regulation of IGFBP5 expression in adipogenesis. This study reports novel effects of IGFBP5 over-expression and silencing on 3T3-L1 differentiation, however further characterisation of IGFBP5 function and activity is required to elucidate its dynamic role in the process of adipogenesis.

Preliminary manipulations of PTPRQ in this cell system identified novel effects of PTPRQ silencing on adipogenesis. However, difficulties were encountered in the detection and manipulation of the lowly expressed PTPRQ, in this cell model. Both IGFBP5 and PTPRQ were investigated with the intention of identifying factors that

might enhance adipogenesis through simple manipulation, for example the addition of IGFBP5 protein to the cells, or the inhibition of PTPRQ with recently developed PTPRQ inhibitors [325]. Neither of these factors were seen to stimulate adipogenesis in this context and thus are not suitable candidates for therapeutic manipulation.

Wnt6 activity was addressed in this system under the hypothesis that Wnt6 silencing, which is known to enhance adipogenesis [184], might be sufficient to rescue the LMNA mediated block in adipogenesis. However, previously reported difficulties in detecting Wnt6 silencing in these cells rendered this gene very problematic to work with. Aside from issues in consistent candidate gene detection and manipulation, the major limitation of this study in the lengthy and arduous nature of 3T3-L1 transfection and differentiation experiments. This dynamic process is highly variable and producing consistent result in this system proved challenging.

Finally, characterisation of ITM2A in adipogenesis was successful as this work uncovered a role for ITM2A in the regulation of adipogenesis and suggests a modulatory relationship between LMNA and ITM2A within this context. This study describes a novel stimulatory effect of ITM2A silencing in adipogenesis, which is sufficient to rescue the LMNA mediated block in adipogenesis. Throughout this study, ITM2A knockdown robustly enhanced 3T3-L1 differentiation by increasing PPARγ protein levels in these cells, and ITM2A manipulation in this context has suggested a possible role for autophagy modulation in the treatment of FPLD2 and for exploration for treatment of HAART associated partial lipodystrophies.

BIBLIOGRAPHY

1. Dechat, T., Adam, S. A., Taimen, P., Shimi, T. & Goldman, R. D. Nuclear lamins. *Cold Spring Harb. Perspect. Biol.* **2,** a000547 (2010).
2. Capelson, M., Doucet, C. & Hetzer, M. W. Nuclear Pore Complexes: Guardians of the Nuclear Genome. *Cold Spring Harb. Symp. Quant. Biol.* **75,** 585–597 (2010).
3. Méndez-López, I. & Worman, H. J. Inner nuclear membrane proteins: impact on human disease. *Chromosoma* **121,** 153–167 (2012).
4. Worman, H. J. *et al.* Laminopathies and the long strange trip from basic cell biology to therapy. *J. Clin. Invest.* **119,** 1825–36 (2009).
5. Worman, H. J., Fong, L. G., Muchir, A. & Young, S. G. Laminopathies and the long strange trip from basic cell biology to therapy. *J. Clin. Invest.* **119,** 1825–1836 (2009).
6. Camozzi, D. *et al.* Diverse lamin-dependent mechanisms interact to control chromatin dynamics. Focus on laminopathies. *Nucleus* **5,** 427–40
7. Worman, H. J. Nuclear lamins and laminopathies. *J. Pathol.* **226,** 316–325 (2012).
8. Dechat, T. *et al.* Nuclear lamins: major factors in the structural organization and function of the nucleus and chromatin. *Genes Dev.* **22,** 832–53 (2008).
9. Capell, B. C. & Collins, F. S. Human laminopathies: nuclei gone genetically awry. *Nat. Rev. Genet.* **7,** 940–952 (2006).
10. Holtz, D., Tanaka, R. A., Hartwig, J. & McKeon, F. The CaaX motif of lamin A functions in conjunction with the nuclear localization signal to target assembly to the nuclear envelope. *Cell* **59,** 969–77 (1989).
11. Dechat, T., Adam, S. A., Taimen, P., Shimi, T. & Goldman, R. D. Nuclear lamins. *Cold Spring Harb. Perspect. Biol.* **2,** a000547 (2010).
12. Crisp, M. & Burke, B. The nuclear envelope as an integrator of nuclear and cytoplasmic architecture. *FEBS Lett.* **582,** 2023–2032 (2008).
13. Moir, R. D., Yoon, M., Khuon, S. & Goldman, R. D. Nuclear lamins A and B1: different pathways of assembly during nuclear envelope formation in living cells. *J. Cell Biol.* **151,** 1155–68 (2000).
14. Liu, B. *et al.* Genomic instability in laminopathy-based premature aging. *Nat. Med.* **11,** 780–785 (2005).

15. Spann, T. P., Goldman, A. E., Wang, C., Huang, S. & Goldman, R. D. Alteration of nuclear lamin organization inhibits RNA polymerase II–dependent transcription. *J. Cell Biol.* **156,** 603–608 (2002).
16. Johnson, B. R. *et al.* A-type lamins regulate retinoblastoma protein function by promoting subnuclear localization and preventing proteasomal degradation. *Proc. Natl. Acad. Sci.* **101,** 9677–9682 (2004).
17. Dorner, D. *et al.* Lamina-associated polypeptide 2α regulates cell cycle progression and differentiation via the retinoblastoma–E2F pathway. *J. Cell Biol.* **173,** 83–93 (2006).
18. Favreau, C. *et al.* Expression of lamin A mutated in the carboxyl-terminal tail generates an aberrant nuclear phenotype similar to that observed in cells from patients with Dunnigan-type partial lipodystrophy and Emery-Dreifuss muscular dystrophy. *Exp. Cell Res.* **282,** 14–23 (2003).
19. Robinson, L. J., Karlsson, N. G., Weiss, A. S. & Packer, N. H. Proteomic analysis of the genetic premature aging disease Hutchinson Gilford progeria syndrome reveals differential protein expression and glycosylation. *J. Proteome Res.* **2,** 556–7
20. Boguslavsky, R. L., Stewart, C. L. & Worman, H. J. Nuclear lamin A inhibits adipocyte differentiation: implications for Dunnigan-type familial partial lipodystrophy. *Hum. Mol. Genet.* **15,** 653–63 (2006).
21. Goldberg, M. *et al.* The tail domain of lamin Dm0 binds histones H2A and H2B. *Proc. Natl. Acad. Sci. U. S. A.* **96,** 2852–7 (1999).
22. Dorner, D., Gotzmann, J. & Foisner, R. Nucleoplasmic lamins and their interaction partners, LAP2alpha, Rb, and BAF, in transcriptional regulation. *FEBS J.* **274,** 1362–73 (2007).
23. Foisner, R. & Gerace, L. Integral membrane proteins of the nuclear envelope interact with lamins and chromosomes, and binding is modulated by mitotic phosphorylation. *Cell* **73,** 1267–79 (1993).
24. Mattout-Drubezki, A. & Gruenbaum, Y. Dynamic interactions of nuclear lamina proteins with chromatin and transcriptional machinery. *Cell. Mol. Life Sci.* **60,** 2053–2063 (2003).
25. Taniura, H., Glass, C. & Gerace, L. A chromatin binding site in the tail domain of nuclear lamins that interacts with core histones. *J. Cell Biol.* **131,** 33–44 (1995).

26. Goldman, R. D., Gruenbaum, Y., Moir, R. D., Shumaker, D. K. & Spann, T. P. Nuclear lamins: building blocks of nuclear architecture. *Genes Dev.* **16,** 533–547 (2002).
27. Gruenbaum, Y. *et al.* The nuclear lamina and its functions in the nucleus. *Int. Rev. Cytol.* **226,** 1–62 (2003).
28. Lund, E. *et al.* Lamin A/C-promoter interactions specify chromatin state-dependent transcription outcomes. *Genome Res.* **23,** 1580–9 (2013).
29. Sullivan, T. *et al.* Loss of A-type lamin expression compromises nuclear envelope integrity leading to muscular dystrophy. *J. Cell Biol.* **147,** 913–20 (1999).
30. Nikolova, V. *et al.* Defects in nuclear structure and function promote dilated cardiomyopathy in lamin A/C–deficient mice. *J. Clin. Invest.* **113,** 357–369 (2004).
31. Bertrand, A. T., Chikhaoui, K., Yaou, R. Ben & Bonne, G. Clinical and genetic heterogeneity in laminopathies. *Biochem. Soc. Trans.* **39,** (2011).
32. Worman, H. J. & Bonne, G. 'Laminopathies': A wide spectrum of human diseases. *Exp. Cell Res.* **313,** 2121–2133 (2007).
33. Burke, B. & Stewart, C. L. in *Current topics in developmental biology* **109,** 1–52 (2014).
34. Agarwal, A. K., Fryns, J.-P., Auchus, R. J. & Garg, A. Zinc metalloproteinase, ZMPSTE24, is mutated in mandibuloacral dysplasia. *Hum. Mol. Genet.* **12,** 1995–2001 (2003).
35. Bergo, M. O. *et al.* Zmpste24 deficiency in mice causes spontaneous bone fractures, muscle weakness, and a prelamin A processing defect. *Proc. Natl. Acad. Sci. U. S. A.* **99,** 13049–54 (2002).
36. Pendás, A. M. *et al.* Defective prelamin A processing and muscular and adipocyte alterations in Zmpste24 metalloproteinase–deficient mice. *Nat. Genet.* **31,** 94 (2002).
37. Moulson, C. L. *et al.* Increased progerin expression associated with unusual *LMNA* mutations causes severe progeroid syndromes. *Hum. Mutat.* **28,** 882–889 (2007).
38. Navarro, C. L. *et al.* Lamin A and ZMPSTE24 (FACE-1) defects cause nuclear disorganization and identify restrictive dermopathy as a lethal neonatal laminopathy. *Hum. Mol. Genet.* **13,** 2493–2503 (2004).

39. Scharner, J., Gnocchi, V. F., Ellis, J. A. & Zammit, P. S. Genotype–phenotype correlations in laminopathies: how does fate translate? *Biochem. Soc. Trans.* **38,** 257–262 (2010).
40. Schirmer, E. C. & Foisner, R. Proteins that associate with lamins: Many faces, many functions. *Exp. Cell Res.* **313,** 2167–2179 (2007).
41. Eriksson, M. *et al.* Recurrent de novo point mutations in lamin A cause Hutchinson–Gilford progeria syndrome. *Nature* **423,** 293–298 (2003).
42. Glynn, M. W. & Glover, T. W. Incomplete processing of mutant lamin A in Hutchinson-Gilford progeria leads to nuclear abnormalities, which are reversed by farnesyltransferase inhibition. *Hum. Mol. Genet.* **14,** 2959–2969 (2005).
43. Gonzalez, J. M., Pla, D., Perez-Sala, D. & Andres, V. A-type lamins and Hutchinson-Gilford progeria syndrome: pathogenesis and therapy. *Front. Biosci. (Schol. Ed).* **3,** 1133–46 (2011).
44. Guénantin, A. C. *et al.* Nuclear envelope-related lipodystrophies. *Semin. Cell Dev. Biol.* **29,** 148–57 (2014).
45. Bidault, G., Vatier, C., Capeau, J., Vigouroux, C. & Béréziat, V. *LMNA* - linked lipodystrophies: from altered fat distribution to cellular alterations. *Biochem. Soc. Trans.* **39,** 1752–1757 (2011).
46. Worman, H. J. & Courvalin, J.-C. The nuclear lamina and inherited disease. *Trends Cell Biol.* **12,** 591–8 (2002).
47. Robbins, A. L. & Savage, D. B. The genetics of lipid storage and human lipodystrophies. *Trends Mol. Med.* **21,** 433–8 (2015).
48. Vigouroux, C. *et al.* Lamin A/C gene: sex-determined expression of mutations in Dunnigan-type familial partial lipodystrophy and absence of coding mutations in congenital and acquired generalized lipoatrophy. *Diabetes* **49,** 1958–62 (2000).
49. Wiltshire, K. M., Hegele, R. A., Innes, A. M. & Brownell, A. K. W. Homozygous lamin A/C familial lipodystrophy R482Q mutation in autosomal recessive Emery Dreifuss muscular dystrophy. *Neuromuscul. Disord.* **23,** 265–8 (2013).
50. Mounkes, L. C., Kozlov, S., Hernandez, L., Sullivan, T. & Stewart, C. L. A progeroid syndrome in mice is caused by defects in A-type lamins. *Nature* **423,** 298–301 (2003).

51. Arimura, T. *et al.* Mouse model carrying H222P-Lmna mutation develops muscular dystrophy and dilated cardiomyopathy similar to human striated muscle laminopathies. *Hum. Mol. Genet.* **14,** 155–169 (2004).
52. Mounkes, L. C., Kozlov, S. V, Rottman, J. N. & Stewart, C. L. Expression of an LMNA-N195K variant of A-type lamins results in cardiac conduction defects and death in mice. *Hum. Mol. Genet.* **14,** 2167–2180 (2005).
53. Yang, S. H. *et al.* Blocking protein farnesyltransferase improves nuclear blebbing in mouse fibroblasts with a targeted Hutchinson-Gilford progeria syndrome mutation. *Proc. Natl. Acad. Sci.* **102,** 10291–10296 (2005).
54. Yang, S. H. *et al.* A farnesyltransferase inhibitor improves disease phenotypes in mice with a Hutchinson-Gilford progeria syndrome mutation. *J. Clin. Invest.* **116,** 2115–2121 (2006).
55. Wojtanik, K. M. *et al.* The role of LMNA in adipose: a novel mouse model of lipodystrophy based on the Dunnigan-type familial partial lipodystrophy mutation. *J. Lipid Res.* **50,** 1068–1079 (2009).
56. Cristancho, A. G. & Lazar, M. A. Forming functional fat: a growing understanding of adipocyte differentiation. *Nat. Rev. Mol. Cell Biol.* **12,** 722–34 (2011).
57. Lee, M.-J., Wu, Y. & Fried, S. K. Adipose tissue heterogeneity: implication of depot differences in adipose tissue for obesity complications. *Mol. Aspects Med.* **34,** 1–11 (2013).
58. Bjørndal, B., Burri, L., Staalesen, V., Skorve, J. & Berge, R. K. Different adipose depots: their role in the development of metabolic syndrome and mitochondrial response to hypolipidemic agents. *J. Obes.* **2011,** 490650 (2011).
59. Gimble, J. M. *et al.* Adipose-derived stromal/stem cells: a primer. *Organogenesis* **9,** 3–10 (2013).
60. Smorlesi, A., Frontini, A., Giordano, A. & Cinti, S. The adipose organ: white-brown adipocyte plasticity and metabolic inflammation. *Obes. Rev.* **13,** 83–96 (2012).
61. Mattson, M. P. Perspective: Does brown fat protect against diseases of aging? *Ageing Res. Rev.* **9,** 69–76 (2010).
62. Virtanen, K. A. *et al.* Functional Brown Adipose Tissue in Healthy Adults. *N. Engl. J. Med.* **360,** 1518–1525 (2009).

63. van Marken Lichtenbelt, W. D. *et al.* Cold-Activated Brown Adipose Tissue in Healthy Men. *N. Engl. J. Med.* **360,** 1500–1508 (2009).
64. Zhang, Y. *et al.* Positional cloning of the mouse obese gene and its human homologue. *Nature* **372,** 425–432 (1994).
65. Hotamisligil, G. S., Shargill, N. S. & Spiegelman, B. M. Adipose expression of tumor necrosis factor-alpha: direct role in obesity-linked insulin resistance. *Science* **259,** 87–91 (1993).
66. Galic, S., Oakhill, J. S. & Steinberg, G. R. Adipose tissue as an endocrine organ. *Mol. Cell. Endocrinol.* **316,** 129–139 (2010).
67. Hamdy, O., Porramatikul, S. & Al-Ozairi, E. Metabolic obesity: the paradox between visceral and subcutaneous fat. *Curr. Diabetes Rev.* **2,** 367–73 (2006).
68. Schleinitz, D., Böttcher, Y., Blüher, M. & Kovacs, P. The genetics of fat distribution. *Diabetologia* **57,** 1276–1286 (2014).
69. Kaur, J. A Comprehensive Review on Metabolic Syndrome. *Cardiol. Res. Pract.* **2014,** 1–21 (2014).
70. Savage, D. B., Petersen, K. F. & Shulman, G. I. Disordered Lipid Metabolism and the Pathogenesis of Insulin Resistance. *Physiol. Rev.* **87,** (2007).
71. Savage, D. B. Mouse models of inherited lipodystrophy. *Dis. Model. Mech.* **2,** 554–562 (2009).
72. Garg, A. & Agarwal, A. K. Caveolin-1: a new locus for human lipodystrophy. *J. Clin. Endocrinol. Metab.* **93,** 1183–5 (2008).
73. Asterholm, I. W., Halberg, N. & Scherer, P. E. Mouse Models of Lipodystrophy Key reagents for the understanding of the metabolic syndrome. *Drug Discov. Today. Dis. Models* **4,** 17–24 (2007).
74. Koutkia, P. & Grinspoon, S. HIV–Associated Lipodystrophy: Pathogenesis, Prognosis, Treatment, and Controversies. *Annu. Rev. Med.* **55,** 303–317 (2004).
75. Herbst, K. L. *et al.* Köbberling type of familial partial lipodystrophy: an underrecognized syndrome. *Diabetes Care* **26,** 1819–24 (2003).
76. Savage, D. B. *et al.* Human metabolic syndrome resulting from dominant-negative mutations in the nuclear receptor peroxisome proliferator-activated receptor-gamma. *Diabetes* **52,** 910–7 (2003).
77. Agostini, M. *et al.* Non-DNA binding, dominant-negative, human PPARγ mutations cause lipodystrophic insulin resistance. *Cell Metab.* **4,** 303–311

(2006).

78. Huang-Doran, I., Sleigh, A., Rochford, J. J., O'Rahilly, S. & Savage, D. B. Lipodystrophy: metabolic insights from a rare disorder. *J. Endocrinol.* **207,** 245–255 (2010).
79. Pendás, A. M. *et al.* Defective prelamin A processing and muscular and adipocyte alterations in Zmpste24 metalloproteinase–deficient mice. *Nat. Genet.* **31,** 94–9 (2002).
80. George, S. *et al.* A Family with Severe Insulin Resistance and Diabetes Due to a Mutation in AKT2. *Science (80-.).* **304,** 1325–1328 (2004).
81. Rubio-Cabezas, O. *et al.* Partial lipodystrophy and insulin resistant diabetes in a patient with a homozygous nonsense mutation in *CIDEC*. *EMBO Mol. Med.* **1,** 280–287 (2009).
82. Cortés, V. A. *et al.* Molecular Mechanisms of Hepatic Steatosis and Insulin Resistance in the AGPAT2-Deficient Mouse Model of Congenital Generalized Lipodystrophy. *Cell Metab.* **9,** 165–176 (2009).
83. Razani, B. *et al.* Caveolin-1-deficient Mice Are Lean, Resistant to Diet-induced Obesity, and Show Hypertriglyceridemia with Adipocyte Abnormalities. *J. Biol. Chem.* **277,** 8635–8647 (2002).
84. Linhart, H. G. *et al.* C/EBP is required for differentiation of white, but not brown, adipose tissue. *Proc. Natl. Acad. Sci.* **98,** 12532–12537 (2001).
85. Duan, S. Z. *et al.* Hypotension, lipodystrophy, and insulin resistance in generalized PPARγ-deficient mice rescued from embryonic lethality. *J. Clin. Invest.* **117,** 812–822 (2007).
86. Horton, J. D., Goldstein, J. L. & Brown, M. S. SREBPs: activators of the complete program of cholesterol and fatty acid synthesis in the liver. *J. Clin. Invest.* **109,** 1125–31 (2002).
87. Shimomura, I. *et al.* Insulin resistance and diabetes mellitus in transgenic mice expressing nuclear SREBP-1c in adipose tissue: model for congenital generalized lipodystrophy. *Genes Dev.* **12,** 3182–94 (1998).
88. Tang, Q. Q. & Lane, M. D. Adipogenesis: From Stem Cell to Adipocyte. *Annu. Rev. Biochem.* **81,** 715–736 (2012).
89. Kim, J. B. & Spiegelman, B. M. ADD1/SREBP1 promotes adipocyte differentiation and gene expression linked to fatty acid metabolism. *Genes Dev.* **10,** 1096–107 (1996).

90. Horton, J. D. *et al.* Combined analysis of oligonucleotide microarray data from transgenic and knockout mice identifies direct SREBP target genes. *Proc. Natl. Acad. Sci. U. S. A.* **100,** 12027–32 (2003).
91. Otto, T. C. & Lane, M. D. Adipose Development: From Stem Cell to Adipocyte. *Crit. Rev. Biochem. Mol. Biol.* **40,** 229–242 (2005).
92. Rosen, E. D. & MacDougald, O. A. Adipocyte differentiation from the inside out. *Nat. Rev. Mol. Cell Biol.* **7,** 885–96 (2006).
93. Bowers, R. R., Kim, J. W., Otto, T. C. & Lane, M. D. Stable stem cell commitment to the adipocyte lineage by inhibition of DNA methylation: role of the BMP-4 gene. *Proc. Natl. Acad. Sci. U. S. A.* **103,** 13022–7 (2006).
94. Zehentner, B. K., Dony, C. & Burtscher, H. The Transcription Factor Sox9 Is Involved in BMP-2 Signaling. *J. Bone Miner. Res.* **14,** 1734–1741 (1999).
95. Ross, S. E. *et al.* Inhibition of adipogenesis by Wnt signaling. *Science* **289,** 950–3 (2000).
96. Bowers, R. R. & Lane, M. D. Wnt signaling and adipocyte lineage commitment. *Cell Cycle* **7,** 1191–1196 (2008).
97. Spinella-Jaegle, S. *et al.* Opposite effects of bone morphogenetic protein-2 and transforming growth factor-beta1 on osteoblast differentiation. *Bone* **29,** 323–30 (2001).
98. McBeath, R., Pirone, D. M., Nelson, C. M., Bhadriraju, K. & Chen, C. S. Cell shape, cytoskeletal tension, and RhoA regulate stem cell lineage commitment. *Dev. Cell* **6,** 483–95 (2004).
99. Fève, B. Adipogenesis: cellular and molecular aspects. *Best Pract. Res. Clin. Endocrinol. Metab.* **19,** 483–499 (2005).
100. Zhang, J.-W., Klemm, D. J., Vinson, C. & Lane, M. D. Role of CREB in transcriptional regulation of CCAAT/enhancer-binding protein beta gene during adipogenesis. *J. Biol. Chem.* **279,** 4471–8 (2004).
101. Lane, M. D., Tang, Q. Q. & Jiang, M. S. Role of the CCAAT enhancer binding proteins (C/EBPs) in adipocyte differentiation. *Biochem. Biophys. Res. Commun.* **266,** 677–83 (1999).
102. Tang, Q.-Q., Otto, T. C. & Lane, M. D. Mitotic clonal expansion: A synchronous process required for adipogenesis. *Proc. Natl. Acad. Sci.* **100,** 44–49 (2003).
103. Tang, Q.-Q. *et al.* Sequential phosphorylation of CCAAT enhancer-binding

protein by MAPK and glycogen synthase kinase 3 is required for adipogenesis. *Proc. Natl. Acad. Sci.* **102,** 9766–9771 (2005).

104. Wu, Z. *et al.* Cross-Regulation of C/EBPα and PPARγ Controls the Transcriptional Pathway of Adipogenesis and Insulin Sensitivity. *Mol. Cell* **3,** 151–158 (1999).
105. Rosen, E. D. *et al.* C/EBPalpha induces adipogenesis through PPARgamma: a unified pathway. *Genes Dev.* **16,** 22–6 (2002).
106. Elberg, G., Gimble, J. M. & Tsai, S. Y. Modulation of the murine peroxisome proliferator-activated receptor gamma 2 promoter activity by CCAAT/enhancer-binding proteins. *J. Biol. Chem.* **275,** 27815–22 (2000).
107. Christy, R. J. *et al.* Differentiation-induced gene expression in 3T3-L1 preadipocytes: CCAAT/enhancer binding protein interacts with and activates the promoters of two adipocyte-specific genes. *Genes Dev.* **3,** 1323–35 (1989).
108. MacDougald, O. A. & Lane, M. D. Transcriptional Regulation of Gene Expression During Adipocyte Differentiation. *Annu. Rev. Biochem.* **64,** 345–373 (1995).
109. Lefterova, M. I. *et al.* PPAR and C/EBP factors orchestrate adipocyte biology via adjacent binding on a genome-wide scale. *Genes Dev.* **22,** 2941–2952 (2008).
110. Zhang, J.-W., Klemm, D. J., Vinson, C. & Lane, M. D. Role of CREB in Transcriptional Regulation of CCAAT/Enhancer-binding Protein Gene during Adipogenesis. *J. Biol. Chem.* **279,** 4471–4478 (2003).
111. Tanaka, T., Yoshida, N., Kishimoto, T. & Akira, S. Defective adipocyte differentiation in mice lacking the C/EBPbeta and/or C/EBPdelta gene. *EMBO J.* **16,** 7432–7443 (1997).
112. Lin, F. T. & Lane, M. D. CCAAT/enhancer binding protein alpha is sufficient to initiate the 3T3-L1 adipocyte differentiation program. *Proc. Natl. Acad. Sci. U. S. A.* **91,** 8757–61 (1994).
113. Lin, F. T. & Lane, M. D. Antisense CCAAT/enhancer-binding protein RNA suppresses coordinate gene expression and triglyceride accumulation during differentiation of 3T3-L1 preadipocytes. *Genes Dev.* **6,** 533–44 (1992).
114. Wang, N. D. *et al.* Impaired energy homeostasis in C/EBP alpha knockout mice. *Science* **269,** 1108–12 (1995).

115. Rosen, E. D. *et al.* C/EBPalpha induces adipogenesis through PPARgamma : a unified pathway. *Genes Dev.* **16,** 22–26 (2002).
116. Zuo, Y., Qiang, L. & Farmer, S. R. Activation of CCAAT/Enhancer-binding Protein (C/EBP) Expression by C/EBPbeta during Adipogenesis Requires a Peroxisome Proliferator-activated Receptor- -associated Repression of HDAC1 at the C/ebp Gene Promoter. *J. Biol. Chem.* **281,** 7960–7967 (2006).
117. Rosen, E. D. *et al.* PPAR gamma is required for the differentiation of adipose tissue in vivo and in vitro. *Mol. Cell* **4,** 611–7 (1999).
118. Ahmadian, M. *et al.* PPARγ signaling and metabolism: the good, the bad and the future. *Nat. Med.* **99,** 557–566 (2013).
119. Gearing, K. L., Göttlicher, M., Teboul, M., Widmark, E. & Gustafsson, J. A. Interaction of the peroxisome-proliferator-activated receptor and retinoid X receptor. *Proc. Natl. Acad. Sci. U. S. A.* **90,** 1440–4 (1993).
120. IJpenberg, A. *et al.* In vivo activation of PPAR target genes by RXR homodimers. *EMBO J.* **23,** 2083–2091 (2004).
121. Siersbaek, R., Nielsen, R. & Mandrup, S. Transcriptional networks and chromatin remodeling controlling adipogenesis. doi:10.1016/j.tem.2011.10.001
122. Zhu, Y. *et al.* Structural organization of mouse peroxisome proliferator-activated receptor y (mPPARy) gene: Alternative promoter use and different splicing yield two mPPARy isoforms (peroxisome proliferation/nuclear receptor superfamily/fatty acid P-oxidation). *Biochemistry* **92,** 7921–7925 (1995).
123. Ahmadian, M. *et al.* PPARγ signaling and metabolism: the good, the bad and the future. *Nat. Med.* **19,** 557–66 (2013).
124. Rosen, E. D. & Spiegelman, B. M. PPARgamma : a nuclear regulator of metabolism, differentiation, and cell growth. *J. Biol. Chem.* **276,** 37731–4 (2001).
125. Aprile, M. *et al.* PPARG in Human Adipogenesis: Differential Contribution of Canonical Transcripts and Dominant Negative Isoforms. *PPAR Res.* **2014,** 537865 (2014).
126. Matsusue, K. *et al.* Liver-specific disruption of PPARγ in leptin-deficient mice improves fatty liver but aggravates diabetic phenotypes. *J. Clin. Invest.* **111,** 737–747 (2003).

127. He, W. *et al.* Adipose-specific peroxisome proliferator-activated receptor knockout causes insulin resistance in fat and liver but not in muscle. *Proc. Natl. Acad. Sci.* **100,** 15712–15717 (2003).
128. Ricote, M., Li, A. C., Willson, T. M., Kelly, C. J. & Glass, C. K. The peroxisome proliferator-activated receptor-gamma is a negative regulator of macrophage activation. *Nature* **391,** 79–82 (1998).
129. Siersbæk, R. *et al.* Transcriptional networks and chromatin remodeling controlling adipogenesis. *Trends Endocrinol. Metab.* **23,** 56–64 (2012).
130. Sauer, S. Ligands for the Nuclear Peroxisome Proliferator- Activated Receptor Gamma. *Trends Pharmacol. Sci.* **36,** 688–704 (2015).
131. Schupp, M. & Lazar, M. A. Endogenous Ligands for Nuclear Receptors: Digging Deeper. *J. Biol. Chem.* **285,** 40409–40415 (2010).
132. Tontonoz, P., Hu, E. & Spiegelman, B. M. Stimulation of adipogenesis in fibroblasts by PPARγ2, a lipid-activated transcription factor. *Cell* **79,** 1147–1156 (1994).
133. Rosen, E. D. *et al.* PPAR gamma is required for the differentiation of adipose tissue in vivo and in vitro. *Mol. Cell* **4,** 611–7 (1999).
134. He, W. *et al.* Adipose-specific peroxisome proliferator-activated receptor knockout causes insulin resistance in fat and liver but not in muscle. *Proc. Natl. Acad. Sci.* **100,** 15712–15717 (2003).
135. Jones, J. R. *et al.* Deletion of PPAR in adipose tissues of mice protects against high fat diet-induced obesity and insulin resistance. *Proc. Natl. Acad. Sci.* **102,** 6207–6212 (2005).
136. Zhang, J. *et al.* Selective disruption of PPAR 2 impairs the development of adipose tissue and insulin sensitivity. *Proc. Natl. Acad. Sci.* **101,** 10703–10708 (2004).
137. Medina-Gomez, G. *et al.* The link between nutritional status and insulin sensitivity is dependent on the adipocyte-specific peroxisome proliferator-activated receptor-gamma2 isoform. *Diabetes* **54,** 1706–16 (2005).
138. Tsai, Y.-S. *et al.* Hypertension and abnormal fat distribution but not insulin resistance in mice with P465L PPARγ. *J. Clin. Invest.* **114,** 240–249 (2004).
139. Freedman, B. D., Lee, E.-J., Park, Y. & Jameson, J. L. A Dominant Negative Peroxisome Proliferator-activated Receptor- Knock-in Mouse Exhibits Features of the Metabolic Syndrome. *J. Biol. Chem.* **280,** 17118–17125

(2005).

140. Gray, S. L., Dalla Nora, E. & Vidal-Puig, A. J. Mouse models of PPAR-γ deficiency: dissecting PPAR-γ's role in metabolic homoeostasis. *Biochem. Soc. Trans.* **33,** 1053 (2005).
141. Lund, E. *et al.* Lamin A/C-promoter interactions specify chromatin state-dependent transcription outcomes. *Genome Res.* **23,** 1580–9 (2013).
142. Stierlé, V. *et al.* The Carboxyl-Terminal Region Common to Lamins A and C Contains a DNA Binding Domain †. *Biochemistry* **42,** 4819–4828 (2003).
143. Barrowman, J., Wiley, P. A., Hudon-Miller, S. E., Hrycyna, C. A. & Michaelis, S. Human ZMPSTE24 disease mutations: residual proteolytic activity correlates with disease severity. *Hum. Mol. Genet.* **21,** 4084–4093 (2012).
144. Maraldi, N. M. *et al.* A pathogenic mechanism leading to partial lipodistrophy and prospects for pharmacological treatment of insulin resistance syndrome. *Acta Biomed.* **78 Suppl 1,** 207–15 (2007).
145. Capanni, C. *et al.* Altered pre-lamin A processing is a common mechanism leading to lipodystrophy. *Hum. Mol. Genet.* **14,** 1489–502 (2005).
146. Tu, Y., Sánchez-Iglesias, S., Araújo-Vilar, D., Fong, L. G. & Young, S. G. *LMNA* missense mutations causing familial partial lipodystrophy do not lead to an accumulation of prelamin A. *Nucleus* **7,** 512–521 (2016).
147. Kim, J. B. *et al.* Nutritional and insulin regulation of fatty acid synthetase and leptin gene expression through ADD1/SREBP1. *J. Clin. Invest.* **101,** 1–9 (1998).
148. Goldstein, J. L., DeBose-Boyd, R. A. & Brown, M. S. Protein Sensors for Membrane Sterols. *Cell* **124,** 35–46 (2006).
149. Shimano, H. Sterol regulatory element-binding proteins (SREBPs): transcriptional regulators of lipid synthetic genes. *Prog. Lipid Res.* **40,** 439–52 (2001).
150. Amemiya-Kudo, M. *et al.* Transcriptional activities of nuclear SREBP-1a, -1c, and -2 to different target promoters of lipogenic and cholesterogenic genes. *J. Lipid Res.* **43,** 1220–35 (2002).
151. Lloyd, D. J., Trembath, R. C. & Shackleton, S. A novel interaction between lamin A and SREBP1: implications for partial lipodystrophy and other laminopathies. *Hum. Mol. Genet.* **11,** 769–77 (2002).

152. Duband-Goulet, I. *et al.* Subcellular localization of SREBP1 depends on its interaction with the C-terminal region of wild-type and disease related A-type lamins. *Exp. Cell Res.* **317,** 2800–13 (2011).
153. Sabatino, L. *et al.* A novel peroxisome proliferator-activated receptor gamma isoform with dominant negative activity generated by alternative splicing. *J. Biol. Chem.* **280,** 26517–25 (2005).
154. Vadrot, N. *et al.* The p.R482W substitution in A-type lamins deregulates SREBP1 activity in Dunnigan-type familial partial lipodystrophy. *Hum. Mol. Genet.* **24,** 2096–2109 (2015).
155. Oldenburg, A. R., Delbarre, E., Thiede, B., Vigouroux, C. & Collas, P. Deregulation of Fragile X-related protein 1 by the lipodystrophic lamin A p.R482W mutation elicits a myogenic gene expression program in preadipocytes. *Hum. Mol. Genet.* **23,** 1151–1162 (2014).
156. Fiorenza, C. G., Chou, S. H. & Mantzoros, C. S. Lipodystrophy: pathophysiology and advances in treatment. *Nat. Rev. Endocrinol.* **7,** 137–50 (2011).
157. Oral, E. A. *et al.* Leptin-Replacement Therapy for Lipodystrophy. *N. Engl. J. Med.* **346,** 570–578 (2002).
158. Ludtke, A. *et al.* Long-term treatment experience in a subject with Dunnigan-type familial partial lipodystrophy: efficacy of rosiglitazone. *Diabet. Med.* **22,** 1611–1613 (2005).
159. Luedtke, A. *et al.* Thiazolidinedione Response in Familial Lipodystrophy Patients with LMNA Mutations: A Case Series. *Horm. Metab. Res.* **44,** 306–311 (2012).
160. McLaughlin, P. D., Ryan, J., Hodnett, P. A., O'Halloran, D. & Maher, M. M. Quantitative Whole-Body MRI in Familial Partial Lipodystrophy Type 2: Changes in Adipose Tissue Distribution Coincide With Biochemical Improvement. *Am. J. Roentgenol.* **199,** W602–W606 (2012).
161. Arioglu, E. *et al.* Efficacy and safety of troglitazone in the treatment of lipodystrophy syndromes. *Ann. Intern. Med.* **133,** 263–74 (2000).
162. Vatier, C., Gautier, J.-F. & Vigouroux, C. Therapeutic use of recombinant methionyl human leptin. *Biochimie* **94,** 2116–2125 (2012).
163. Park, J. Y., Javor, E. D., Cochran, E. K., DePaoli, A. M. & Gorden, P. Long-term efficacy of leptin replacement in patients with Dunnigan-type familial

partial lipodystrophy. *Metabolism* **56,** 508–516 (2007).

164. Agostini, M. *et al.* Non-DNA binding, dominant-negative, human PPARgamma mutations cause lipodystrophic insulin resistance. *Cell Metab.* **4,** 303–11 (2006).
165. Cadiñanos, J. & Bradley, A. Generation of an inducible and optimized piggyBac transposon system. *Nucleic Acids Res.* **35,** e87 (2007).
166. Mehlem, A., Hagberg, C. E., Muhl, L., Eriksson, U. & Falkevall, A. Imaging of neutral lipids by oil red O for analyzing the metabolic status in health and disease. *Nat. Protoc.* **8,** 1149–54 (2013).
167. Arsenijevic, T. *et al.* Murine 3T3-L1 Adipocyte Cell Differentiation Model: Validated Reference Genes for qPCR Gene Expression Analysis. *PLoS One* **7,** e37517 (2012).
168. Deleersnijder, W. *et al.* Isolation of markers for chondro-osteogenic differentiation using cDNA library subtraction. Molecular cloning and characterization of a gene belonging to a novel multigene family of integral membrane proteins. *J. Biol. Chem.* **271,** 19475–82 (1996).
169. Hedlund, J., Johansson, J. & Persson, B. BRICHOS - a superfamily of multidomain proteins with diverse functions. *BMC Res. Notes* **2,** 180 (2009).
170. Boeuf, S. *et al.* Enhanced ITM2A expression inhibits chondrogenic differentiation of mesenchymal stem cells. *Differentiation.* **78,** 108–15
171. Lagha, M. *et al.* Itm2a is a Pax3 target gene, expressed at sites of skeletal muscle formation in vivo. *PLoS One* **8,** e63143 (2013).
172. Tai, T.-S., Pai, S.-Y. & Ho, I.-C. Itm2a, a target gene of GATA-3, plays a minimal role in regulating the development and function of T cells. *PLoS One* **9,** e96535 (2014).
173. Van den Plas, D. & Merregaert, J. Constitutive overexpression of the integral membrane protein Itm2A enhances myogenic differentiation of C2C12 cells. *Cell Biol. Int.* **28,** 199–207 (2004).
174. Namkoong, S. *et al.* The integral membrane protein ITM2A, a transcriptional target of PKA-CREB, regulates autophagic flux via interaction with the vacuolar ATPase. *Autophagy* **11,** 756–768 (2015).
175. Van den Plas, D. & Merregaert, J. In vitro studies on Itm2a reveal its involvement in early stages of the chondrogenic differentiation pathway. *Biol. cell* **96,** 463–70 (2004).

176. Bermeo, S., Vidal, C., Zhou, H. & Duque, G. Lamin A/C Acts as an Essential Factor in Mesenchymal Stem Cell Differentiation Through the Regulation of the Dynamics of the Wnt/β-Catenin Pathway. *J. Cell. Biochem.* **116,** 2344–53 (2015).
177. Wojtanik, K. M. *et al.* The role of LMNA in adipose: a novel mouse model of lipodystrophy based on the Dunnigan-type familial partial lipodystrophy mutation. *J. Lipid Res.* **50,** 1068–79 (2009).
178. Mikkelsen, T. S. *et al.* Comparative epigenomic analysis of murine and human adipogenesis. *Cell* **143,** 156–69 (2010).
179. Tang, Q. Q. & Lane, M. D. Adipogenesis: from stem cell to adipocyte. *Annu. Rev. Biochem.* **81,** 715–36 (2012).
180. Petersen, R. K. *et al.* Cyclic AMP (cAMP)-mediated stimulation of adipocyte differentiation requires the synergistic action of Epac- and cAMP-dependent protein kinase-dependent processes. *Mol. Cell. Biol.* **28,** 3804–16 (2008).
181. Yang, D.-C. *et al.* cAMP/PKA regulates osteogenesis, adipogenesis and ratio of RANKL/OPG mRNA expression in mesenchymal stem cells by suppressing leptin. *PLoS One* **3,** e1540 (2008).
182. Tong, Q. *et al.* Function of GATA transcription factors in preadipocyte-adipocyte transition. *Science* **290,** 134–8 (2000).
183. Wang, L. & Di, L. Wnt/β-Catenin Mediates AICAR Effect to Increase GATA3 Expression and Inhibit Adipogenesis. *J. Biol. Chem.* **290,** 19458–19468 (2015).
184. Cawthorn, W. P. *et al.* Wnt6, Wnt10a and Wnt10b inhibit adipogenesis and stimulate osteoblastogenesis through a β-catenin-dependent mechanism. *Bone* **50,** 477–89 (2012).
185. Stambolic, V., Ruel, L. & Woodgett, J. R. Lithium inhibits glycogen synthase kinase-3 activity and mimics wingless signalling in intact cells. *Curr. Biol.* **6,** 1664–8 (1996).
186. Hernandez, L. *et al.* Functional coupling between the extracellular matrix and nuclear lamina by Wnt signaling in progeria. *Dev. Cell* **19,** 413–25 (2010).
187. Mitsui, S., Osako, Y. & Yuri, K. Mental retardation-related protease, motopsin (prss12), binds to the BRICHOS domain of the integral membrane protein 2a. *Cell Biol. Int.* **38,** 117–23 (2014).
188. Kirchner, J. & Bevan, M. J. ITM2A is induced during thymocyte selection

and T cell activation and causes downregulation of CD8 when overexpressed in CD4(+)CD8(+) double positive thymocytes. *J. Exp. Med.* **190,** 217–28 (1999).

189. Martin, L. *et al.* Regulated intramembrane proteolysis of Bri2 (Itm2b) by ADAM10 and SPPL2a/SPPL2b. *J. Biol. Chem.* **283,** 1644–52 (2008).
190. Marcora, M. S. *et al.* Amyloid peptides ABri and ADan show differential neurotoxicity in transgenic Drosophila models of familial British and Danish dementia. *Mol. Neurodegener.* **9,** 5 (2014).
191. Vadrot, N. *et al.* The p.R482W substitution in A-type lamins deregulates SREBP1 activity in Dunnigan-type familial partial lipodystrophy. *Hum. Mol. Genet.* **24,** 2096–109 (2015).
192. Oldenburg, A. R., Delbarre, E., Thiede, B., Vigouroux, C. & Collas, P. Deregulation of Fragile X-related protein 1 by the lipodystrophic lamin A p.R482W mutation elicits a myogenic gene expression program in preadipocytes. *Hum. Mol. Genet.* **23,** 1151–62 (2014).
193. Yang, Z. & Klionsky, D. J. Mammalian autophagy: core molecular machinery and signaling regulation. *Curr. Opin. Cell Biol.* **22,** 124–31 (2010).
194. Baerga, R., Zhang, Y., Chen, P.-H., Goldman, S. & Jin, S. Targeted deletion of autophagy-related 5 (atg5) impairs adipogenesis in a cellular model and in mice. *Autophagy* **5,** 1118–30 (2009).
195. Singh, R. *et al.* Autophagy regulates adipose mass and differentiation in mice. *J. Clin. Invest.* **119,** 3329–39 (2009).
196. Kovsan, J. *et al.* Altered autophagy in human adipose tissues in obesity. *J. Clin. Endocrinol. Metab.* **96,** E268-77 (2011).
197. Skop, V. *et al.* Autophagy inhibition in early but not in later stages prevents 3T3-L1 differentiation: Effect on mitochondrial remodeling. *Differentiation.* **87,** 220–9 (2014).
198. Guo, L. *et al.* Transactivation of Atg4b by C/EBPβ promotes autophagy to facilitate adipogenesis. *Mol. Cell. Biol.* **33,** 3180–90 (2013).
199. Zhang, C. *et al.* Autophagy is involved in adipogenic differentiation by repressesing proteasome-dependent PPARγ2 degradation. *Am. J. Physiol. Endocrinol. Metab.* **305,** E530-9 (2013).
200. Forgac, M. Vacuolar ATPases: rotary proton pumps in physiology and pathophysiology. *Nat. Rev. Mol. Cell Biol.* **8,** 917–29 (2007).

201. Choi, J. C. & Worman, H. J. Reactivation of autophagy ameliorates LMNA cardiomyopathy. *Autophagy* **9,** 110–1 (2013).
202. Cao, K. *et al.* Rapamycin Reverses Cellular Phenotypes and Enhances Mutant Protein Clearance in Hutchinson-Gilford Progeria Syndrome Cells. *Sci. Transl. Med.* **3,** (2011).
203. Siddle, K. Molecular basis of signaling specificity of insulin and IGF receptors: neglected corners and recent advances. *Front. Endocrinol. (Lausanne).* **3,** 34 (2012).
204. Nakae, J., Kido, Y. & Accili, D. Distinct and Overlapping Functions of Insulin and IGF-I Receptors.
205. Liu, J. P., Baker, J., Perkins, A. S., Robertson, E. J. & Efstratiadis, A. Mice carrying null mutations of the genes encoding insulin-like growth factor I (Igf-1) and type 1 IGF receptor (Igf1r). *Cell* **75,** 59–72 (1993).
206. Bunner, A. E., Chandrasekera, P. C. & Barnard, N. D. Knockout mouse models of insulin signaling: Relevance past and future. *World J. Diabetes* **5,** 146–59 (2014).
207. Boucher, J. *et al.* Impaired thermogenesis and adipose tissue development in mice with fat-specific disruption of insulin and IGF-1 signalling. *Nat. Commun.* **3,** 902 (2012).
208. Schneider, M. R., Wolf, E., Hoeflich, A. & Lahm, H. IGF-binding protein-5: flexible player in the IGF system and effector on its own. *J. Endocrinol.* **172,** 423–40 (2002).
209. Beattie, J., Allan, G. J., Lochrie, J. D. & Flint, D. J. Insulin-like growth factor-binding protein-5 (IGFBP-5): a critical member of the IGF axis. *Biochem. J.* **395,** (2006).
210. Hwa, V., Oh, Y. & Rosenfeld, R. G. The Insulin-Like Growth Factor-Binding Protein (IGFBP) Superfamily [1]. *Endocr. Rev.* **20,** 761–787 (1999).
211. Imai, Y. *et al.* Substitutions for hydrophobic amino acids in the N-terminal domains of IGFBP-3 and -5 markedly reduce IGF-I binding and alter their biologic actions. *J. Biol. Chem.* **275,** 18188–94 (2000).
212. James, P. L., Jones, S. B., Busby, W. H., Clemmons, D. R. & Rotwein, P. A highly conserved insulin-like growth factor-binding protein (IGFBP-5) is expressed during myoblast differentiation. *J. Biol. Chem.* **268,** 22305–12 (1993).

213. Twigg, S. M. & Baxter, R. C. Insulin-like growth factor (IGF)-binding protein 5 forms an alternative ternary complex with IGFs and the acid-labile subunit. *J. Biol. Chem.* **273,** 6074–9 (1998).
214. Andress, D. L. Heparin modulates the binding of insulin-like growth factor (IGF) binding protein-5 to a membrane protein in osteoblastic cells. *J. Biol. Chem.* **270,** 28289–96 (1995).
215. Jones, J. I., Gockerman, A., Busby, W. H., Wright, G. & Clemmons, D. R. Insulin-like growth factor binding protein 1 stimulates cell migration and binds to the alpha 5 beta 1 integrin by means of its Arg-Gly-Asp sequence. *Proc. Natl. Acad. Sci. U. S. A.* **90,** 10553–7 (1993).
216. Fowlkes, J. L., Thrailkill, K. M., George-Nascimento, C., Rosenberg, C. K. & Serra, D. M. Heparin-Binding, Highly Basic Regions within the Thyroglobulin Type-1 Repeat of Insulin-Like Growth Factor (IGF)-Binding Proteins (IGFBPs) -3, -5, and -6 Inhibit IGFBP-4 Degradation [1]. *Endocrinology* **138,** 2280–2285 (1997).
217. Nam, T.-J., Busby, W. H., Rees, C. & Clemmons, D. R. Thrombospondin and Osteopontin Bind to Insulin-Like Growth Factor (IGF)-Binding Protein-5 Leading to an Alteration in IGF-I-Stimulated Cell Growth [1]. *Endocrinology* **141,** 1100–1106 (2000).
218. Conover, C. A. in *The IGF System* 355–376 (Humana Press, 1999). doi:10.1007/978-1-59259-712-3_16
219. Coverley, J. A. & Baxter, R. C. Phosphorylation of insulin-like growth factor binding proteins. *Mol. Cell. Endocrinol.* **128,** 1–5 (1997).
220. Camacho-Hubner, C., Busby, W. H., McCusker, R. H., Wright, G. & Clemmons, D. R. Identification of the forms of insulin-like growth factor-binding proteins produced by human fibroblasts and the mechanisms that regulate their secretion. *J. Biol. Chem.* **267,** 11949–56 (1992).
221. Arai, T., Arai, A., Busby, W. H. & Clemmons, D. R. Glycosaminoglycans inhibit degradation of insulin-like growth factor-binding protein-5. *Endocrinology* **135,** 2358–2363 (1994).
222. Duan, C. & Clemmons, D. R. Transcription factor AP-2 regulates human insulin-like growth factor binding protein-5 gene expression. *J. Biol. Chem.* **270,** 24844–51 (1995).
223. Conover, C. A., Bale, L. K., Clarkson, J. T. & Tørring, O. Regulation of

insulin-like growth factor binding protein-5 messenger ribonucleic acid expression and protein availability in rat osteoblast-like cells. *Endocrinology* **132,** 2525–2530 (1993).

224. Chevalley, T., Strong, D. D., Mohan, S., Baylink, D. & Linkhart, T. A. Evidence for a role for insulin-like growth factor binding proteins in glucocorticoid inhibition of normal human osteoblast-like cell proliferation. *Eur. J. Endocrinol.* **134,** 591–601 (1996).
225. Boonyaratanakornkit, V. *et al.* Progesterone stimulation of human insulin-like growth factor-binding protein-5 gene transcription in human osteoblasts is mediated by a CACCC sequence in the proximal promoter. *J. Biol. Chem.* **274,** 26431–8 (1999).
226. McCarthy, T. L. *et al.* Promoter-dependent and -independent activation of insulin-like growth factor binding protein-5 gene expression by prostaglandin E2 in primary rat osteoblasts. *J. Biol. Chem.* **271,** 6666–71 (1996).
227. Gabbitas, B. & Canalis, E. Insulin-like growth factors sustain insulin-like growth factor-binding protein-5 expression in osteoblasts. *Am. J. Physiol. - Endocrinol. Metab.* **275,** (1998).
228. Yeh, L.-C. C. & Lee, J. C. Identification of an Osteogenic Protein-1 (Bone Morphogenetic Protein-7)-Responsive Element in the Promoter of the Rat Insulin-Like Growth Factor-Binding Protein-5 Gene [1]. *Endocrinology* **141,** 3278–3286 (2000).
229. Perez-Casellas, L. Regulation of IGFBP-5 and osteoblast functions by Nuclear Factor I.
230. CESI, V. *et al.* C/EBP ? and ? mimic retinoic acid activation of IGFBP-5 in neuroblastoma cells by a mechanism independent from binding to their site. *Exp. Cell Res.* **305,** 179–189 (2005).
231. Meester-Smoor, M. A. *et al.* The MN1 oncoprotein activates transcription of the IGFBP5 promoter through a CACCC-rich consensus sequence. *J. Mol. Endocrinol.* **38,** 113–25 (2007).
232. Tanno, B. *et al.* Expression of insulin-like growth factor-binding protein 5 in neuroblastoma cells is regulated at the transcriptional level by c-Myb and B-Myb via direct and indirect mechanisms. *J. Biol. Chem.* **277,** 23172–80 (2002).
233. YOSHIZAWA, A. & OGIKUBO, S. IGF Binding Protein-5 Synthesis is

Regulated by Testosterone through Transcriptional Mechanisms in Androgen Responsive Cells. *Endocr. J.* **53,** 811–818 (2006).

234. Duan, C., Liimatta, M. B. & Bottum, O. L. Insulin-like growth factor (IGF)-I regulates IGF-binding protein-5 gene expression through the phosphatidylinositol 3-kinase, protein kinase B/Akt, and p70 S6 kinase signaling pathway. *J. Biol. Chem.* **274,** 37147–53 (1999).
235. Marshman, E. *et al.* Insulin-like growth factor binding protein 5 and apoptosis in mammary epithelial cells. *J. Cell Sci.* **116,** 675–82 (2003).
236. Akkiprik, M. *et al.* Multifunctional roles of insulin-like growth factor binding protein 5 in breast cancer. *Breast Cancer Res.* **10,** 212 (2008).
237. Miyake, H., Pollak, M. & Gleave, M. E. Castration-induced up-regulation of insulin-like growth factor binding protein-5 potentiates insulin-like growth factor-I activity and accelerates progression to androgen independence in prostate cancer models. *Cancer Res.* **60,** 3058–64 (2000).
238. Wang, H. *et al.* Insulin-like growth factor-binding protein 2 and 5 are differentially regulated in ovarian cancer of different histologic types. *Mod. Pathol.* **19,** 1149–1156 (2006).
239. Liu, Y. *et al.* Identification of genes differentially expressed in human primary lung squamous cell carcinoma. *Lung Cancer* **56,** 307–317 (2007).
240. Johnson, S. K. & Haun, R. S. Insulin-like growth factor binding protein-5 influences pancreatic cancer cell growth. *World J. Gastroenterol.* **15,** 3355–66 (2009).
241. Stolf, B. S. *et al.* Differential expression of IGFBP-5 and two human ESTs in thyroid glands with goiter, adenoma and papillary or follicular carcinomas. *Cancer Lett.* **191,** 193–202 (2003).
242. Lin, S.-C. *et al.* Regulation of IGFBP-5 expression during tumourigenesis and differentiation of oral keratinocytes. *J. Pathol.* **198,** 317–325 (2002).
243. Hung, P.-S. *et al.* Insulin-like growth factor binding protein-5 (IGFBP-5) suppresses the tumourigenesis of head and neck squamous cell carcinoma. *J. Pathol.* **214,** 368–376 (2008).
244. Miyatake, T. *et al.* Down-regulation of insulin-like growth factor binding protein-5 (IGFBP-5): Novel marker for cervical carcinogenesis. *Int. J. Cancer* **120,** 2068–2077 (2007).
245. James, P. L., Stewart, C. E. & Rotwein, P. Insulin-like growth factor binding

protein-5 modulates muscle differentiation through an insulin-like growth factor-dependent mechanism. *J. Cell Biol.* **133,** 683–93 (1996).

246. Cobb, L. J. *et al.* Partitioning of IGFBP-5 actions in myogenesis: IGF-independent anti-apoptotic function. *J. Cell Sci.* **117,** 1737–1746 (2004).
247. Mukherjee, A. & Rotwein, P. Insulin-like growth factor binding protein-5 in osteogenesis: Facilitator or inhibitor? *Growth Horm. IGF Res.* **17,** 179–185 (2007).
248. Richman, C., Baylink, D. J., Lang, K., Dony, C. & Mohan, S. Recombinant Human Insulin-Like Growth Factor-Binding Protein-5 Stimulates Bone Formation Parameters *in Vitro* and *in Vivo* [1]. *Endocrinology* **140,** 4699–4705 (1999).
249. Durant, D., Pereira, R., Stadmeyer, L. & Canalis, E. Transgenic mice expressing selected insulin-like growth factor-binding protein-5 fragments do not exhibit enhanced bone formation. *Growth Horm. IGF Res.* **14,** 319–327 (2004).
250. Bauss, F., Lang, K., Dony, C. & Kling, L. The complex of recombinant human insulin-like growth factor-I (rhIGF-I) and its binding protein-5 (IGFBP-5) induces local bone formation in murine calvariae and in rat cortical bone after local or systemic administration. *Growth Horm. IGF Res.* **11,** 1–9 (2001).
251. Devlin, R. D., Du, Z., Buccilli, V., Jorgetti, V. & Canalis, E. Transgenic Mice Overexpressing Insulin-Like Growth Factor Binding Protein-5 Display Transiently Decreased Osteoblastic Function and Osteopenia. doi:10.1210/en.2002-220129
252. Salih, D. A. M. *et al.* Insulin-like growth factor-binding protein 5 (Igfbp5) compromises survival, growth, muscle development, and fertility in mice. *Proc. Natl. Acad. Sci.* **101,** 4314–4319 (2004).
253. Sekiya, I., Vuoristo, J. T., Larson, B. L. & Prockop, D. J. In vitro cartilage formation by human adult stem cells from bone marrow stroma defines the sequence of cellular and molecular events during chondrogenesis. *Proc. Natl. Acad. Sci.* **99,** 4397–4402 (2002).
254. Kiepe, D., Ciarmatori, S., Haarmann, A. & Tönshoff, B. Differential expression of IGF system components in proliferating vs. differentiating growth plate chondrocytes: the functional role of IGFBP-5. *AJP Endocrinol.*

Metab. **290,** E363–E371 (2005).

255. Samuel, W. *et al.* Decreased expression of insulin-like growth factor binding protein-5 during N-(4-hydroxyphenyl)retinamide-induced neuronal differentiation of ARPE-19 human retinal pigment epithelial cells: Regulation by CCAAT/enhancer-binding protein. *J. Cell. Physiol.* **224,** 827–836 (2010).
256. Samuel, W. *et al.* Mitogen-activated protein kinase pathway mediates *N* -(4-hydroxyphenyl)retinamide-induced neuronal differentiation in the ARPE-19 human retinal pigment epithelial cell line. *J. Neurochem.* **106,** 591–602 (2008).
257. Tanno, B. *et al.* Silencing of endogenous IGFBP-5 by micro RNA interference affects proliferation, apoptosis and differentiation of neuroblastoma cells. *Cell Death Differ.* **12,** 213–223 (2005).
258. Cheng, H.-L., Shy, M. & Feldman, E. L. Regulation of Insulin-Like Growth Factor-Binding Protein-5 Expression during Schwann Cell Differentiation*. *Endocrinology* **140,** 4478–4485 (1999).
259. Naspi, A. *et al.* IGFBP-3 inhibits Wnt signaling in metastatic melanoma cells. *Mol. Carcinog.* **56,** 681–693 (2017).
260. Wu, K. *et al.* The role of IGFBP-5 in mediating the anti-proliferation effect of tetrandrine in human colon cancer cells. *Int. J. Oncol.* (2014). doi:10.3892/ijo.2014.2800
261. Liu, B. Y. *et al.* Mammary Tumor Regression Elicited by Wnt Signaling Inhibitor Requires IGFBP5. *Cancer Res.* **72,** 1568–1578 (2012).
262. Zhu, W. *et al.* IGFBP-4 is an inhibitor of canonical Wnt signalling required for cardiogenesis. *Nature* **454,** 345–349 (2008).
263. Wo, D. *et al.* Opposing Roles of Wnt Inhibitors IGFBP-4 and Dkk1 in Cardiac Ischemia by Differential Targeting of LRP5/6 and β-catenin. *Circulation* (2016).
264. Boney, C. M., Moats-Staats, B. M., Stiles, A. D. & D'Ercole, A. J. Expression of insulin-like growth factor-I (IGF-I) and IGF-binding proteins during adipogenesis. *Endocrinology* **135,** 1863–1868 (1994).
265. Siddals, K. W., Westwood, M., Gibson, J. M. & White, A. IGF-binding protein-1 inhibits IGF effects on adipocyte function: implications for insulin-like actions at the adipocyte. *J. Endocrinol.* **174,** 289–97 (2002).
266. Rajkumar, K., Modric, T. & Murphy, L. J. Impaired adipogenesis in insulin-

like growth factor binding protein-1 transgenic mice. *J. Endocrinol.* **162,** 457–65 (1999).

267. Wheatcroft, S. B. *et al.* IGF-Binding Protein-2 Protects Against the Development of Obesity and Insulin Resistance. *Diabetes* **56,** 285–294 (2007).
268. Baxter, R. C. & Twigg, S. M. Actions of IGF binding proteins and related proteins in adipose tissue. *Trends Endocrinol. Metab.* **20,** 499–505 (2009).
269. Chan, S. S. Y., Twigg, S. M., Firth, S. M. & Baxter, R. C. Insulin-Like Growth Factor Binding Protein-3 Leads to Insulin Resistance in Adipocytes. *J. Clin. Endocrinol. Metab.* **90,** 6588–6595 (2005).
270. Chan, S. S. Y., Schedlich, L. J., Twigg, S. M. & Baxter, R. C. Inhibition of adipocyte differentiation by insulin-like growth factor-binding protein-3. *AJP Endocrinol. Metab.* **296,** E654–E663 (2009).
271. Wabitsch, M., Heinze, E., Debatin, K.-M. & Blum, W. IGF-I- and IGFBP-3-Expression in Cultured Human Preadipocytes and Adipocytes. *Horm. Metab. Res.* **32,** 555–559 (2000).
272. Gardan, D., Mourot, J. & Louveau, I. Decreased expression of the IGF-II gene during porcine adipose cell differentiation. *Mol. Cell. Endocrinol.* **292,** (2008).
273. Hausman, G. J., Richardson, R. L. & Simmen, F. A. Secretion of insulin-like growth factor (IGF)-I and -II and IGF binding proteins (IGFBPs) in fetal stromal-vascular (S-V) cell cultures obtained before and after the onset of adipogenesis in vivo. *Growth. Dev. Aging* **66,** 11–26 (2002).
274. Gehrke, S. *et al.* Epigenetic Regulation of Depot-Specific Gene Expression in Adipose Tissue. *PLoS One* **8,** e82516 (2013).
275. Tonner, E. *et al.* Insulin-like growth factor binding protein-5 (IGFBP-5) induces premature cell death in the mammary glands of transgenic mice. *Development* **129,** 4547–57 (2002).
276. Ning, Y. *et al.* Diminished Growth and Enhanced Glucose Metabolism in Triple Knockout Mice Containing Mutations of Insulin-Like Growth Factor Binding Protein-3, -4, and -5. doi:10.1210/me.2005-0196
277. Ning, Y. *et al.* Delayed Mammary Gland Involution in Mice with Mutation of the Insulin-Like Growth Factor Binding Protein 5 Gene. doi:10.1210/en.2006-0041

278. Andres-Leon, E., Gonzalez Pena, D., Gomez-Lopez, G. & Pisano, D. G. miRGate: a curated database of human, mouse and rat miRNA-mRNA targets. *Database* **2015,** bav035-bav035 (2015).
279. Rosen, E. D. & MacDougald, O. A. Adipocyte differentiation from the inside out. *Nat. Rev. Mol. Cell Biol.* **7,** 885–896 (2006).
280. Singh, R. *et al.* Testosterone Inhibits Adipogenic Differentiation in 3T3-L1 Cells: Nuclear Translocation of Androgen Receptor Complex with β-Catenin and T-Cell Factor 4 May Bypass Canonical Wnt Signaling to Down-Regulate Adipogenic Transcription Factors. *Endocrinology* **147,** 141–154 (2006).
281. Blouin, K. *et al.* Effects of androgens on adipocyte differentiation and adipose tissue explant metabolism in men and women. *Clin. Endocrinol. (Oxf).* **72,** 176–188 (2010).
282. Chazenbalk, G. *et al.* Androgens inhibit adipogenesis during human adipose stem cell commitment to preadipocyte formation. *Steroids* **78,** 920–6 (2013).
283. Garten, A., Schuster, S. & Kiess, W. The Insulin-Like Growth Factors in Adipogenesis and Obesity.
284. Tardif, G., Hum, D., Pelletier, J.-P., Duval, N. & Martel-Pelletier, J. Regulation of the IGFBP-5 and MMP-13 genes by the microRNAs miR-140 and miR-27a in human osteoarthritic chondrocytes. *BMC Musculoskelet. Disord.* **10,** 148 (2009).
285. Silha, J. V., Gui, Y. & Murphy, L. J. Impaired glucose homeostasis in insulin-like growth factor-binding protein-3-transgenic mice. *Am. J. Physiol. - Endocrinol. Metab.* **283,** E937–E945 (2002).
286. Stoker, A. W. REVIEW Protein tyrosine phosphatases and signalling. *J. Endocrinol.* **185,** 19–33 (2005).
287. Andersen, J. N. *et al.* Structural and evolutionary relationships among protein tyrosine phosphatase domains. *Mol. Cell. Biol.* **21,** 7117–36 (2001).
288. Oganesian, A. *et al.* Protein tyrosine phosphatase RQ is a phosphatidylinositol phosphatase that can regulate cell survival and proliferation.
289. Schraders, M. *et al.* Mutations in PTPRQ Are a Cause of Autosomal-Recessive Nonsyndromic Hearing Impairment DFNB84 and Associated with Vestibular Dysfunction. doi:10.1016/j.ajhg.2010.02.015
290. Shahin, H. *et al.* Nonsense mutation of the stereociliar membrane protein gene PTPRQ in human hearing loss DFNB84. *J. Med. Genet.* **47,** 643–645 (2010).

291. Goodyear, R. J. *et al.* A receptor-like inositol lipid phosphatase is required for the maturation of developing cochlear hair bundles. *J. Neurosci.* **23,** 9208–19 (2003).
292. Sakaguchi, H. *et al.* Dynamic compartmentalization of protein tyrosine phosphatase receptor Q at the proximal end of stereocilia: Implication of myosin VI-based transport. *Cell Motil. Cytoskeleton* **65,** 528–538 (2008).
293. Nayak, G., Goodyear, R. J., Legan, P. K., Noda, M. & Richardson, G. P. Evidence for multiple, developmentally regulated isoforms of Ptprq on hair cells of the inner ear. *Dev. Neurobiol.* **71,** 129–141 (2011).
294. Seifert, R. A. *et al.* PTPRQ is a novel phosphatidylinositol phosphatase that can be expressed as a cytoplasmic protein or as a subcellularly localized receptor-like protein. *Exp. Cell Res.* **287,** 374–386 (2003).
295. Andersen, J. N. *et al.* Structural and Evolutionary Relationships among Protein Tyrosine Phosphatase Domains. *Mol. Cell. Biol.* **21,** 7117–7136 (2001).
296. Elson, A., Leder, P. & By, C. Identification of a cytoplasmic, phorbol ester-inducible isoform of protein tyrosine phosphatase E. *Cell Biol.* **92,** 12235–12239 (1995).
297. Oganesian, A. *et al.* Protein tyrosine phosphatase RQ is a phosphatidylinositol phosphatase that can regulate cell survival and proliferation. *Proc. Natl. Acad. Sci.* **100,** 7563–7568 (2003).
298. Jung, H. *et al.* Involvement of PTP-RQ in differentiation during adipogenesis of human mesenchymal stem cells. (2009). doi:10.1016/j.bbrc.2009.04.001
299. Yu, K. R. *et al.* Structural basis for the dephosphorylating activity of PTPRQ towards phosphatidylinositide substrates. *Acta Crystallogr. Sect. D Biol. Crystallogr.* **69,** 1522–1529 (2013).
300. Peng, X.-D. *et al.* Dwarfism, impaired skin development, skeletal muscle atrophy, delayed bone development, and impeded adipogenesis in mice lacking Akt1 and Akt2. *Genes Dev.* **17,** 1352–65 (2003).
301. Fan, W. *et al.* FOXO1 Transrepresses Peroxisome Proliferator-activated Receptor Transactivation, Coordinating an Insulin-induced Feed-forward Response in Adipocytes. *J. Biol. Chem.* **284,** 12188–12197 (2009).
302. Xu, J. & Liao, K. Protein kinase B/AKT 1 plays a pivotal role in insulin-like growth factor-1 receptor signaling induced 3T3-L1 adipocyte differentiation.

J. Biol. Chem. **279,** 35914–22 (2004).

303. Kim, J. E. & Chen, J. regulation of peroxisome proliferator-activated receptor-gamma activity by mammalian target of rapamycin and amino acids in adipogenesis. *Diabetes* **53,** 2748–56 (2004).
304. Heneberg, P. *et al.* Use of Protein Tyrosine Phosphatase Inhibitors as Promising Targeted Therapeutic Drugs. *Curr. Med. Chem.* **16,** 706–733 (2009).
305. Kestler, H. A. & Kuhl, M. From individual Wnt pathways towards a Wnt signalling network. *Philos. Trans. R. Soc. B Biol. Sci.* **363,** 1333–1347 (2008).
306. van Amerongen, R. & Nusse, R. Towards an integrated view of Wnt signaling in development. *Development* **136,** 3205–3214 (2009).
307. MacDonald, B. T., Tamai, K. & He, X. Wnt/beta-catenin signaling: components, mechanisms, and diseases. *Dev. Cell* **17,** 9–26 (2009).
308. Cristancho, A. G. & Lazar, M. A. Forming functional fat: a growing understanding of adipocyte differentiation. *Nat. Rev. Mol. Cell Biol.* **12,** 722–734 (2011).
309. Bennett, C. N. *et al.* Regulation of osteoblastogenesis and bone mass by Wnt10b. *Proc. Natl. Acad. Sci.* **102,** 3324–3329 (2005).
310. Kennell, J. A. & MacDougald, O. A. Wnt signaling inhibits adipogenesis through beta-catenin-dependent and -independent mechanisms. *J. Biol. Chem.* **280,** 24004–10 (2005).
311. Nishizuka, M., Koyanagi, A., Osada, S. & Imagawa, M. Wnt4 and Wnt5a promote adipocyte differentiation. *FEBS Lett.* **582,** 3201–3205 (2008).
312. Kanazawa, A. *et al.* Wnt5b partially inhibits canonical Wnt/β-catenin signaling pathway and promotes adipogenesis in 3T3-L1 preadipocytes. *Biochem. Biophys. Res. Commun.* **330,** 505–510 (2005).
313. Tong, J. *et al.* Lamin A/C deficiency is associated with fat infiltration of muscle and bone. *Mech. Ageing Dev.* **132,** 552–559 (2011).
314. Tseng, Y.-H., Kriauciunas, K. M., Kokkotou, E. & Kahn, C. R. Differential roles of insulin receptor substrates in brown adipocyte differentiation. *Mol. Cell. Biol.* **24,** 1918–29 (2004).
315. Moldes, M. *et al.* Peroxisome-proliferator-activated receptor gamma suppresses Wnt/beta-catenin signalling during adipogenesis. *Biochem. J.* **376,** 607–13 (2003).

316. Lagathu, C. *et al.* Secreted frizzled-related protein 1 regulates adipose tissue expansion and is dysregulated in severe obesity. *Int. J. Obes. (Lond).* **34,** 1695–705 (2010).
317. O'Reilly, M. W., House, P. J. & Tomlinson., J. W. Understanding androgen action in adipose tissue. *J. Steroid Biochem. Mol. Biol.* **143,** 277–284 (2014).
318. DESLYPERE, J. P., VERDONCK, L. & VERMEULEN, A. Fat Tissue: A Steroid Reservoir and Site of Steroid Metabolism. *J. Clin. Endocrinol. Metab.* **61,** 564–570 (1985).
319. Huang, C.-K. *et al.* Loss of androgen receptor promotes adipogenesis but suppresses osteogenesis in bone marrow stromal cells. *Stem Cell Res.* **11,** 938–50 (2013).
320. Kawano, H. *et al.* Suppressive function of androgen receptor in bone resorption.
321. Yeh, S. *et al.* Generation and characterization of androgen receptor knockout (ARKO) mice: an in vivo model for the study of androgen functions in selective tissues. *Proc. Natl. Acad. Sci. U. S. A.* **99,** 13498–503 (2002).
322. Hartig, S. M. *et al.* Androgen receptor agonism promotes an osteogenic gene program in preadipocytes. *Biochem. Biophys. Res. Commun.* **434,** 357–62 (2013).
323. Feleke, Y., Fekade, D. & Mezegebu, Y. Prevalence of highly active antiretroviral therapy associated metabolic abnormalities and lipodystrophy in HIV infected patients. *Ethiop. Med. J.* **50,** 221–30 (2012).
324. Baril, J.-G. *et al.* HIV-associated lipodystrophy syndrome: A review of clinical aspects. *Can. J. Infect. Dis. Med. Microbiol. = J. Can. des Mal. Infect. la Microbiol. medicale* **16,** 233–43 (2005).
325. Park, H., Yu, K. R., Ku, B., Kim, B. Y. & Kim, S. J. Identification of novel PTPRQ phosphatase inhibitors based on the virtual screening with docking simulations. *Theor. Biol. Med. Model.* **10,** 49 (2013).